Sara Fathollahi, M.Sc.

Continuous feeding of low-dose pharmaceuticals with regard to material properties and process stability

DOCTORAL THESIS

to achieve the university degree of
“Doktorin der technischen Wissenschaften”
submitted to

Graz University of Technology

Supervisor

Univ.-Prof. Dipl.-Ing. Dr. techn. Johannes G. Khinast
Institute for Process and Particle Engineering, Technical University, Graz

Graz, May 2021

First assessor and supervisor

Univ.-Prof. Dipl.-Ing. Dr. techn. Johannes G. Khinast

Institute for Process and Particle Engineering, Technical University, Graz

Research Center Pharmaceutical Engineering GmbH, Graz

Second assessor

Univ.-Prof. Dr. Dr.h.c. Stane Srčič, M.Sc. Pharm

Department of Pharmaceutical Technology, Faculty of Pharmacy, University of Ljubljana

EIDESSTATTLICHE ERKLÄRUNG

Ich erkläre an Eides statt, dass ich die vorliegende Arbeit selbstständig verfasst, andere als die angegebenen Quellen/Hilfsmittel nicht benutzt, und die den benutzten Quellen wörtlich und inhaltlich entnommenen Stellen als solche kenntlich gemacht habe. Das in TUGRAZonline hochgeladene Textdokument ist mit der vorliegenden Dissertation identisch.

....

Datum Unterschrift

AFFIDAVIT

I declare that I have authored this thesis independently, that I have not used other than the declared sources/resources, and that I have explicitly indicated all material which has been quoted either literally or by content from the sources used. The text document uploaded to TUGRAZonline is identical to the present doctoral thesis.

....

Date Signiture

„The science of today is the technology of tomorrow“

Edward Teller

Acknowledgments

I first would like to thank professor Johannes Khinast for his guidance, motivation, and patience. I appreciated the opportunity he gave me to conduct this PhD thesis.

I am thankful to all people who contributed to this work and supported me during the difficult times. I would like to acknowledge Stephan Sacher for his help and support in challenges and scientific questions. Special thanks go to my collaboration partners Benjamin Glasser (Rutgers University) and Sebastian Manuel Escotet Espinoza (Merck). I am gratefully indebted to them for their cooperation and very valuable comments on the published papers.

I would like to thank Julia Kruisz, Jakob Rehrl, and Luca Orefice for their cooperation and helpful discussions during the last years.

I especially want to thank my colleagues Viktoria Magosi, Mohammed Feroz Bhuiyan, Michael Piller, and Elliot Koh for technical and graphical support.

Furthermore, I would like to thank interns Martina Kotzent, and Hasan Mahmud Chowdhury for technical support of the experimental studies.

Finally, I must express my very profound gratitude to my family and my friends for providing me with unfailing support and continuous encouragement throughout my years of study and through the process of researching and writing this thesis. This accomplishment would not have been possible without them.

Abstract

The influence of powder composition on packing density and other processing-relevant properties of binary mixtures, including powder flowability is highly relevant in the context of continuous manufacturing. To study this, binary mixtures of pharmaceutical powders with different particle size ratios, α, and varying fractions of large and small particles were analyzed systematically. The results show that the ideal mixture rules do not apply to the mixtures with strongly asymmetric particles, but there is a non-linear and non-monotonic relation between powder composition and the macroscopic powder properties. The results have relevance to pharmaceutical particle processing operations where constant powder mixture properties are needed to ensure quality standards are met e.g., capsule or die filling during tableting, and the continuous feeding of powders via screw feeders.

Powder feeding is a critical unit operation in continuous manufacturing. If the feeding is inconsistent or inaccurate, it will pass the inconsistency and inaccuracy to downstream unit operations such as blending. Especially, high-potency active pharmaceutical ingredients and low-dose excipients, or excipients with very low density, are notoriously hard to feed with currently available commercial technology. The micro-feeder system presented in this thesis is capable of feeding low-dose rates (down to 1 g/h) of powders with different particle sizes and flow properties. The novel micro-feeder can feed the materials that are typically difficult to accurately feed using conventional continuous feeders due to high cohesion, poor flow properties, or low density.

In general, there is a relation between powder properties and feeding performance in most feeders as well as in the micro-feeder system. In the micro-feeder system, powders with finer particles and higher compressibility show densification during their feeding process. However, powders with larger particles and lower compressibility show both “densification” and “powder bed expansion” which is the manifestation of dilation and elastic recovery of particles during the micro-feeding process. These material-specific behaviors (unique but reproducible) were characterized via a displacement feed factor profile for each powder. Through the application of this displacement feed factor, it is possible to provide precise feeding accuracy of low-dose materials. This profile was applied in the micro-feeder system to proactively control the feed rate by manipulating the powder displacement rate. Based on the displacement feed factor profile, which is reproducible and independent from the feed rate set-point, the feed rate can be predicted during the feeding process and at any feed rate set-point. A significant improvement in the feeding performance was achieved for all investigated materials.

In addition, a combined feed-forward/iterative learning control is proposed for the micro-feeder, which realizes a corridor control of low-dose feeding of pharmaceutical raw materials. This control strategy with its reference tracking method enables a constant feed rate with a minimum deviation from the set-point.

Zusammenfassung

Der Einfluss der Zusammensetzung eines Pulvers auf die Packungsdichte und andere verarbeitungsrelevante Eigenschaften von binären Mischungen, wie das Fließverhalten des Pulvers, sind von großer Bedeutung für die kontinuierliche Fertigung. Um dies zu untersuchen, wurden binäre Mischungen von pharmazeutischen Pulvern mit verschiedenen Partikelgrößen, α, und verschiedenen Teilmengen von großen und kleinen Partikel systematisch analysiert. Die Ergebnisse zeigen, dass die idealen Mischungsregeln für stark asymetrische Partikel nicht anwendbar sind, jedoch eine nicht-lineare, nicht-monotone Relation zwischen der Pulverzusammensetzung und den makroskopischen Pulvereigenschaften besteht.

Die Ergebnisse sind von großer Relevanz für pharmazeutische Prozesse mit pulverförmigen Materialien, bei der konstante Mischungseigenschaften zur Sicherstellung der Qualitätsstandards benötigt werden.. Beispiele dafür sind das Füllen von Kapseln oder der Matrix während der Tablettierung oder kontinuierliches Dosieren von Pulvern mittels Schneckenförderelementen.

Das Dosieren von Pulver ist ein kritischer Vorgang bei kontinuierlicher Fertigung. Wenn das Dosieren inkonsistent oder ungenau ist, werden die Inkonsistenzen und Ungenauigkeiten an nachgeschaltete Vorgänge wie das Mischen weitergegeben. Besonders, hochwirksame pharmazeutische Wirkstoffe, gering dosierte Hilfsstoffe oder Hilfsstoffe mit sehr geringer Dichte sind mit aktuell bekannten Methoden schwierig zu dosieren. Das Micro-feeder System, welches in dieser Arbeit präsentiert wird, ermöglicht das Dosieren geringer Mengen (bis zu 1g/h) von Pulvern mit unterschiedlichen Partikelgrößen und Fließeigenschaften. Der neuartige Micro-feeder kann Materialien verarbeiten, die typischerweise aufgrund von hoher Kohäsion, schlechten Fließeigenschaften oder niedriger Dichte mit konventionellen Feedern sehr schwierig zu dosieren sind.

Grundsätzlich gibt es für die meisten Dosierer wie auch für den Micro-feeder eine Abhängigkeit zwischen den Pulvereigenschaften und der Dosierleistung und dem Verhalten beim Dosieren . Im Micro-feeder System weisen Pulver mit feineren Partikelgrößen und höherer Komprimierbarkeit eine Verdichtung (densification) während des Dosierprozesses auf. Pulver mit größerer Partikelgröße und niedrigerer Komprimierbarkeit zeigen sowohl „densification“ als auch Expansion (powder bed expansion). Dies ist die Manifestation der Erweiterung und elastischen Entspannung von Partikeln im Micro-feeding Prozess. Dieses materialspezifische Verhalten (einzigartig aber reproduzierbar) wurde mittels eines „displacement feed factor“-Profiles für jedes Pulver charakterisiert. Die Anwendung des „displacement feed factor”-

Profiles ermöglicht präzises Dosieren niedrig dosierter Materialien. Für das Micro-feeder System werden Profile verwendet, um die Dosierrate mittels der Pulver „displacement“-Rate proaktiv zu verändern. Basierend auf dem „displacement feed factor”-Profil, welches reproduzierbar und unabhängig vom Sollwert der Dosierrate ist, kann die Dosierrate während des Dosier-Prozesses und bei jedem beliebigen Sollwert vorhergesagt werden.

Für alle betrachteten Materialien wurde eine signifikante Verbesserung der Dosierleistung erreicht. Zusätzlich wurde ein kombinierter „feed-forward/iterative learning“ Kontrollmechanismus für den Micro-feeder eingesetzt. Dieser regelt die Dosierung von niedrig dosierten pharmazeutischen Materialien innerhalb eines Korridors. Diese Kontrollstrategie basierend auf der Verfolgung eines Referenzwertes ermöglicht eine konstante Dosierrate mit minimaler Abweichung vom Sollwert.

Table of Contents

1 Introduction and Motivation

A pharmaceutical product is consisting of two materials, active pharmaceutical ingredients (APIs) and excipients e.g., fillers, disintegrants, compaction aids, coloring, and lubricants. Pharmaceutical manufacturing is divided into primary manufacturing and secondary manufacturing (1).

Primary manufacturing consists of API synthesis (by chemical synthesis or biological processing) followed by API finish processes such as drying, purification, and size reduction (1,2). Secondary manufacturing turns the API into the final dosage form. For instance, tablet manufacturing includes feeding, blending, granulation drying, milling, blending, tableting, and coating. Packaging of the final dosage form and warehousing distribution is the last process chain in the pharmaceutical manufacturing process (1,2).
All pharmaceutical products need to be manufactured in line with good manufacturing practice (GMP) in order to enter the market (2). The requirements for GMP in EU are covered by Directive 2003/94/EC (2).

1.1 Process Intensification

The "European Roadmap for Processes Intensification" defined process intensification (PI) as "PI provides radically innovative principles ('paradigm shift') in process and equipment design which can benefit (often with more than a factor two) process and chain efficiency, capital and operating expenses, quality, wastes, process safety and more" (3).
The pharmaceutical industry is paying attention to process intensification (PI) mainly for the potential benefits of it such as selectivity, process safety, reliability, sustainability, smaller process plant, overall cost reduction, and related energy saving (3). PI provides great opportunities to significantly improve the performance of pharmaceutical processes (4). It has been demonstrated in pharmaceutical industry through the implementation of continuous manufacturing (5).

1.2 Continuous manufacturing

Pharmaceutical industry is shifting from batch to continuous manufacturing in both primary manufacturing and secondary manufacturing for many potential benefits (1,6,7), e.g., faster production with a higher flexibility of production volume, modular manufacturing, reducing environmental footprints and operating costs, better monitoring and control over the individual

processes, and therefore more consistent product quality (1,8). In the continuous manufacturing process, multiple batches of materials can be manufactured continuously.

In general, continuous manufacturing is characterized by the connection of the individual processes into one line, e.g., in the ConSigma continuous tableting line from GEA, the final tablet product is produced from raw API and excipients in one manufacturing line. Continuous manufacturing has been increasingly applied in the pharmaceutical industry after the FDA encouraging innovation and rational manufacturing (9–11). In the last years, Several modular continuous manufacturing implementations have been commercialized by different equipment companies, including GEA, Glatt, or Bosch to name a few.

Common to all continuous manufacturing operations, APIs and excipients are continuously fed and blended as a first step (12). In particular, feeders play an important role: they maintain the steady-state of the process and deliver the pharmaceutical ingredients to the downstream process (7,13), e.g., continuous granulation, tableting, and coating. Individual feeders continuously deliver the APIs and excipients according to the formulation and at pre-defined feed rates (7). Consistent feeding of materials requires a good understanding of the material properties and the manufacturing process.

1.3 Challenges and opportunities

There is an increasing need in pharmaceutical industry for more efficient manufacturing processes. The reasons are market competition due to patent expirations of many drugs, high cost of research and development for new drugs, great demand for reducing environmental footprints, and desire for innovation within the industry (4). Hence, there is a great opportunity to adopt innovations in the pharmaceutical industry. This requires a good understanding of the manufacturing process and the material properties (including in-process properties).

1.3.1 Impact of powder properties

Powder properties are highly relevant in the pharmaceutical industry, since the quality and therapeutic effect of the individual product, i.e., a tablet or capsule, is directly connected to powder properties, such as density and flowability (14,15). For example, during tableting, a die is filled gravimetrically with powder, which is subsequently compressed. Other examples include the feeding capacity of screw feeders (16) or hot-melt extruders (17), which are a function of powder density at the screw inlet and flowability, the amount of powder filled into capsules during tamping or dosator filling, or the ability to blend powders (agglomeration versus segregation) (18,19). These effects are especially important during continuous

processing since in such processes, not the powder mass is relevant, which can be accurately measured by weighing, but the mass flow rate, for which no sensors exist (16). Thus, flowability, segregation tendency, and adhesiveness strongly impact the processability and relate to the quality of the final product in terms of weight and content uniformity (14,20).

Depending on the specific material density, fine powders with a particle size below 50-100 μm experience significant cohesive forces between individual particles (21). Van der Waals forces, electrostatic forces, and capillary forces are predominant in the dispersion of fine powders (21). These forces can lead to agglomeration and adhesion of particles to the walls of feeders (21). Many APIs are powders with particles in the cohesive range. Thus, especially the continuous blending and feeding of APIs in a continuous manufacturing framework is challenging.

1.3.1.1 Powder blending

In pharmaceutical manufacturing, secondary manufacturing (drug production manufacturing) starts with blending the API and excipients (2,22). Deviations of the API concentration in the blend, even at a micro-scale, affect the safety and quality of the final drug products (12,23). Traditionally powder blending was done in a batch-wise process in blenders and was stored and transported between unit operations batch-wise (22). The main disadvantage of batch-wise blending is the scale-up since the blend size is limited to the blender size. This problem can be solved by using a continuous blender (22).

Powder blending is an essential unit operation in the pharmaceutical manufacturing line. Homogeneity of powder mixture is the goal of this unit operation. In the context of continuous manufacturing, the powder blend concentration is determined by the feed rate of the API feeder in relation to the feed rate of the excipient feeder(s). The blending performance is dependent on process parameters and design as well as on material properties e.g., particle size distribution, flow properties such as cohesion, bulk, and tapped density.

In-process powder density and flowability are complex properties of powders and depend on many factors, such as particle size distribution, particle shape, moisture, inter-particle cohesion, and friction coefficients, as well as processing history (24–26). Unfortunately, it is difficult to predict these properties for arbitrary powders and each powder measurements of the relevant properties, including bulk density, tapped density, compressibility, cohesiveness, flow function, permeability, and many others is required. In addition, environmental conditions have an impact. In particular, relative humidity (impacting the moisture uptake) and temperature affect these properties (27,28).

Knowing processing-relevant mixture properties is important for the design and the optimization of powder processing operations, especially in the context of continuous pharmaceutical manufacturing, where powders are in motion at all times, and thus, the flow properties of mixtures are critical. Unfortunately, the dependence of macroscopic powder properties on the composition is far from linear with respect to the mass fractions of the components.

A good understanding of the relationship between powder composition and critical quality attributes (CQAs) of a drug product is required for the rational development of solid dosage forms and manufacturing processes (29). Therefore, the ability to predict the properties of powders as a function of composition is critical for ensuring controllable processes and reproducible products (12).

1.3.1.2 Powder feeding

In the context of continuous manufacturing, continuous feeding (30–33) of materials is one of the most critical unit operations in the entire line. Powder behavior should be fully understood to prevent over or under-dosing. For instance, powder flowability is an important powder property, which can affect the feeding process (18,20). Flowability is a complex property of a powder and depends on many factors such as particle size distribution, particle shape, moisture, inter-particle cohesion, and friction forces (14,24,34).

Especially continuous low-dose feeding of sticky and cohesive powder is a challenge in the pharmaceutical industry (12,35). While feed rates of kilograms per hour can be obtained using standard equipment, low feed rates in the range of grams per hour are difficult to achieve due to the intermittent nature of granular flows from small-scale screw conveyors. Even more problematic is the continuous feeding of cohesive or electrostatic materials, which flow in chunks or agglomerates.

Continuous low-dose feeding is highly important for two reasons: First, the pharmaceutical industry is in the process of adopting continuous manufacturing. Second, high-potency active pharmaceutical ingredients (HPAPIs), with doses in the range of milligrams or even micrograms per tablet, are becoming more frequent (15,16,36). Currently, no reliable equipment exists that can be used for continuous low-dose feeding of powders (37–41). Continuous feeding of fine powder at the low ratios needed for a given formulation is one of the key issues in continuous manufacturing processes (21,36).

1.3.1.2.1 Loss in weight feeder

Loss-in-weight (LIW) feeder is the most common feeder used in continuous pharmaceutical manufacturing lines. This gravimetric feeder consists of a volumetric feeder with rotating screws for powder dispensing, which is located on a weighing platform, and a gravimetric controller (42). The controller receives a signal from the load cell of the weighing platform as a function of time (42). This signal is used to calculate the instantaneous feed rate of the LIW feeder. The instantaneous feed rate is compared to the desired feed rate (set-point) and in case of any deviation, an appropriate correction to the rotating speed of the screws is applied (42).

The feeding range of the LIW feeder depends on the feeder's size and tooling such as screws and screens (36,42). Especially at low feed rates of < 1 kg/h, LIW feeding is challenging due to feed-rate fluctuations associated with the screw conveying principle, problems during the hopper refilling, and associated feed-rate variations due to changes in the powder bed height. Moreover, bridging and adhesion of cohesive materials are associated with the screw conveying method, leading potentially to blockage of the feed channel (36,42–44).

The LIW feeder operates temporarily in volumetric mode during the start-up and refilling procedure (42). In this mode, similar to any other volumetric feeder, the bulk properties are highly relevant in order to achieve constant and non-fluctuating feed rates. Powder bulk density is a strong function of other powder properties, such as particle size distribution, shape, packing properties, processing history, as well as environmental conditions such as vibration and humidity (35,45). Even batch-to-batch variations in the powder properties may introduce errors in the feeding system.

1.4 Reference

1. Rantanen J, Khinast J. The Future of Pharmaceutical Manufacturing Sciences. J Pharm Sci [Internet]. 2015;104(11):3612–38. Available from: https://doi.org/10.1002/jps.24594
2. Plumb K. Continuous processing in the pharmaceutical industry: Changing the mind set. Chem Eng Res Des. 2005;83(6 A):730–8.
3. DECHEMA. European roadmap for process intensification [Internet]. 2005. Available from: https://dechema.de/efce_media/-p-531-EGOTEC-9a551f7b3fe98d8e9b2fdfdda75ae7ff.pdf
4. Wang J, Li F, Lakerveld R. Process intensification for pharmaceutical crystallization. Chem Eng Process - Process Intensif [Internet]. 2018;127(January):111–26. Available from: https://doi.org/10.1016/j.cep.2018.03.018
5. Nima Yazdanpanah. Continuous Manufacturing in the Pharmaceutical Industry. aiche.org/cep. 2021;
6. Vanarase A, Ricart B, Almaya A, Debelder L, Wyatt J. Results and Discussion Corporate Strategy for CM Implementation. 2020;(August):1–18.
7. Hanson J. Control of a system of loss-in-weight feeders for drug product continuous manufacturing. Powder Technol [Internet]. 2018;331:236–43. Available from: https://doi.org/10.1016/j.powtec.2018.03.027
8. Schaber SD, Gerogiorgis DI, Ramachandran R, Evans JMB, Barton PI, Trout BL. Economic analysis of integrated continuous and batch pharmaceutical manufacturing: A case study. Ind Eng Chem Res. 2011;50(17):10083–92.
9. FDA. Quality Considerations for Continuous Manufacturing Guidance for Industry. Food Drug Adm [Internet]. 2019;(February):1–27. Available from: https://www.fda.gov/Drugs/GuidanceComplianceRegulatoryInformation/Guidances/default.htm
10. Administration F and D. Guidance for Industry, PAT-A Framework for Innovative Pharmaceutical Development, Manufacturing and Quality Assurance. 2004;(September). Available from: http://www.fda.gov/downloads/Drugs/GuidanceComplianceRegulatoryInformation/Guidances/ucm070305.pdf

11. FDA. Advancement of Emerging Technology Applications for Pharmaceutical Innovation and Modernization Guidance for Industry. Food Drug Adm [Internet]. 2017;(September):1–8. Available from: http://www.fda.gov/Drugs/GuidanceComplianceRegulatoryInformation/Guidances/default.htm

12. Wang Y, Koynov S, Glasser BJ, Muzzio FJ. A method to analyze shear cell data of powders measured under different initial consolidation stresses. Powder Technol [Internet]. 2016;294:105–12. Available from: http://dx.doi.org/10.1016/j.powtec.2016.02.027

13. Moghtadernejad S, Escotet-Espinoza MS, Oka S, Singh R, Liu Z, Román-Ospino AD, et al. A Training on: Continuous Manufacturing (Direct Compaction) of Solid Dose Pharmaceutical Products. J Pharm Innov. 2018;13(2):155–87.

14. Sandler N, Wilson D. Prediction of granule packing and flow behavior based on particle size and shape analysis. J Pharm Sci [Internet]. 2010;99(2):958–68. Available from: http://dx.doi.org/10.1002/jps.21884

15. Bostijn N, Dhondt J, Ryckaert A, Szabó E, Dhondt W, Van Snick B, et al. A multivariate approach to predict the volumetric and gravimetric feeding behavior of a low feed rate feeder based on raw material properties. Int J Pharm [Internet]. 2019;557(September 2018):342–53. Available from: https://doi.org/10.1016/j.ijpharm.2018.12.066

16. Stauffer F, Vanhoorne V, Pilcer G, Chavez PF, Schubert MA, Vervaet C, et al. Managing active pharmaceutical ingredient raw material variability during twin-screw blend feeding. Eur J Pharm Biopharm. 2019;135(October 2018):49–60.

17. Matić J, Witschnigg A, Zagler M, Eder S, Khinast J. A novel in silico scale-up approach for hot melt extrusion processes. Chem Eng Sci. 2019;204:257–69.

18. Van Snick B, Grymonpré W, Dhondt J, Pandelaere K, Di Pretoro G, Remon JP, et al. Impact of blend properties on die filling during tableting. Int J Pharm [Internet]. 2018;549(1–2):476–88. Available from: https://doi.org/10.1016/j.ijpharm.2018.08.015

19. Van Snick B, Dhondt J, Pandelaere K, Bertels J, Mertens R, Klingeleers D, et al. A multivariate raw material property database to facilitate drug product development and enable in-silico design of pharmaceutical dry powder processes. Int J Pharm [Internet]. 2018;549(1–2):415–35. Available from: https://doi.org/10.1016/j.ijpharm.2018.08.014

20. Grymonpré W, Vanhoorne V, Van Snick B, Blahova Prudilova B, Detobel F, Remon JP,

et al. Optimizing feed frame design and tableting process parameters to increase die-filling uniformity on a high-speed rotary tablet press. Int J Pharm [Internet]. 2018;548(1):54–61. Available from: https://doi.org/10.1016/j.ijpharm.2018.06.047

21. Leschonski K, Rüthele S, Menzel U. A Special Feeder for Diffraction Pattern Analysis of Dry Powders. Part Part Syst Charact. 1984;1(1–4):161–6.

22. Jaspers M, de Wit MTW, Kulkarni SS, Meir B, Janssen PHM, van Haandel MMW, et al. Impact of excipients on batch and continuous powder blending. Powder Technol [Internet]. 2021;384:195–9. Available from: https://doi.org/10.1016/j.powtec.2021.02.014

23. Forte G, Clark PJ, Yan Z, Stitt EH, Marigo M. Using a Freeman FT4 rheometer and Electrical Capacitance Tomography to assess powder blending. Powder Technol [Internet]. 2018; Available from: http://linkinghub.elsevier.com/retrieve/pii/S0032591017309701

24. Prescott JK, Barnum RA. On powder flowability. Pharm Technol [Internet]. 2000;(October). Available from: www.pharmaportal.com

25. Capece M, Silva KR, Sunkara D, Strong J, Gao P. On the relationship of inter-particle cohesiveness and bulk powder behavior: Flowability of pharmaceutical powders. Int J Pharm [Internet]. 2016 Sep 10 [cited 2019 Feb 5];511(1):178–89. Available from: https://www.sciencedirect.com/science/article/pii/S037851731630549X?via%3Dihub

26. Leung LY, Mao C, Srivastava I, Du P, Yang C-Y. Flow Function of Pharmaceutical Powders Is Predominantly Governed by Cohesion, Not by Friction Coefficients. J Pharm Sci [Internet]. 2017 Jul 1 [cited 2019 Jan 23];106(7):1865–73. Available from: https://www.sciencedirect.com/science/article/pii/S0022354917302447#!

27. Vandewalle N, Lumay G, Ludewig F, Fiscina JE. How relative humidity affects random packing experiments. Phys Rev E - Stat Nonlinear, Soft Matter Phys. 2012;85(3):1–5.

28. Teunou E, Fitzpatrick JJ. Effect of relative humidity and temperature on food powder. J Food Eng. 1999;42:109–16.

29. Worku ZA, Kumar D, Gomes JV, He Y, Glennon B, Ramisetty KA, et al. Modelling and understanding powder flow properties and compactability of selected active pharmaceutical ingredients, excipients and physical mixtures from critical material properties. Int J Pharm [Internet]. 2017;531(1):191–204. Available from: http://dx.doi.org/10.1016/j.ijpharm.2017.08.063

30. Rogers L, Briggs N, Achermann R, Adamo A, Azad M, Brancazio D, et al. Continuous Production of Five APIs in Flexible Plug-and-Play Modules - A Demonstration Campaign. Org Process Res Dev. 2020;

31. Azad MA, Osorio JG, Brancazio D, Hammersmith G, Klee DM, Rapp K, et al. A compact, portable, re-configurable, and automated system for on-demand pharmaceutical tablet manufacturing. Int J Pharm [Internet]. 2018;539(1–2):157–64. Available from: https://doi.org/10.1016/j.ijpharm.2018.01.027

32. Adamo A, Beingessner RL, Behnam M, Chen J, Jamison TF, Jensen KF, et al. On-demand continuous-flow production of pharmaceuticals in a compact, reconfigurable system. Science (80-). 2016;352(6281):61–7.

33. Stelzer T, Wong SY, Chen J, Myerson AS. Evaluation of PAT Methods for Potential Application in Small-Scale, Multipurpose Pharmaceutical Manufacturing Platforms. Org Process Res Dev. 2016;20(8):1431–8.

34. Yu W, Muteki K, Zhang L, Kim G. Prediction of bulk powder flow performance using comprehensive particle size and particle shape distributions. J Pharm Sci [Internet]. 2011;100(1):284–93. Available from: http://dx.doi.org/10.1002/jps.22254

35. Yang S, Evans JRG. Metering and dispensing of powder; the quest for new solid freeforming techniques. Powder Technol. 2007 Sep;178(1):56–72.

36. Engisch WE, Muzzio FJ. Loss-in-Weight Feeding Trials Case Study: Pharmaceutical Formulation. J Pharm Innov. 2014;10(1):56–75.

37. Lu X, Yang S, Evans JRG. Studies on ultrasonic microfeeding of fine powders. J Phys D Appl Phys. 2006;39(11):2444–53.

38. Lu X, Yang S, Evans JRG. Ultrasound-assisted microfeeding of fine powders. Particuology. 2008 Feb;6(1):2–8.

39. Matsusaka S, Yamamoto K, Masuda H. Micro-feeding of a fine powder using a vibrating capillary tube. Adv Powder Technol. 1996;7(2):141–51.

40. Qi L, Zeng X, Zhou J, Luo J, Chao Y. Stable micro-feeding of fine powders using a capillary with ultrasonic vibration. Powder Technol. 2011 Dec;214(2):237–42.

41. Chen X, Seyfang K, Steckel H. Development of a micro-dosing system for fine powder using a vibrating capillary. Part 2. The implementation of a process analytical technology tool in a closed-loop dosing system. Int J Pharm. 2012 Aug;433(1–2):42–50.

42. C.A. Blackshields AMC. Continuous powder feeding for pharmaceutical solid dosage form manufacture: a short review. Pharm Dev Technol [Internet]. 2017; Available from: https://doi.org/10.1080/10837450.2017.1339197

43. Engisch WE, Muzzio FJ. Feedrate deviations caused by hopper refill of loss-in-weight feeders. Powder Technol. 2015;283:389–400.

44. Engisch WE, Muzzio FJ. Method for characterization of loss-in-weight feeder equipment. Powder Technol. 2012;228:395–403.

45. Yu AB, Standish N. Estimation of the Porosity of Particle Mixtures by a Linear-Mixture Packing Model. Ind Eng Chem Res. 1991;30(6):1372–85.

2 Impact of Powder Composition on Processing-relevant Properties of Pharmaceutical materials: An Experimental Study

(This chapter is based on the publication Sara Fathollahi, Eva Faulhammer, Benjamin J. Glasser, Johannes G. Khinast, Impact of Powder Composition on Processing-relevant Properties of Pharmaceutical Materials: An Experimental Study, Advanced Powder Technology, Volume 31, Issue 7, July 2020, Pages 2991-3003)

2.1 Abstract

In this work, we studied the influence of powder composition on packing density and other processing-relevant properties of binary mixtures, including powder flowability. Binary mixtures of pharmaceutical powders with different particle size ratios, α and varying fractions of large and small particles were analyzed systematically. Mixtures of three excipients and one API with different composition (2, 5, 10, 30, 50, 70, 90, 95 and 98 %wt.) were prepared in a Turbula mixer. Powders with different properties and particle size distribution were chosen, in order to obtain three binary mixtures with different size ratios. Then, macroscopic powder properties including bulk (poured) and tapped density (BD and TD) were measured. A powder rheometer was used to measure the flow function coefficient (ffc), cohesion, compressibility and permeability of the binary mixtures. We considered experimentally three classes of binary mixtures, which are characterized by two critical ratios of particle diameter: the critical size ratio of entrance (α_c) and the critical size ratio of replacement (α_r), where $\alpha_c = 0.154$ and $\alpha_r = 0.741$. Below the critical size ratio of entrance (α_c), the particle asymmetry (ratio between large and small particle diameters) is high and small particles can fill the voids between larger ones. Between α_c and the critical size ratio of replacement (α_r), the smaller particles are too large to fit in the voids between larger particles (packing structure changes). Above α_r, the particles are more or less symmetric in size and overall packing structure does not change by mixing the particles. Our experiments show that there is a non-linear and non-monotonic dependence of all relevant properties on composition for powder mixtures that have an $\alpha < \alpha_r$. This non-linear behavior is even more significant for strongly asymmetric binary mixtures with $\alpha < \alpha_c$. We argue that this behavior is related to the composition dependence of random packing of particulate systems. Our results have relevance to pharmaceutical particle processing operations where constant powder mixture properties are needed to ensure quality standards are met; such operations include capsule or die filling during tableting, and the continuous feeding of powders

via screw feeders. Our results suggest that for pharmaceutical particle processing operations, where constant powder mixture properties are a prerequisite for process robustness, the size ratio of API and excipient particles, α should not be smaller than $\alpha_r = 0.741$.

2.2 Introduction

Macroscopic powder properties, such as bulk (poured) density, average particle size, width of the particle size distribution (PSD) and, especially, the flowability, have significant impact on the processability of a particulate material [1], [2]. This is true for many industries, including the chemical and catalyst industry or companies that make agricultural products, fertilizers, metal powders and concrete, or consumer products. However, in the pharmaceutical industry, powder properties are even more relevant, since the quality and therapeutic effect of the individual product, i.e., a tablet or capsule, is directly connected to powder properties, such as the density [1], [3]. For example, during tableting a die is filled gravimetrically with powder, which is subsequently compressed [2], [4]. The mass of powder in the die (and thus the tablet mass) is directly related to the density, permeability and often, to the flowability of the powder [4], since die filling has to occur in a fraction of a second [1]. Other examples include the feeding capacity of screw feeders [5] or hot-melt extruders [6], which are a function of powder density at the screw inlet and flowability, the amount of powder filled into capsules during tamping or dosator filling, or the ability to blend powders (agglomeration versus segregation) [4], [7]. These effects are especially important during continuous processing, since in such processes not the powder mass is relevant (which can be accurately measured by weighing) but the mass flow rate, for which no sensors exist [5]. Thus, flowability, segregation tendency and adhesiveness strongly impact the processability and relate to the quality of the final product in terms of weight and content uniformity [1], [2].

In-process powder density and flowability are complex properties of powders and depend on many factors, such as particle size distribution, particles shape, moisture, inter-particle cohesion and friction coefficients, as well as processing history [8]–[10]. Unfortunately, it is difficult to predict these properties for arbitrary powders and for each powder measurements of the relevant properties, including bulk density, tapped density, compressibility, cohesiveness, flow function, permeability and many others are required. In addition, environmental conditions have an impact. In particular, relative humidity (impacting the moisture uptake) and temperature affect these properties [11], [12].

While the experimental determination of powder properties for defined materials can be readily carried out, and data-base approaches have been proposed by several groups [3], [7], [13]–[16], the problem in the design of continuous powder processing operations is the fact that typically mixtures of powders have to be processed, often involving 4-10 different materials. Unfortunately, the dependence of macroscopic powder properties on the composition is far from linear with respect to the mass fractions of the components. Binary packings of particles, ternary and multi-component packings are well studied, e.g., in the book of German [17]. In fact, even addition of small quantities of one powder to another powder may strongly affect the mixture properties. A typical example is the addition of colloidal silica to strongly cohesive powders. Blending of colloidal silicon dioxide (used as a glidant) with strongly cohesive active pharmaceutical ingredients (APIs) or excipients can significantly enhance flowability, even at silica mass fractions of less than 1% [18], [19]. Adding smaller particles to larger ones can change the bulk density dramatically, since the small particles can occupy the space between larger particles, reducing the void fraction (air space or porosity) [20]–[22]. In addition, the compressibility of powders, i.e., the ability to form stable bonds that withstand a tensile stress, is affected by composition [23].

As pointed out above, in pharmaceutical manufacturing the API is commonly mixed with excipients (e.g., fillers, disintegrants, compaction aids and lubricants) in order to produce the final product forms. Clearly, deviations of the API concentration in the blend, even at a micro-scale, affect the safety and quality of the final drug products [24], [25]. In the context of continuous manufacturing, the powder blend concentration is determined by the feed rate of the API feeder in relation the feed rate of the excipient feeder(s). Bulk properties of the mixtures are highly relevant to achieve constant, non-fluctuating feed rates, especially in volumetric feeders. Therefore, the density and porosity of particulate mixtures are important factors to consider [21] [22]. Similarly, powder flowability is an important powder property, which can affect the filling and feeding process [2], [4]. Flowability is a complex property of a powder and depends on many factors such as particle size distribution, particles shape, moisture, inter-particle cohesion and friction forces [1], [8], [26].

The development of solid dosage forms and manufacturing processes requires a good understanding of the relationship between powder composition and critical quality attributes (CQAs) of a drug product [27]. Therefore, the ability to predict the properties of powders as a function of composition is critical for ensuring controllable processes and reproducible products [24].

In the literature it is well-known that many macroscopic properties of powder mixtures do not depend in a linear way on the mixture fraction. However, in these studies, packing density and porosity of mixtures have been studied mostly theoretically [20]–[22], [28]–[34]. Moreover, mathematical models were developed based on the packing theory of spherical particles and subsequently, the similarity between the spherical and non-spherical particle packings [31]. These models were used to predict the packing density [20], [21], [28]–[30] and porosity [22], [31]–[34] of binary mixtures. The accuracy of the models has been evaluated with experimental packing density results [35]–[37] of binary mixtures of mono-sized spherical particles. In more recent experimental studies [38], [39], also only the packing density of spherical and mono-sized particles was measured. However, industrial materials are usually not mono-sized, i.e., they have a wide particle size distribution (PSD).

There are only a few studies [40]–[42], where other processing-relevant powder properties, such as compressibility, cohesiveness, flow function, friction coefficient and permeability have been studied for binary mixtures of powders. Odeniyi et al. [41] investigated the compressibility index (calculated from the bulk and tapped density measurement), angle of internal flow (also derived from tapping experiments) and angle of repose of binary mixtures. Verthalis and Pilpel [40] measured the mean particle size, tensile strength and angle of internal flow (derived from tapping experiment) of binary mixtures. In a recent publication of Alshafiee et al. [42], the ffc of binary blends at three blend compositions was measured using a ring shear tester.

Knowing processing-relevant mixture properties is important for the design and the optimization of powder processing operations, especially in the context of continuous pharmaceutical manufacturing, where powders are in motion at all times, and thus, flow properties of mixtures are critical. Therefore, the goal of this study was to identify the relationship between powder composition and macroscopic, processing-relevant powder properties for a binary mixture of powders (API and excipients). This is important to better understand the downstream processability and to form the basis for predictive models, needed for the design of advanced continuous manufacturing operations. For this purpose, three different binary material mixtures with different size ratios have been investigated. For each binary mixture, nine fractions of 2, 5, 10, 30, 50, 70, 90, 95 and 98% by mass were prepared. Mixtures were fully characterized by a FT4 powder rheometer system and a Pharmatest system (in order to measure the macroscopic powder properties including bulk density (BD) and tapped density (TD)). In Section 2 the materials and methods are described, followed by results and discussion (Section 3) and conclusions, in Section 4.

In summary, we aimed to experimentally study in detail the impact of pharmaceutical materials composition on process-relevant properties, including frictional and flowability parameters. The obtained data were qualitatively explained by the "theory of random packing properties".

2.3 Materials and Methods

2.3.1 Materials

Three different α-lactose-monohydrate excipients and one active pharmaceutical ingredient (API) were used in this study. Powders with different particle sizes and properties were chosen for this study. Lactose is mostly used in pharmaceutical industry as a filler for tableting and capsule filling [43], or as a carrier for dry-powder inhalers. CapsuLac60 (CL) is a sieved lactose with excellent flow properties. SorboLac400 (SL) is a milled lactose with good compactability and Inhalac70 (InL) is a sieved lactose, which is a standard inhalation carrier material [44]. All three α-lactose-monohydrate excipients were supplied by Meggle, Germany. Ascorbic acid (AA; Vitamin C) is an essential nutrient widely used in the food and pharmaceutical industries [45]. Ascorbic acid was obtained as a pharmaceutical grade API from Mühlenchemie, Germany and has poor flowability.

2.3.2 Mixture preparation

Three binary mixtures with different size ratios were prepared for this study. Nine mixtures (600g total mixture weight) of CL and AA with AA:CL mass fractions of 98:2, 95:5, 90:10, 70:30, 50:50, 30:70, 10:90, 5:95 and 2:98 were weighed and placed into nine plastic vessels. The powders in the plastic vessels were mixed for 15 minutes at 60rpm in a Turbula blender TC2 (Willy A. Bachofen Maschinenfabrik, Switzerland). The Turbula blender combines rotation, translation and inversion in a low shear mixing process. The same procedure was used for preparing SL:CL as well as InL:CL mixtures. For the binary system SL:CL, four additional mixtures with SL:CL mass fraction of 20:80, 40:60, 60:40 and 80:20 were prepared.

2.3.3 Powder characterization

2.3.3.1 Particle size distributions

Particle size distributions (PSDs) of the materials were measured by using laser light diffraction techniques and optical methods. PSDs of SL and AA were determined by Helos/KR (OASIS/L dry dispersing system Sympatec, Clausthal-Zellerfeld, Germany), measuring particle size range of 0.45 µm to 875 µm. PSDs of CL and InL were determined by QICPIC (OASIS/L dry

dispersing system Sympatec, Clausthal-Zellerfeld, Germany), measuring particle size range of 20 µm to 7308 µm. In both systems, a vibrating chute was used to transport the powder in a controlled way to the dispersing unit.

The PSDs of the AA:CL mixtures were also measured by QICPIC. Since mixtures were prepared by mass, the cumulative distribution can be calculated by the following equation:

$$Q_{3,m(x)} = Q_{3,A(x)} * w_A + Q_{3,B(x)} * w_B \quad \text{Eq. 1}$$

where w_A and w_B are respectively the mass fraction of CL and AA in the mixture. $Q_{3,A}$ and $Q_{3,B}$ are the cumulative PSDs of CL and AA, respectively.

Comparing calculated PSDs of the mixtures with the measured ones is a good measure of the mixing quality after blending of the powders. In the case of AA:CL mixtures, samples for measuring PSDs were taken carefully from the upper part of the container by a spoon.

Since the materials' PSDs are very similar for the InL:CL mixture, such an analysis was not performed. Moreover, the analysis was not done for SL:CL mixtures, since the particle size distribution of the mixture ranges over a wide range, requiring laser diffraction and image analysis simultaneously, which was not feasible.

2.3.3.2 Powder density measurement

The bulk (poured) and tapped densities (BD and TD) of materials and mixtures were analyzed by a Phamatest PT-TD200, which is a standardized method described in the United States Pharmacopeia (USP 2011, h616i) [46]. The standard 250 mL cylinder was filled with powder and powder mass was recorded ($BD = \frac{\text{mass [g]}}{\text{volume [cm3]}}$). The tapped density was determined after mechanically tapping the powder sample in three steps of 500, 750 and 1250 strokes ($TD = \frac{\text{mass [g]}}{\text{volume [cm3]}}$). Hausner ratio is the ratio of TD to BD, which provides information on powder flowability. In general, it is expected that a lower Hausner ratio indicates better flowability.

True density of the material was measured by a helium pycnometer (AccuPyc II 1340, Micromeritics, Norcross, USA). The AccuPyc was operated with a 10 cm^3 module sample. Prior to true density measurements, AccuPyc was calibrated with a calibration standard volume of 6.37 cm^3. Volume of solid samples (excluding all voids and pores) were determined by measuring the pressure change of helium in the calibrated volume. Details of this methodology can be found in the work of Viana et al. [47].

2.3.3.3 Powder properties obtained from FT4 powder rheometer

The FT4 powder rheometer system (Freeman Technology, Tewkesbury, UK) was used to characterize powder properties, such as flow properties, compressibility and permeability. For each sample in the glass test vessel (10 mL shear cell with diameter of 25 mm) a conditioning step was performed first: The blade was rotated and moved downwards and upwards to generate a standardized preconditioned powder bed under defined conditions.

2.3.3.4 Shear cell test

The shear cell test consists of conditioning, consolidation, pre-shearing and shearing steps [24]. After filling the sample powder into the glass test vessel, a conditioning step was performed by the blade, as described above. Afterward the powder was consolidated at an initial consolidation stress of 9kPa by a vented piston. To achieve a steady state, the powder was then sheared. The pre-sheared point was indicated here by recording the shear stress at an initial consolidation stress of 9kPa by using the shear cell piston. After the conditioning, consolidation and pre-shearing, shear stresses under decreasing normal stresses of 7, 6, 5, 4 and 3kPa were measured and recorded during the shear cell test runs. A linear yield locus was fitted to the recorded data. From this linear yield locus two semicircles can be generated. The small circle describes the unconfined yield stress (σ_c) and the large one describes the principal consolidating stress (σ_1). Flow Function coefficient ($ffc = \frac{\sigma_1}{\sigma_c}$), cohesion (T1) and angle of internal friction (φ) were also obtained from the shear cell test. Further details on the shear cell measurements are presented in Freeman [48] and Wang et al. [24].

2.3.3.5 Bulk properties: compressibility and permeability tests

Compressibility and permeability are important properties of powders, which can be measured by the FT4 rheometer. After conditioning the powder by the blade, compressibility and permeability were measured as follows:

Compressibility was determined by applying an increasing direct consolidation load by the piston to the conditioned powder and measuring the changes in powder bed height. The vented piston consists of a mesh form surface, which allows air to penetrate through the piston while applying direct normal pressure to the powder bed. Compressibility percentage was measured at increasing consolidation loads of 1-15 kPa.

Permeability was measured as the pressure drop across the powder bed at increasing consolidation loads of 1-15 kPa (applied via the vented piston). A large pressure drop indicates

high bed resistance to flow of air and thus low permeability. Large pressure drops are obtained, according to the Carman-Kozeny (or Ergun) equation for low void space and small particles. Pressure drop is proportional to the inverse third power of porosity in the low porosity range. Thus, small reductions in porosity (and increases in density) will lead to significant pressure loss. Pressure loss is also inversely proportional to the square of the channel diameters (and thus, equivalent particle diameter of the bed).

2.4 Results and discussion

2.4.1 Characterizing binary mixtures

In this study, the binary mixtures were characterized by two dimensionless ratios: size ratio and fraction of components [29]. The size ratio $\alpha = d/D$ (ratio of small to large particle diameter) was used which always has a value smaller than unity ($\alpha \leq 1$); and the mass fraction of larger particles is defined as:

$$\mathfrak{f} = \frac{m_L}{m_L + m_S}, \qquad \text{Eq. 2}$$

where m_L is the mass of large particles (D) and m_S is the mass of small particles (d).

A random close packing (RCP) of equal size spheres is reported [29], [38] to have the packing fraction (volume fraction of solids) of $\Phi_{rcp} \approx 0.64$. However, the close packing fraction of binary mixtures varies with size ratio and the fraction of large particles. For example, at a fixed fraction of large particles, the packing fraction increases with decreasing mixture size ratio ($\alpha \rightarrow 0$). This behavior can be justified by the "infinite asymmetry limit (IAL)" model [29]. This model describes the packing fraction in the large-particle dominant and the small-particle dominant regions. In binary mixtures with high fraction of large particles ($\mathfrak{f} \rightarrow 100\%$), the large particles dominate the packing structure. The IAL model describes the random close packing fraction of binary mixtures of spheres with high fraction of large particles as follows:

$$\Phi = \frac{\Phi_{rcp}}{f} \qquad \text{Eq. 3}$$

Here Φ_{rcp} is the random close packing fraction of mono-sized spheres (≈ 0.64) and f is the fraction of larger particles (see Eq. 2). For a low fraction of large particles, where the small particles dominate the packing, the model leads to:

$$\Phi = \frac{\Phi_{rcp}}{1 - f\,(1 - \Phi_{rcp})} \qquad \text{Eq. 4}$$

In contrast to idealized binary-sphere packings, real powders have distributions in size and shape. In addition, cohesive forces are present (for smaller particles) leading potentially to agglomeration; which is not the case in the large spherical particles (used to develop the mathematical models) [17]. Thus, the goal of this study was to examine binary mixtures of pharmaceutically relevant powders. Studies of powders, together with idealized sphere modeling, are needed to fully understand the characteristics of packed particles.

2.4.2 Classification of binary mixtures

PSDs (Q_3) of all pure materials used in this study are shown in Figure 1. CL and InL have the largest average particle size and SL has the finest particles. Pure materials properties are summarized in Table 1. Span ($= (x_{90} - x_{10)}/x_{50}$) indicates the width of the PSD, i.e., how far the x_{10} and x_{90} deviate from the average particle size (x_{50}). SL has the widest PSD among all the materials.

Table 1. List of material properties. All measurements were done in triplicate.

Materials	CapsuLac60 (CL)	InhaLac70 (InL)	Ascorbic Acid (AA)	SorboLac400 (SL)
x_{10} ± SD [µm]	120 ± 1	147 ± 0	18 ± 0	1 ± 0
x_{50} ± SD [µm]	221 ± 4	227 ± 1	57 ± 1	7 ± 0
x_{90} ± SD [µm]	337 ± 7	301 ± 1	119 ± 1	17 ± 0
Bulk (poured) density BD [g/cm3]	0.59	0.66	0.65	0.41
Tapped density TD [g/cm3]	0.70	0.74	0.91	0.69
Span [-]	0.98	0.68	1.77	2.19
Hausner ratio [-]	1.19	1.12	1.38	1.68
True density [g/cm3]	1.54	1.54	1.69	1.55
Porosity in tapped state [-]	0.54	0.52	0.46	0.56
Sphericity [-]	0.88	0.88	0.90	*
Aspect ratio [-]	0.74	0.74	0.69	*

*QICPIC is not able to measure the sphericity and aspect ratio of very fine particles

Three sets of material mixtures were prepared, always containing CL as the base material. The goal was to analyze in which way the mixture material properties change, if the second

compound has a similar PSD (InL), has smaller particles (AA) or contains much smaller particles (SL). Smaller particles could occupy the interstitial spaces of larger ones, with dimensions in the order of the hydraulic radius (d_{SV} ε/6(1-ε)).

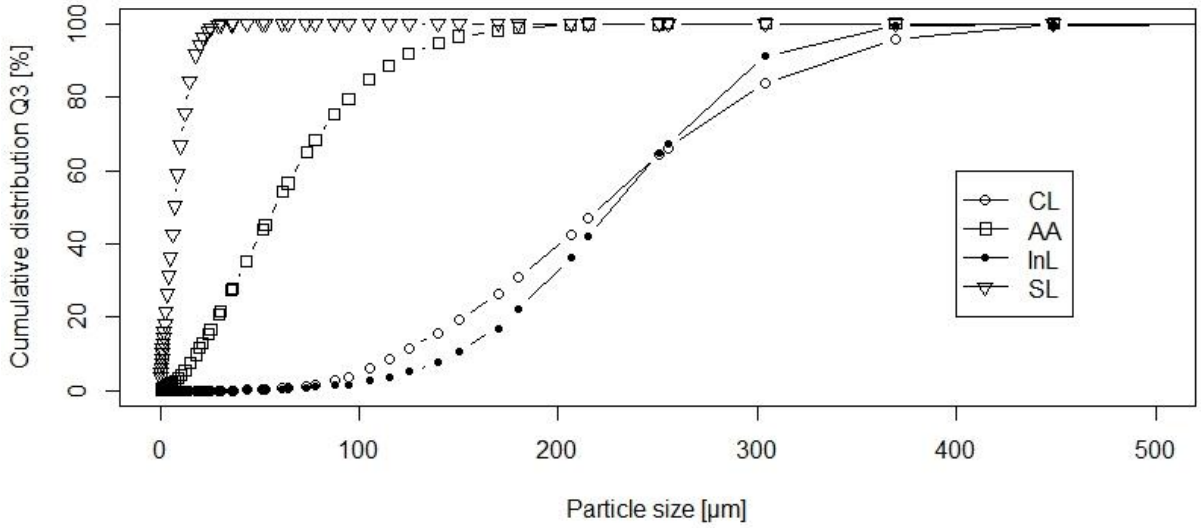

Figure 1. Cumulative distribution Q_3 of materials. SL and AA were measured by Helos. CL and InL were measured by QICPIC. All measurements were done in triplicate (n=3).

A binary mixture with equal-density spheres of diameter D and d with D>>d is being called "non-crowding binary systems" according to Stovall et al. [20]. In such a binary system, either large-particles or small-particles are densely packed (only one component controls the packing arrangement) [20], [49]. In this case, adding either large or small particles does not change the overall packing structure of the mixture. In Figure 2 typical packing arrangements of such binary mixtures are shown. In Figure 2 A and B, the large-particles are densely packed and introducing smaller particles into the mixture, the packing density increases (since the voids are filled with smaller particles, therefore density increases and porosity decreases). However, the overall packing structure remains the same. In Figure 2 C and D, the small-particles are densely packed and by introducing the larger particles they remain densely packed in the entire volume minus that taken up by the larger particles. Larger particles replace many small particles and are surrounded by the smaller ones, therefore density increases and porosity decreases. This mechanism (Figure 2 B and D) is the so-called "filling mechanism" [21], [22]. It happens when the size ratio of d/D is smaller than the "critical ratio of entrance, α_c" of 0.154 (given by McGeary) [21]. This critical ratio ($\alpha_c = \frac{1}{3+\sqrt{12}} = 0.154$) is demonstrated by Descartes [38] as

well. The strong asymmetric particle size allows the small particles to pass through the gaps between the large ones and fill the voids.

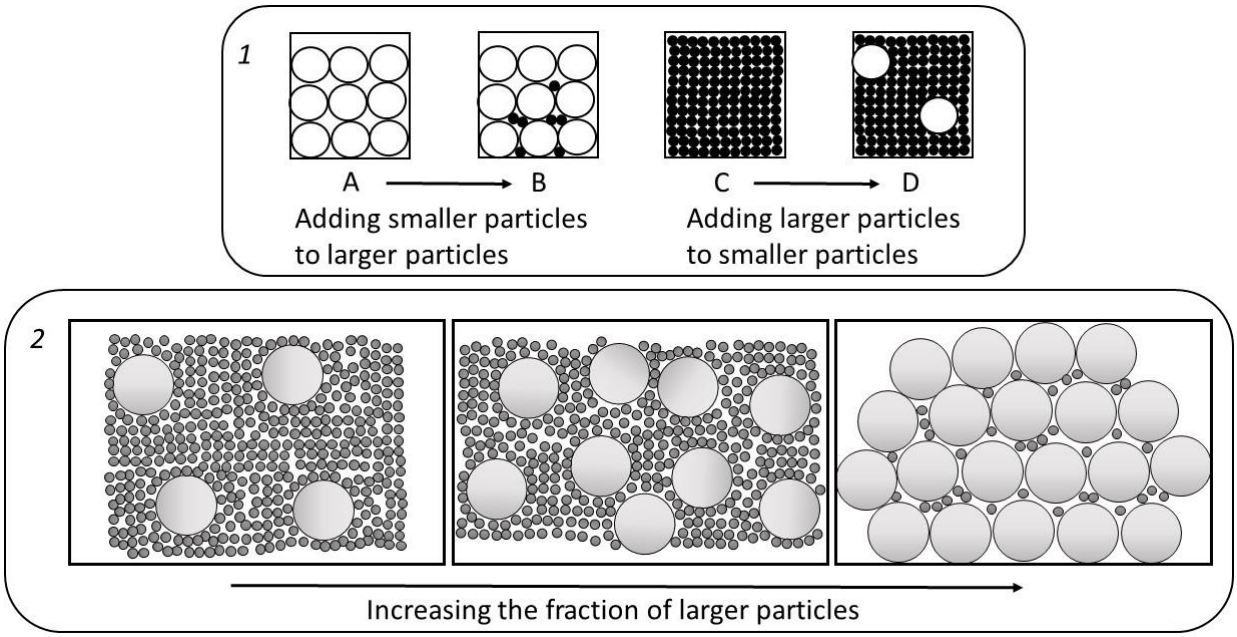

Figure 2. Schematic of typical packing arrangement of particles in "non-crowding" binary mixtures. (1): Adding smaller particles to densely packed large particles (A→B); Adding larger particles to densely packed small particles (C→D). (2): Changing of the packing control: smaller particles define the packing structure of the binary mixture if small particles dominate (left). Larger particles control overall packing structure when large particles dominate (right). In between both particles control the structure (middle).

In binary systems with D>d (called "crowding binary systems" by Stoval et al. [20]), not one component controls the packing arrangement. Unlike the "non-crowding binary systems", adding one of the components changes the packing arrangement of particles. This mechanism is so-called "occupation mechanism" [20]–[22]. The packing density here depends on the fraction of the components in the system (higher fraction of larger particles increase the porosity and decrease the packing density). "Occupation mechanism" happens when the α is smaller than the "critical ratio of replacement, α_r" of 0.741 (given by McGeary) [21]. When $\alpha > \alpha_r = 0.741$, the two size particles can replace each other and result in no change in overall volume and therefore the packing density [21].

Powders with different particle diameter (see Table 1) were selected in this study to obtain binary mixtures with $\alpha < \alpha_c$ (SL:CL), $\alpha_c < \alpha < \alpha_r$ (AA:CL) and $\alpha > \alpha_r$ (InL:CL). PSDs of AA:CL mixtures with different fractions were measured by QICPIC immediately after blending and were calculated according to Eq. 1. with data from the pure materials. Figure 3 shows measured

PSDs of CL and AA with AA:CL fractions of 100:0, 98:2, 95:5, 90:10, 70:30, 50:50, 30:70, 10:90, 5:95, 2:98 and 0:100.

Difference in PSDs between experimentally measured and theoretically calculated ones are rather low. This low difference (<5%) in cumulative distribution, considering the sampling errors, is acceptable, confirming the fact that the powders were well mixed by the chosen mixing procedure. In the case of InL:CL mixtures, the data could not be analyzed in this way since the PSDs are very similar. Moreover, for SL:CL such an analysis could not be performed, since Helos laser diffraction needs to be used, while CL has to be analyzed via the QICPIC. Thus, mixtures cannot be measured due to the wide span. In Figure 4, however, the expected mixture PSD is shown via calculation.

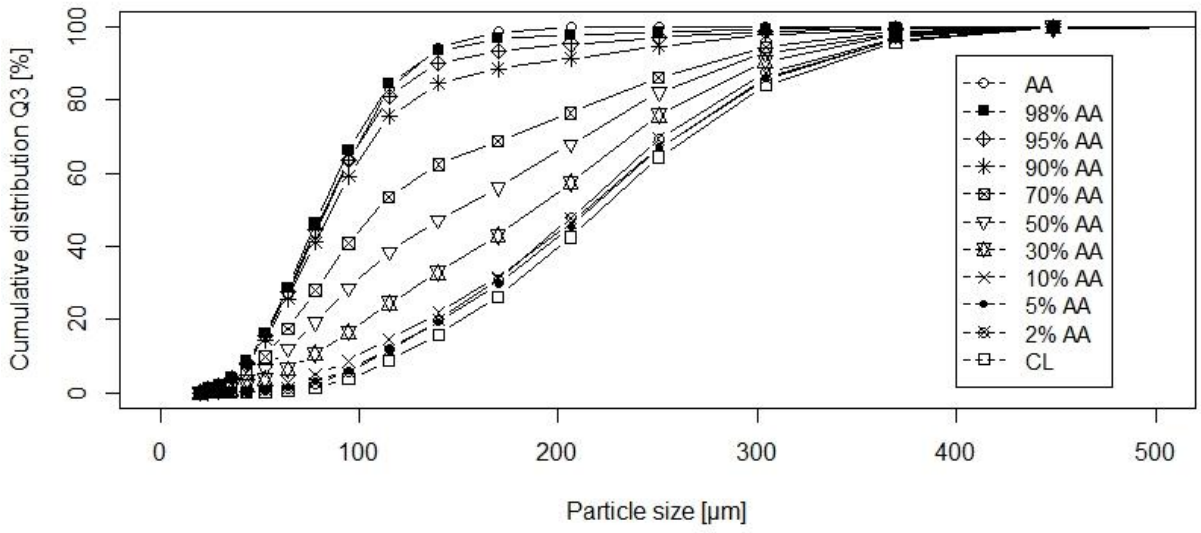

Figure 3. PSDs of AA:CL mixtures, measured by QICPIC.

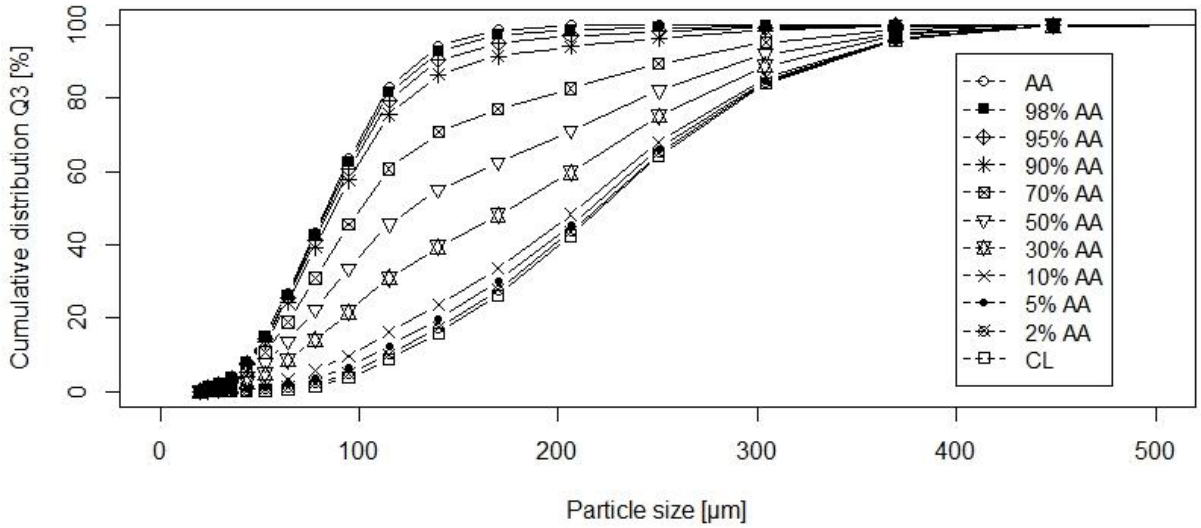

Figure 4. PSDs of AA:CL mixtures, calculated according to Eq. 1.

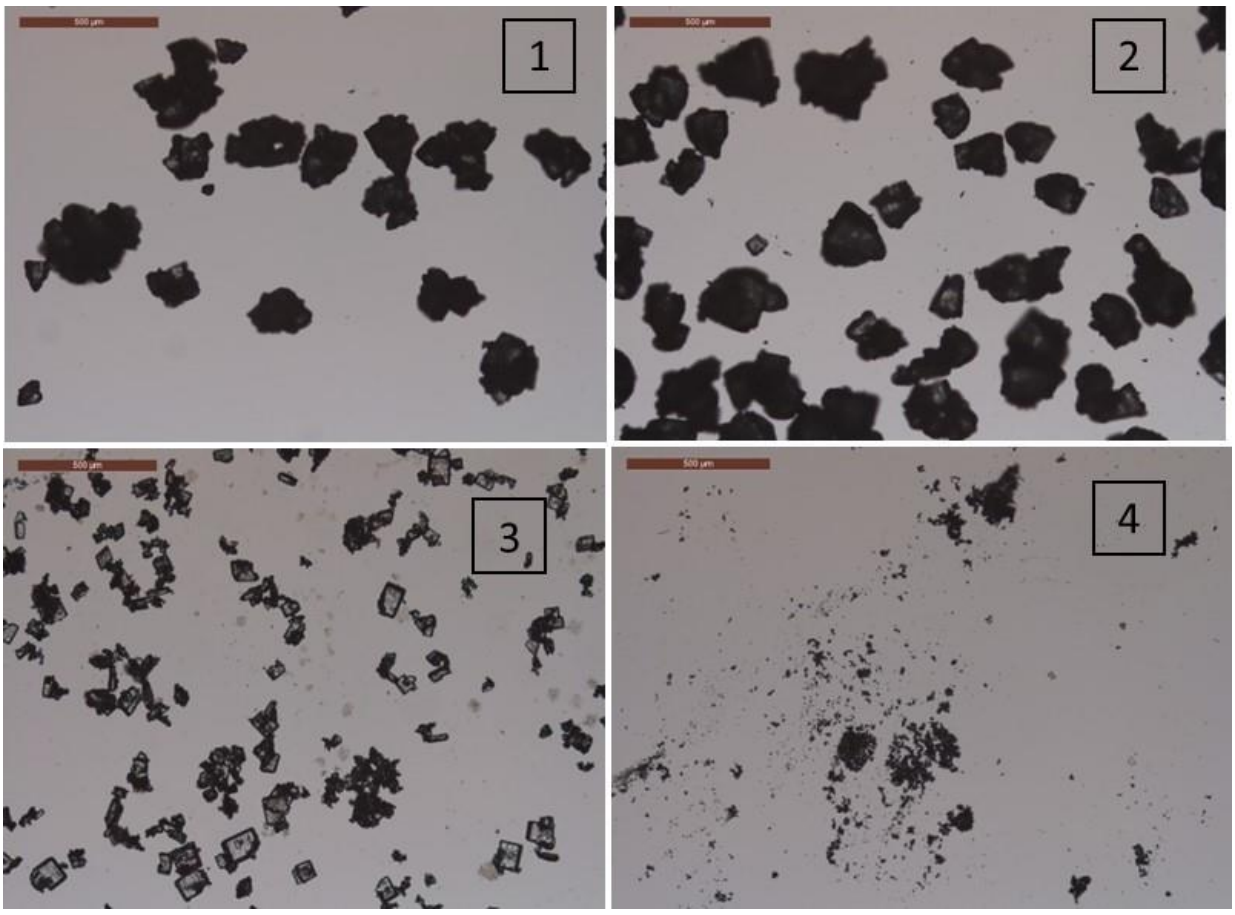

Figure 5. Electron microscope images of the materials; (1) CapsuLac60, (2) Inhalac70, (3) Ascorbic Acid, (4) SorboLac400. A scale bar of 500 µm is shown in the left top corner of each image.

Figure 5 shows electron microscope image of the materials. In addition to particles size, shape of particles is an important factor for mixture packing properties. All three lactose materials are

of irregular shape (SEM pictures provided by the supplier were compared), yet do not take the form of needles, flakes or plates which would lead to significant amounts of interlocking. AA particles are more cubic or prism-like. However for further discussions, considering the sphericity of the materials of > 0.88 (see Table 1), particles of all materials are considered as close-to-spherical particles.

2.4.3 Density dependence on mixture composition

Bulk (poured) and tapped density of all three binary mixtures were measured in triplicate by the PT-TD200 powder density tester. Figure 6 shows the bulk density of the three mixtures as a function of the mass fraction of Capsulac60 (CL) in the mixture. As can be seen, bulk densities of the mixtures are non-linearly related to mass fraction of CL in the mixture. For the mixture with AA (AA:CL), bulk density first increases with increasing CL fraction in the mixture to reach a maximum value of 0.8 g/cm^3 (for the 50:50 mixture) and then decreases. Interestingly, this maximum value is significantly higher than the bulk density values of 100% AA (0.66 g/cm^3) and 100% CL (0.59 g/cm^3).

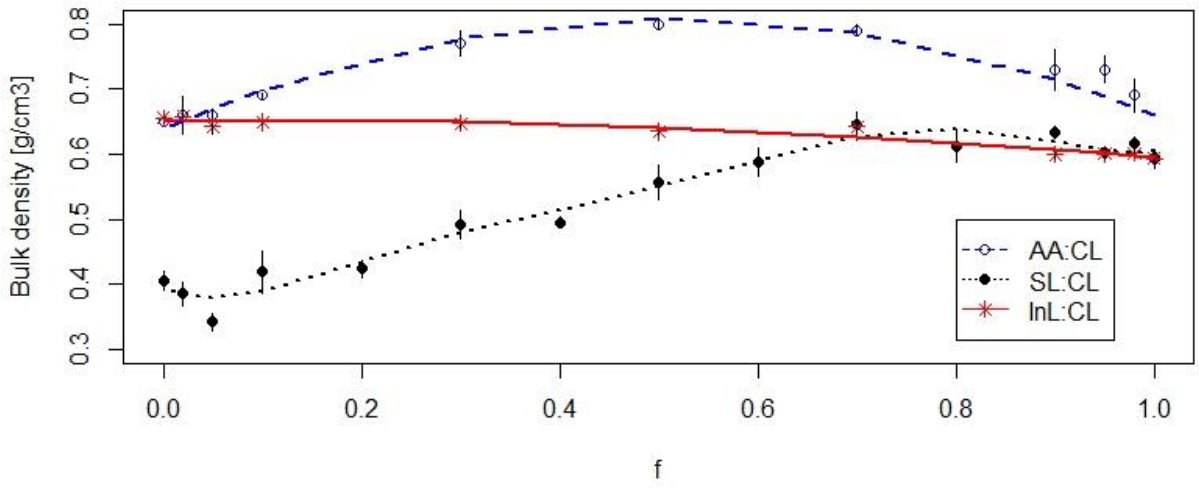

Figure 6. Bulk (poured) density of different mixtures as a function of f (mass fraction of CapsuLac60 (CL) in the binary mixture). Standard deviations of triplicate measurements are shown for each mixture fraction. Y-axis scale range: 0.3-0.8 g/cm^3. Lines are drawn to aid the eye.

For the mixture with the highest size ratio of $d_{50,SL}$:$d_{50,CL}$ = 1:32 , this non-linear relation is even more significant. In this case, the highest BD value is obtained for a 30:70 mixture of SL:CL (0.65 g/cm^3), which is higher than the BD value of pure SL (0.41 g/cm^3) and CL (0.59

g/cm^3). In contrast to the two mixtures with different particle sizes, a (more or less) linear relationship between BD and CL mass fraction is obtained for the InL:CL mixture, as expected.

Figure 7 shows the tapped density (TD) as a function of mass fraction of CL in the mixture. For the SL:CL mixture the highest TD value (0.96 g/cm^3) is obtained for the 30:70. This value is much higher than both pure components TD values. Starting from pure SL (TD=0.69 g/cm^3), TD increases with the CL mass fraction until 70% is reached, and then it decreases to the TD value of pure CL (TD=0.7 g/cm^3). For the AA:CL mixture with size ratio of $d_{50,AA}$:$d_{50,CL}$ = 1:4, the highest TD value (0.93 g/cm^3) occurs again for the 50:50 mixture, which is higher than the tapped densities of the pure materials, i.e., 0.91 g/cm^3 and 0.7 g/cm^3, respectively. For the same-diameter mixture InL:CL, again, there is a linear relation between TD and mixture composition.

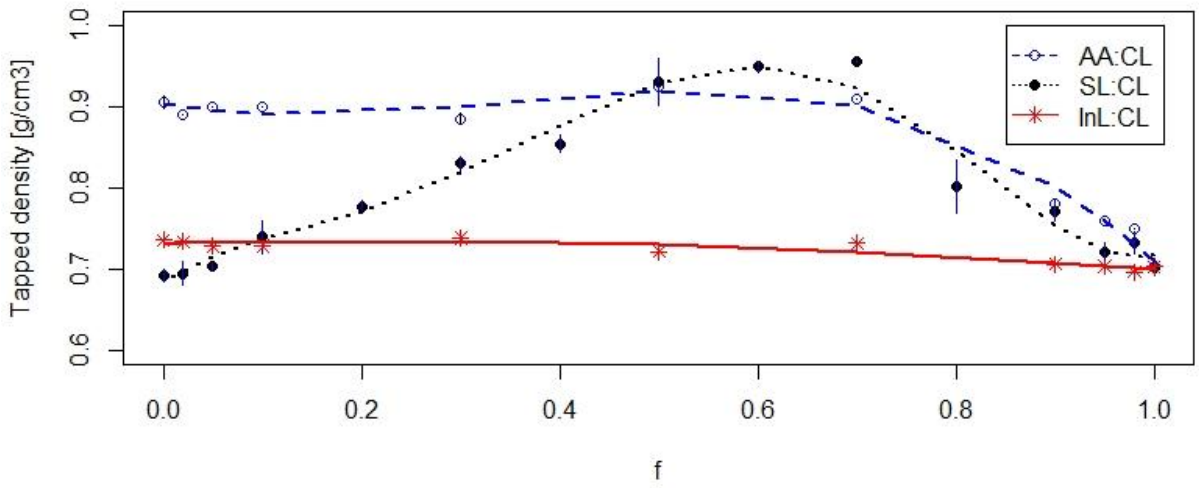

Figure 7. Tapped density of different mixtures as a function of f. Standard deviations of triplicate measurements are shown for each mixture fraction. Y-axis scale range: 0.6-1 g/cm^3. Lines are drawn to aid the eye.

For the discussion of the bulk and tapped density results, we will first discuss the tapped density results in Figure 7, since tapped density is more intuitive and less complex than bulk density (the latter being also strongly influenced by cohesion). The tapped density of the mixture can be explained by understanding the packing structure of the mixtures. After blending the powders and tapping, a random packing in the density tester's glass cylinder can be assumed. According to the theory of random packing [21], when $\alpha < \alpha_c = 0.154$, one of the components takes over control of the overall structure of the packing. A change of the control from one component to the other occurs while changing the fractional solid volume of the components.

This is the so-called “filling mechanism”, where addition of one component does not change the overall structure (i.e., the connective framework) of the other component.

Such a case occurs in the SL:CL mixture with a size ratio of 0.032. In the following discussion we will assume that each mixture consists of more or less spherical particles of the same size (which is only a – not too bad – approximation as shown in Figure 5). Clearly, when a small SL particle is added to a pure SL powder, the density does not change. The same is true for adding a large CL particle to the CL powder. However, when a small particle is added to the large particles, the small particles will occupy the void space between the large particles (filling mechanism). Mass increases; yet volume does not increase. Thus, the density will increase significantly with more small SL particles being added to large CL particles. On the other end of the mixture spectrum, if one large particle is added to many small particles (close to pure SL), the large particle will add mass to the mixture. And also the volume will increase. However, the large particle will not bring with it the same “void” it would occupy if it were placed amongst large particles (porosity of a randomly packed bed of spheres is around 0.37-0.42 [33], [50]). Instead the small particles will occupy the space around the large one. Thus, density will also increase, yet less strongly. The maximum density can be expected when all the voids between the large particles are occupied with small ones. From Table 1, we can see that the porosity (void fraction) of pure CL is approximately 54%. Of course, due to packing restrictions not the whole voidage can be occupied by small particles, and we expect that possibly up to 40-60% of this voidage can be occupied by small particles. Based on this reasoning, we expect a “volcano plot”, with a maximum around 70-80% of CL fraction. Moreover, we expect on both sides of the plot an increase of density from the pure density of the compounds (both being lactose with more or less the same TD of ~0.7 g/cm^3) towards the maximum. For the reasons pointed out above, we expect the increase to be steeper on the right side (pure CL). In fact, this is exactly what is seen in the Figure 7 for the SL:CL mixture.

For the AA:CL mixture with size ratio of 0.258, the size ratio is greater than the “critical ratio of entrance” of 0.154 [21]. It means neither components completely control the packing structure. Both particle collectives interfere with the overall structure of the combination. This so-called “occupation mechanism” happens, when adding a new component does change the skeleton of previous components. Note that AA has a higher true density than CL. Starting with pure AA, if CL particles are added, CL particles require space, yet still the space around the CL particles is occupied by much smaller AA particles. This should lead to an increase in TD. However, CL particles have a lower true density, which decreases the mixture density. Overall, these effects seem to cancel and starting from the left (CL=0%), the density stays constant. At

around 50-60% CL in AA the densest packing structure seems to be reached (maximum TD of ~ 0.93 g/cm^3). Note that this density is more than 30% higher than the density of pure CL and about 15% higher than the density one would obtain when a linear mixture model is assumed. Thus, a volumetric filling method (capsules, dies) would lead to a content uniformity far outside specification.

According to the theory of random packing, when the size ratio of two particle collectives is larger than the "critical ratio of replacement" of 0.741, the overall connective framework of particles does not change [21]. The difference here from the filling mechanism is that the two sized particles can replace each other, resulting in no change in the overall packing structure and the particle connective framework [21].

In contrast, for the InL:CL mixture with a size ratio of 0.97, the composition of the mixture should not affect the overall packing structure [21]. Therefore, there is a linear relation between TD and mixture composition, as can be seen in Figure 7.

The bulk density (also known as poured density) results (see Figure 6) are more complex to interpret since in this case the cohesivity and friction between particles plays a major role. Especially, for small particles which are more affected by cohesion the densities are much smaller than in the tapped (well-packed). Bulk (poured) density is related to both powder properties (PSD, shape, etc.) and cohesive forces between particles, e.g., van der Waals, electrostatic and capillary forces [51].

Even for the large CL particles the bulk density is lower (0.59 g/cm^3) than tapped density (0.7 g/cm^3), leading to a Hausner ratio of 1.19. When small cohesive SL particles are added to the CL particles, again the small particle occupy the interstitial space between the large one. However, since there is significant cohesion, the packing is not as effective and the density does not increase as dramatically (as it does in the tapped case), when the CL fraction is reduced. Thus, the TD increases slightly with decreasing CL fraction (from the right side of Figure 6) and reaches a maximum (again) at around 60-80% CL. When the CL fraction is further decreased, the BD decreases to finally reach the BD of pure SL (left side of Figure 6).

In the case of AA:CL mixture a different situation is obtained: here both particle classes are above a size where Van der Waals forces dominate, and thus, the BD plot resembles the TD features for higher fractions of CL (>40%). A maximum is obtained at around a 50:50 mixture, no filling appears to happening, and the maximum density of the mixture of about 0.8 g/cm^3 is close to the maximum of TD at around 0.92 g/cm^3. Apparently, little energy is required to destroy local arched and frictional structures to achieve a well packed state. In the case of the

SL:CL mixture, the increase of the maximum mixture density is more than 40%, going from BD to TD. Thus, in this case, much more energy is required to destroy structures stabilized by cohesion. This is also underlined by the fact that the maximum TD is obtained with SL:CL mixtures, and the maximum BD with AA: CL mixtures.

For the same-size mixture of InL:CL again a more or less linear dependence on mixture fraction is observed, which is expected since both particle grades have similar size and Hausner ratio.

Hausner ratio and porosity data in the tapped state are summarized for all mixtures in Table 2. Porosity is calculated according to [52]:

$$\varepsilon = 1 - \Phi = 1 - \frac{\rho_{tapped}}{\rho_{true}} \qquad \text{Eq. 5}$$

Pure SL has the highest porosity among all materials. The lowest porosity obtained is 0.43 for the mixture of SL with 70% CL, since much of the voidage is occupied by SL. Interestingly, the porosities in the tapped states are much higher than the ones for tightly packed spherical particles (<0.4). It is well-established that particle shape affects the porosity strongly [31], where porosity increases with decreasing sphericity of particles [31]. Thus, the round (close-to-spherically shaped) particles (see Figure 5) used in this study lead to a much higher porosity, even, in the densest state, likely due to interlocking and wedging.

Table 2. Hausner ratio and porosity in tapped state of all binary mixtures.

AA:CL	Porosity in tapped state [-]	Hausner ratio [-]	**SL:CL**	Porosity in tapped state [-]	Hausner ratio [-]	**InL:CL**	Porosity in tapped state [-]	Hausner ratio [-]
0:100	0.54	1.19	**0:100**	0.54	1.19	**0:100**	0.54	1.19
2:98	0.51	1.09	**2:98**	0.53	1.19	**2:98**	0.55	1.16
5:95	0.51	1.04	**5:95**	0.52	1.20	**5:95**	0.54	1.17
10:90	0.50	1.07	**10:90**	0.51	1.22	**10:90**	0.54	1.18
-	-	-	**20:80**	0.48	1.31	**-**	-	-
30:70	0.43	1.15	**30:70**	0.38	1.48	**30:70**	0.52	1.14
-	-	-	**40:60**	0.38	1.62	**-**	-	-
50:50	0.43	1.16	**50:50**	0.41	1.67	**50:50**	0.53	1.14
-	-	-	**60:40**	0.45	1.72	**-**	-	-
70:30	0.46	1.15	**70:30**	0.47	1.68	**70:30**	0.52	1.14
-	-	-	**80:20**	0.50	1.83	**-**	-	-
90:10	0.46	1.30	**90:10**	0.53	1.76	**90:10**	0.53	1.12
95:5	0.47	1.36	**95:5**	0.55	2.05	**95:5**	0.53	1.13
98:2	0.47	1.35	**98:2**	0.56	1.80	**98:2**	0.52	1.12
100:0	0.46	1.38	**100:0**	0.55	1.68	**100:0**	0.52	1.12

Figure 8 shows the packing fraction (Φ) of the highly asymmetric SL:CL mixture as a function of f (see Eq. 2) compared to the predictions of the IAL model (see Eq. 3 and Eq. 4). Φ_{rcp} is taken as 0.45 (instead of 0.64 for random close packing of equal size spheres), since the packing fraction of both pure CL and SL is 0.45 ($\Phi = \frac{\rho_{\text{tapped}}}{\rho_{\text{true}}}$). In the figure, the points are the experimental data and the solid lines are the theoretical curves for the idealized mixtures of the IAL model (see Eq. 3 and Eq. 4). At low and high f one can see that that our data fits the IAL model very well. At intermediate f there is a deviation between the model and the experimental data. The polydispersity of our materials may explain the deviations from the model at intermediate f.

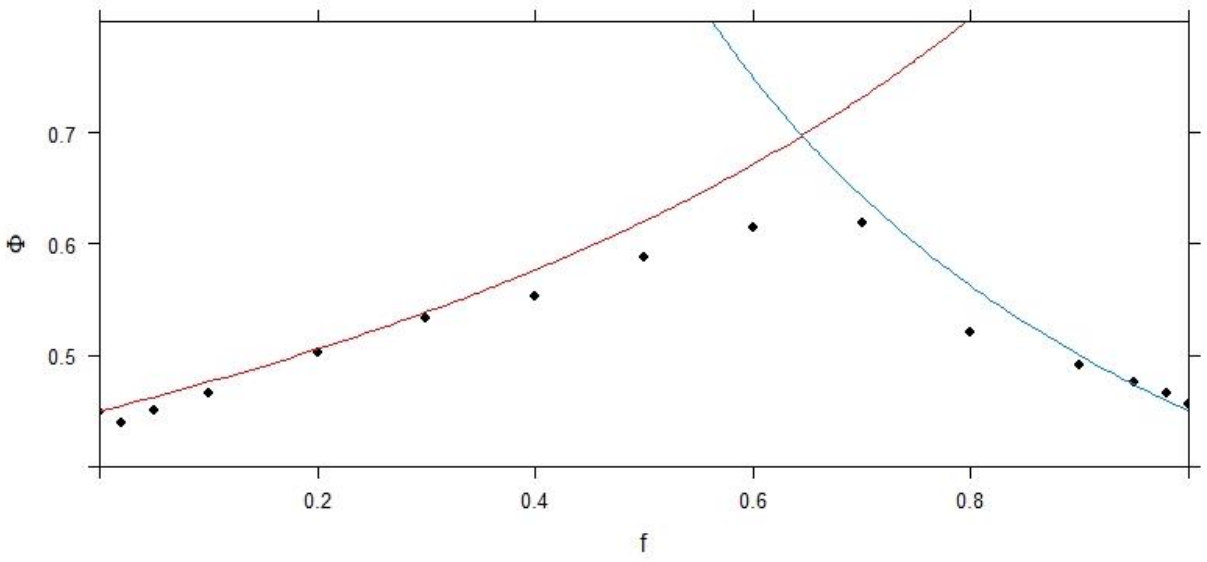

Figure 8. Packing fraction (Φ) of SL:CL mixture as a function of f. The solid lines are the theoretical curves of idealized mixtures (see Eq. 3 and Eq.4).

Hausner ratio HR (i.e., ratio of TD to BD) correlates with the particle size, cohesivity and frictional properties. Lower HRs correlate with lower cohesivity and increase flowability. Despite being criticized as unreliable measure of flowability, HR is widely used in the community to the straightforward way of measuring flowability [53]. Generally, it is assumed that below a HR of 1.18 good flowability is obtained [54]. Data in Table 2 shows that with increasing the fraction of larger particles in the mixtures with smaller particles (i.e., AA:CL and SL:CL), HR decreases. Clearly, with increasing the fraction of larger particles in the mixture, the influence of cohesive force on the powder properties decreases as a function of the particle size. When the average particle size in the mixture decreases, the influence of cohesive forces acting on particles increases as a result of it [51]. The highest HR is thus obtained for the smallest particles.

Agglomeration of cohesive particles has been studied for both the bulk and tapped state of binary mixtures of SL:CL and AA:CL. Since the PSD measurement systems are designed to deagglomerate samples, we studied the possible agglomeration through sieving the samples. After the bulk and tapped density measurement tests, the samples were sieved manually (not via a sieve stack). No significant agglomeration has been observed in the samples.

2.4.4 Permeability and Flowability

FT4 dynamic tests were used for studying the influence of powder composition on powder properties, such as compressibility and permeability. All measurements were done at a minimum in triplicate for each composition of the binary mixtures. Note that after conditioning and applying an initial normal stress (described above) a density is obtained that is between the tapped and bulk (poured) density.

Figure 9 presents the dependence of compressibility (change in volume in %) on the mass fraction of CL for all three binary mixtures when applying a direct consolidation load of 15kPa. As can be seen, the curve is non-linear for the SL:CL mixture. Although there is not a maximum in the compressibility, the curve deviates from a linear interpolation between the two pure materials. Especially, at a CL fraction of 60-80 % the compressibility is significantly higher than a linear mixture model would suggest. Interestingly, this is the mixture with the highest density and lowest porosity. For the AA:CL mixture, the compressibility increases already after adding only 2% CL to AA and then it decreases to the pure CL compressibility value of 5.41%. The correlation between compressibility and CL fraction in the mixture is linear for the InL:CL mixture, which is expected since all other mixture properties of this "same-size" mixture are linear as well.

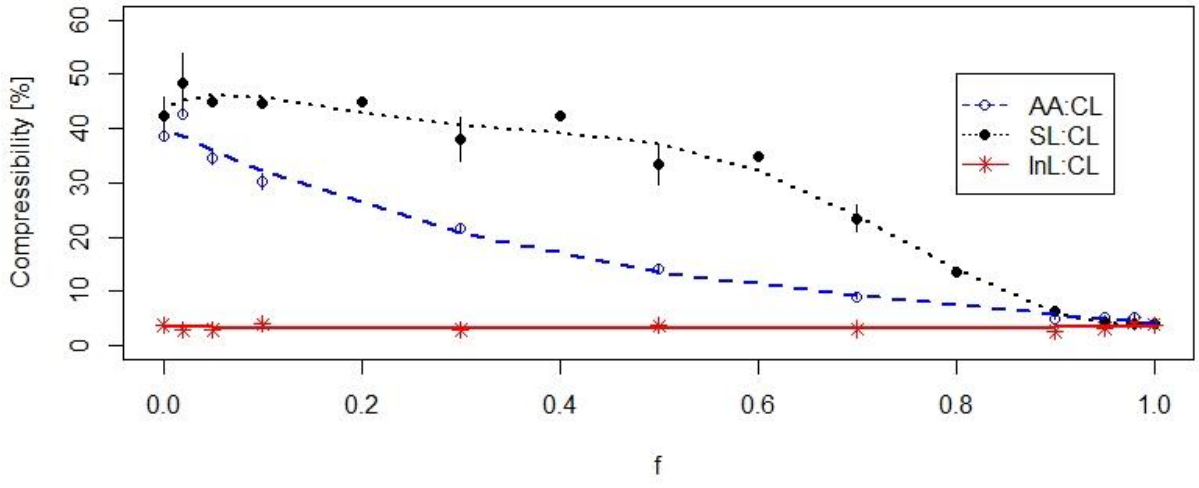

Figure 9. Compressibility of different mixtures as a function of f, at 15KPa. Lines are drawn to aid the eye.

Clearly, there is a relation between porosity in the powder bed and compressibility. For more porous mixtures compressibility is greater, since the applied normal stress leads to rearrangement of particles in the voids of the powder bed.

Figure 10 depicts the pressure drop, ΔP, across the powder bed at 15kPa normal stress as a function of the fraction of larger particles in the mixture. A higher pressure drop indicates a lower permeability of the powder bed. According to the Ergun equation, pressure drop is a strong function of porosity ($\sim 1/\varepsilon^3$) at lower porosities and of particle size ($\sim 1/d_p^2$). Thus, it is expected that the porosity, particle size and permeability correlate.

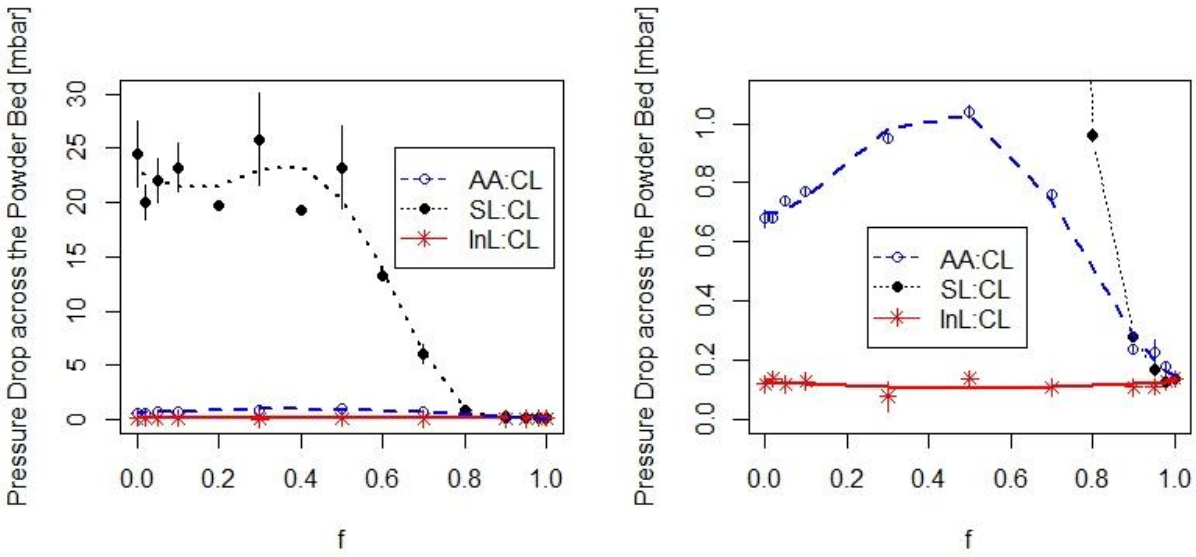

Figure 10. Pressure drop across the powder bed for all three binary mixtures are shown in the left panel. The right panel shows a magnification of the lower part of the plot. Standard deviations of at least triplicate measurements are shown for each mixture fraction. Lines are drawn to aid the eye.

As can be seen in Figure 10, ΔP is significantly larger for the small-particle system (SL:CL) mixture than for the other mixtures. In fact, the maximum pressure loss in the SL:CL mixture is more than 25 times larger than that for the AA:CL mixture and 180 times larger than that for the InL:CL mixture. From these data it is apparent that particle size influences the pressure drop much more strongly than porosity. This is probably due to the fact that porosity never reaches a small enough value to be that significant (porosity >0.4) and thus, the size of channels between the particles is the most important factor. This is underlined by the fact that 70% CL in the mixture has a much higher ΔP than pure CL and the other mixtures. Thus, even at low mass fractions the small particles control the inner structure of the bed (since they occupy the interstitial space as discussed above).

At the maximum the resistance of the powder bed to transmitting air increases to a value of 25.81 mbar (for 70:30 mixture) then it decreases to 0.14 mbar (value for 100% CL).

For the AA:CL mixture a (much lower) maximum ΔP is obtained at about 50% CL with 1.04 mBar. This maximum ΔP coincides also with the maximum for the density (see bulk and tapped densities above) for the 50:50 mixture. Apparently, AA particles are larger and thus, the ΔP is determined by the porosity (or density). Again, for the mixture of InL:CL the correlation is linear.

In summary, the packing structure of the particles (explained above according to theory of random packing) explains the permeability results. The filling mechanisms, occurring in the SL:CL mixtures, leads to filled voids, even at high CL mass fractions. Therefore, the pressure drop increases across the powder bed.

2.4.5 FT4 shear cell measurements

As described above, the FT4 shear cell tests provide information on the cohesivity, the internal angle of friction and the flow function (ffc) of powders. In these tests, slow rotation induces shear. Each shear test is preceded by a pre-shear. Then, the powder bed resists the rotation of the shear head, and the shear stress increases until the bed fails and shears. This shear stress is the called the "point of incipient failure". Each point in the shear vs. normal stress diagram is called the "yield point". A linear yield locus is fitted through these yield points. Cohesion is the intercept of the yield locus with the shear stress τ-axis [24]. The angle of internal friction is the slope of the linearized yield locus. From this linear yield locus two semicircles are generated. The small semi-circle, generated by passing through the origin and tangent to the yield locus, describes the unconfined yield stress (σ_c). The large semi-circle, which is drawn tangent to yield locus and passing through the pre-shear point, describes the principal consolidating stress (σ_1). The flow function coefficient is the ratio of the principal consolidating stress and the unconfined yield stress ($\frac{\sigma_1}{\sigma_c}$) [24].

In the literature it has been shown that the flow function of pharmaceutical powders is predominately governed by cohesion alone, whereas the effect of frictional angles, whether for incipient flow or steady-state flow, is negligible. Flow functions between 1 and 4 are considered to indicate poorly flowing powders. Flow functions above 10 indicate very good flowability.

Cohesivity and ffc data for the three material mixtures, obtained from the FT4 rheometer, are presented in Figure 11 and Figure 12, respectively. As expected, mixtures with lower cohesion have a higher ffc value. SL has the finest particles, and therefore it is the most cohesive and most difficult to flow (ffc=2). Pure CL has very good flowability with a ffc value of above 10. For the SL:CL mixture there is a strong non-linearity observed. Pure CL has good flowability,

yet adding of SL decreases flowability and increases cohesion. With increasing the mass fraction of CL the flowability is decreasing and cohesivity increases. At a 50:50 mixture the poor flowability of SL is reached.

For the AA:CL mixture the situation is similar. Small amounts of AA do not change the flowability (also they do not increase flowability), yet below 95% of CL there is a steady decline of flowability and at approximately a 50:50 mixture an ffc of 4.35 is obtained. Pure AA has somewhat lower ffc of 3.5.

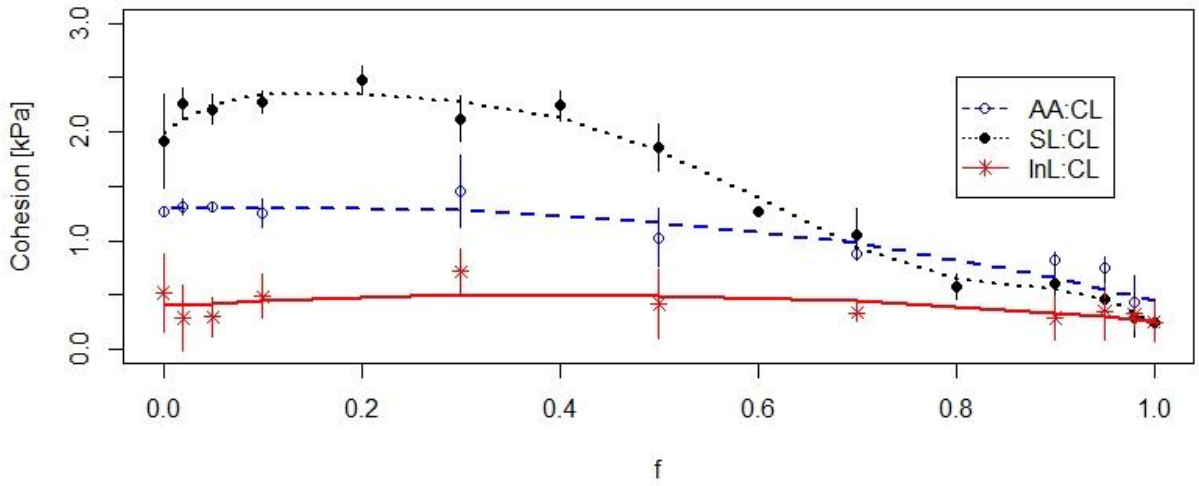

Figure 11. Cohesivity of the three mixtures from the FT4 powder rheometer as a function of f. Standard deviations of triplicate measurements are shown for each mixture fraction. Lines are drawn to aid the eye.

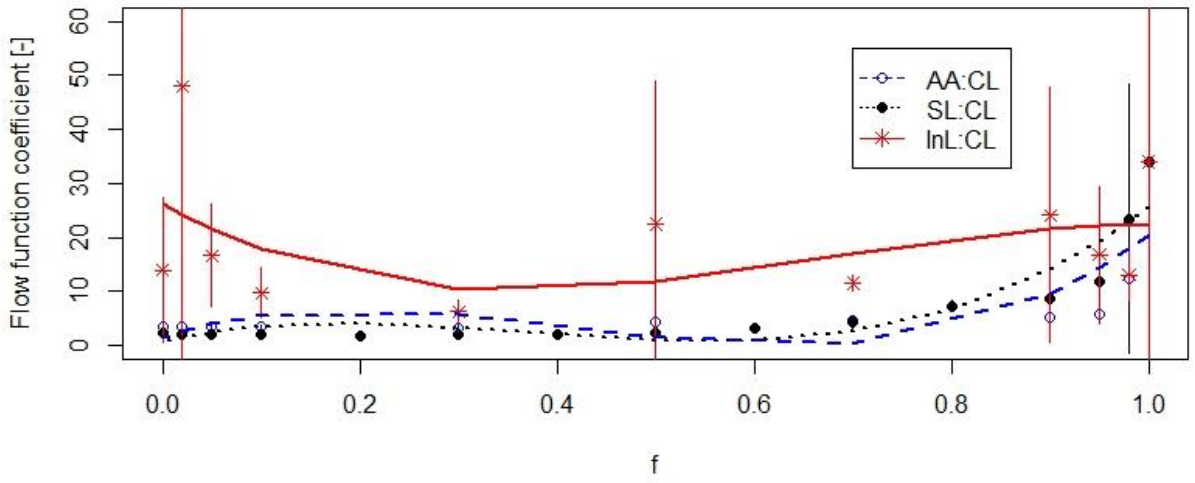

Figure 12. Flow function (ffc) of the three mixtures from the FT4 powder rheometer as a function of f. Standard deviations of triplicate measurements are shown for each mixture's fraction. Lines are drawn to aid the eye.

The ffc values for the same-size InL:CL mixture show high standard deviations compared to the other two binary mixtures (see Figure 12). In both the binary mixtures of SL:CL and AA:CL, the standard deviation increases dramatically by increasing the fraction of CL in the mixture. Since ffc is the ratio of consolidation stress to the unconfined yield strength, it is not a good metric for powders with good flowability. For free flowing powders (powders with larger particle size) unconfined yield strength is zero or nearly zero. Thus, slight variability in the unconfined yield strength may lead to a large variability of ffc [55]. In the large experimental study of Megarry et al., it was shown that powders with bigger particle sizes have a higher variability in the ffc data [56]. In summary, the mixture of InL and CL seems to flow well, with the highest ffc values and the lowest cohesion obtained for mixtures between 10 and 90% CL.

The internal angle of friction data, obtained from the FT4 rheometer, are presented in Figure 13 for the three material mixtures. The data were obtained during measuring cohesion strength with the FT4 rheometer, by creating a plane of failure and measuring the required torque [57]. No significant change in the angle of internal friction is observed for all three binary mixtures. Often, fine materials and those with a wide range of particle sizes are more frictional than coarse materials or powders with a narrow particle size distribution [57]. Certainly, in our case angle of internal friction does not depend on the composition in an apparent non-linear manner.

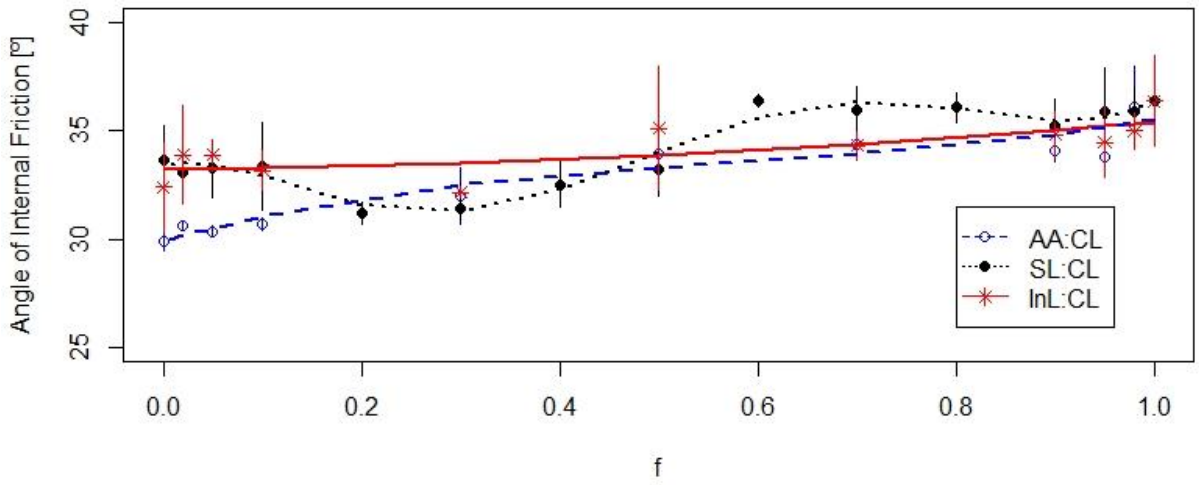

Figure 13. Angle of internal friction of the three mixtures from the FT4 powder rheometer as a function of f. Standard deviation of triplicate measurements are shown for each mixture fraction. Lines are drawn to aid the eye.

2.5 Summary and conclusions

In our work, we investigated the dependence of macroscopic powder properties, including bulk (poured) and tapped density, Hausner ratio, compressibility, permeability, cohesivity and flow function ffc, on the mixture composition of binary powder mixtures from 0-100%. We varied the fraction of large particles for binary mixtures of various size ratios, α. Three classes of binary mixtures with $\alpha < \alpha_c$ (SL:CL), $\alpha_c < \alpha < \alpha_r$ (AA:CL) and $\alpha > \alpha_r$ (InL:CL) were studied. The results are strongly dependent on the size ratio of the binary mixtures and fraction of larger particles. Our results show that there is a smooth linear correlation between macroscopic powder properties for binary mixture of symmetric particle size ($\alpha = 0.97$). However, this simple linear mixture rule does not apply for other binary mixture classes with significantly different size ratios ($\alpha < \alpha_r = 0.741$).

A non-linear non-monotonic dependence of powder properties on composition has been observed for mixtures with size ratios of 1:4 ($\alpha = d/D = 0.258$) and 1:32 ($\alpha = d/D = 0.032$). This behavior can be explained by understanding the random packing structure of the particles. Here, the size ratio of the binary mixtures and fraction of components define the overall packing structure. Bulk and tapped density increase smoothly for the weakly asymmetric binary mixture of AA:CL ($\alpha > \alpha_c$ and $\alpha < \alpha_r$) with increasing the fraction of CL particles (large particles).

The non-linear increase in density is even more significant for the strongly asymmetric binary mixture of SL:CL ($\alpha = 0.032 < \alpha_c = 0.154$). We argue that this non-linear behavior is related to the size ratio and composition dependence of random packing of the particle system. A dramatic increase in bulk and tapped density of both asymmetric binary mixtures was observed for the fractions between 50 and 70 % CL. Thus, these results show that there is a transition from large particles dominating the overall structure to small particles dominating for asymmetric particle sizes ($\alpha < \alpha_r = 0.741$). The maximum bulk and tapped density was observed at the fractions where this transition happens. This is an important result as many powder processing operations are based on volumetric filling or displacement. Quite often excipient particles are large and API particles are smaller, very often with $\alpha < 0.741$. Examples include capsule or die filling during tableting, or the continuous feeding of powders via screw feeders. Since density directly relates to mass in a constant-volume system, changes in density need to be predicted for the design, optimization and control of pharmaceutical manufacturing operations. Considering the non-linear dependence of powder properties on compositions for asymmetric particle sizes ($\alpha < \alpha_r = 0.741$), our results suggest using particle mixtures with $\alpha > \alpha_r$ if stable operation of varying mixtures is needed. This could for example be the case when pharmaceutical ingredients (APIs) are mixed with a carrier and filled into capsules. Capsule filling is a volumetric process and for mixtures with high asymmetry, our results suggest that small changes in the composition could lead to large changes in fill weight due to the large changes in density. Thus, limiting the size ratios of the components in the mixture is a prerequisite for process agility and robustness.

In summary we showed that for particle mixtures with different size, non-linear (non-ideal) mixture rules need to be developed in order to allow for a rational design, optimization, scale-up and control of pharmaceutical manufacturing operations. This is especially relevant in the context of continuous pharmaceutical manufacturing.

2.6 Acknowledgements

RCPE is a K1 COMET Centre within the COMET –Competence Centres for Excellent Technologies programme. The COMET programme is operated by the Austrian Research Promotion Agency (FFG) on behalf of the Federal Ministry for Transport, Innovation and Technology (BMVIT) and the Federal Ministry for Digital and Economic Affairs (BMDW). Our projects are also funded by Land Steiermark and the Styrian Business Development Agency (SFG). Furthermore, we would like to thank Martina Kotzent and Hasan Mahmud Chowdhury for their technical support of the experimental studies presented in this work, as well as Luca Orefice for helpful discussions.

2.7 References

[1] N. Sandler and D. Wilson, "Prediction of granule packing and flow behavior based on particle size and shape analysis," *J. Pharm. Sci.*, vol. 99, no. 2, pp. 958–968, 2010.

[2] W. Grymonpré *et al.*, "Optimizing feed frame design and tableting process parameters to increase die-filling uniformity on a high-speed rotary tablet press," *Int. J. Pharm.*, vol. 548, no. 1, pp. 54–61, 2018.

[3] N. Bostijn *et al.*, "A multivariate approach to predict the volumetric and gravimetric feeding behavior of a low feed rate feeder based on raw material properties," *Int. J. Pharm.*, vol. 557, no. September 2018, pp. 342–353, 2019.

[4] B. Van Snick *et al.*, "Impact of blend properties on die filling during tableting," *Int. J. Pharm.*, vol. 549, no. 1–2, pp. 476–488, 2018.

[5] F. Stauffer *et al.*, "Managing active pharmaceutical ingredient raw material variability during twin-screw blend feeding," *Eur. J. Pharm. Biopharm.*, vol. 135, no. October 2018, pp. 49–60, 2019.

[6] J. Matić, A. Witschnigg, M. Zagler, S. Eder, and J. Khinast, "A novel in silico scale-up approach for hot melt extrusion processes," *Chem. Eng. Sci.*, vol. 204, pp. 257–269, 2019.

[7] B. Van Snick *et al.*, "A multivariate raw material property database to facilitate drug product development and enable in-silico design of pharmaceutical dry powder processes," *Int. J. Pharm.*, vol. 549, no. 1–2, pp. 415–435, 2018.

[8] J. K. Prescott and R. A. Barnum, "On powder flowability," *Pharm. Technol.*, no. October, 2000.

[9] M. Capece, K. R. Silva, D. Sunkara, J. Strong, and P. Gao, "On the relationship of inter-particle cohesiveness and bulk powder behavior: Flowability of pharmaceutical powders," *Int. J. Pharm.*, vol. 511, no. 1, pp. 178–189, Sep. 2016.

[10] L. Y. Leung, C. Mao, I. Srivastava, P. Du, and C.-Y. Yang, "Flow Function of Pharmaceutical Powders Is Predominantly Governed by Cohesion, Not by Friction Coefficients," *J. Pharm. Sci.*, vol. 106, no. 7, pp. 1865–1873, Jul. 2017.

[11] N. Vandewalle, G. Lumay, F. Ludewig, and J. E. Fiscina, "How relative humidity affects random packing experiments," *Phys. Rev. E - Stat. Nonlinear, Soft Matter Phys.*, vol. 85, no. 3, pp. 1–5, 2012.

[12] E. Teunou and J. J. Fitzpatrick, "Effect of relative humidity and temperature on food powder," *J. Food Eng.*, vol. 42, pp. 109–116, 1999.

[13] K. Pingali, R. Mendez, D. Lewis, B. Michniak-Kohn, A. Cuitino, and F. Muzzio, "Mixing order of glidant and lubricant - Influence on powder and tablet properties," *Int. J. Pharm.*, vol. 409, no. 1–2, pp. 269–277, 2011.

[14] A. U. Vanarase, J. G. Osorio, and F. J. Muzzio, "Effects of powder flow properties and shear environment on the performance of continuous mixing of pharmaceutical powders," *Powder Technol.*, vol. 246, pp. 63–72, 2013.

[15] M. S. Escotet-Espinoza *et al.*, "Effect of material properties on the residence time distribution (RTD) characterization of powder blending unit operations. Part II of II: Application of models," *Powder Technol.*, vol. 344, pp. 525–544, 2019.

[16] B. Van Snick *et al.*, "Impact of material properties and process variables on the residence time distribution in twin screw feeding equipment," *Int. J. Pharm.*, vol. 556, no.

December 2018, pp. 200–216, 2019.

[17] R. M. German, *Particle packing characteristics*. Princeton, NJ.

[18] S. VARTHALIS and N. PILPEL, "The action of colloidal silicon dioxide as a glidant for lactose, paracetamol, oxytetracycline and their mixtures," *J. Pharm. Pharmacol.*, vol. 29, no. 1, pp. 37–40, 1977.

[19] S. Jonat, S. Hasenzahl, M. Drechsler, P. Albers, K. G. Wagner, and P. C. Schmidt, "Investigation of compacted hydrophilic and hydrophobic colloidal silicon dioxides as glidants for pharmaceutical excipients," *Powder Technol.*, vol. 141, no. 1–2, pp. 31–43, 2004.

[20] T. Stovall, F. D. E. Larrard, and M. Buil, "Linear Packing density of grain mixtures," vol. 48, pp. 1–12, 1986.

[21] A. B. Yu and N. Standish, "An analytical-parametric theory of the random packing of particles," *Powder Technol.*, vol. 55, no. 3, pp. 171–186, 1988.

[22] A. B. Yu and N. Standish, "Estimation of the Porosity of Particle Mixtures by a Linear-Mixture Packing Model," *Ind. Eng. Chem. Res.*, vol. 30, no. 6, pp. 1372–1385, 1991.

[23] M. C. Leaper, K. Ali, and A. J. Ingham, "Comparing the Dynamic Flow Properties and Compaction Properties of Pharmaceutical Powder Mixtures," *Chem. Eng. Technol.*, vol. 41, no. 1, pp. 102–107, 2018.

[24] Y. Wang, S. Koynov, B. J. Glasser, and F. J. Muzzio, "A method to analyze shear cell data of powders measured under different initial consolidation stresses," *Powder Technol.*, vol. 294, pp. 105–112, 2016.

[25] G. Forte, P. J. Clark, Z. Yan, E. H. Stitt, and M. Marigo, "Using a Freeman FT4 rheometer and Electrical Capacitance Tomography to assess powder blending," *Powder Technol.*, 2018.

[26] W. Yu, K. Muteki, L. Zhang, and G. Kim, "Prediction of bulk powder flow performance using comprehensive particle size and particle shape distributions," *J. Pharm. Sci.*, vol. 100, no. 1, pp. 284–293, 2011.

[27] Z. A. Worku *et al.*, "Modelling and understanding powder flow properties and compactability of selected active pharmaceutical ingredients, excipients and physical mixtures from critical material properties," *Int. J. Pharm.*, vol. 531, no. 1, pp. 191–204, 2017.

[28] L. Meng, P. Lu, and S. Li, "Packing properties of binary mixtures in disordered sphere systems," *Particuology*, vol. 16, pp. 155–166, 2014.

[29] I. Prasad, C. Santangelo, and G. Grason, "Subjamming transition in binary sphere mixtures," *Phys. Rev. E*, vol. 96, no. 5, pp. 1–11, 2017.

[30] R. S. Farr and R. D. Groot, "Close packing density of polydisperse hard spheres," *J. Chem. Phys.*, vol. 131, no. 24, 2009.

[31] A. B. Yu, R. P. Zou, and N. Standish, "Modifying the linear packing model for predicting the porosity of nonspherical particle mixtures," *Ind. Eng. Chem. Res.*, vol. 35, no. 10, pp. 3730–3741, 1996.

[32] J. M. V. Prior, I. Almeida, and J. M. Loureiro, "Prediction of the packing porosity of mixtures of spherical and non-spherical particles with a geometric model," *Powder Technol.*, vol. 249, pp. 482–496, 2013.

[33] N. Ouchiyama and T. Tanaka, "Porosity of a Mass of Solid Particles Having a Range of

Sizes," *Ind. Eng. Chem. Fundam.*, vol. 20, no. 1, pp. 66–71, 1981.

[34] N. Ouchiyama and T. Tanaka, "Porosity Estimation for Random Packings of Spherical Particles," *Ind. Eng. Chem. Fundam.*, vol. 23, no. 4, pp. 490–493, 1984.

[35] R. K. Mcgeary, "Mechanical Packing," *J. Am. Ceram. Soc.*, vol. 58, no. 1931, pp. 513–522, 1955.

[36] A. E. R. Westman and H. R. Hugill, "The Packing of Particles," *J. Am. Ceram. Soc.*, vol. 13, no. 10, pp. 767–779, 1930.

[37] R. K. McGEARY, "Mechanical Packing of Spherical Particles," *J. Am. Ceram. Soc.*, vol. 44, no. 10, pp. 513–522, 1961.

[38] S. Pillitteri, G. Lumay, E. Opsomer, and N. Vandewalle, "From jamming to fast compaction dynamics in granular binary mixtures," *Sci. Rep.*, vol. 9, no. 1, pp. 1–7, 2019.

[39] A. K. H. Kwan, K. W. Chan, and V. Wong, "A 3-parameter particle packing model incorporating the wedging effect," *Powder Technol.*, vol. 237, pp. 172–179, 2013.

[40] S. Varthalis and N. Pilpel, "Anomalies in some properties of powder mixtures," *J. Pharm. Pharmacol.*, vol. 28, no. 5, pp. 415–419, 1976.

[41] M. A. Odeniyi, T. O. Abobarin, and O. A. Itiola, "Compressibility and flow characteristics of binary mixtures of metronidazole with lactose and microcrystalline cellulose," *Farmacia*, vol. 56, no. 6, pp. 625–638, 2008.

[42] M. Alshafiee *et al.*, "A predictive integrated framework based on the radial basis function for the modelling of the flow of pharmaceutical powders," *Int. J. Pharm.*, vol. 568, no. February, p. 118542, 2019.

[43] S. Wang *et al.*, "Novel coprocessed excipients composed of lactose, HPMC, and PVPP for tableting and its application," *Int. J. Pharm.*, vol. 486, no. 1–2, pp. 370–379, 2015.

[44] E. Faulhammer *et al.*, "Low-dose capsule filling of inhalation products: critical material attributes and process parameters," *Int. J. Pharm.*, vol. 473, no. 1–2, pp. 617–626, 2014.

[45] S. Huang *et al.*, "Exploring the effect of PVP on the spherical agglomeration process and micromeritic properties of ascorbic acid," *Powder Technol.*, vol. 342, no. 130, pp. 929–937, 2019.

[46] M. O. Besenhard *et al.*, "Accuracy of micro powder dosing via a vibratory sieve-chute system.," *Eur. J. Pharm. Biopharm.*, vol. 94, pp. 264–272, Jun. 2015.

[47] M. Viana, P. Jouannin, C. Pontier, and D. Chulia, "About pycnometric density measurements," *Talanta*, vol. 57, no. 3, pp. 583–593, 2002.

[48] R. Freeman, "Measuring the flow properties of consolidated, conditioned and aerated powders — A comparative study using a powder rheometer and a rotational shear cell," *Powder Technol.*, vol. 174, no. 1–2, pp. 25–33, May 2007.

[49] J.A. Hersey, "Ordered Mixing: A New Concept in Powder Mixing Practice," vol. 11, pp. 1–4, 1974.

[50] R. F. Benenati and C. B. Brosilow, "Void fraction distribution in beds of spheres," *AIChE J.*, vol. 8, no. 3, pp. 359–361, 1962.

[51] F. Boschini, V. Delaval, K. Traina, N. Vandewalle, and G. Lumay, "Linking flowability and granulometry of lactose powders," *Int. J. Pharm.*, vol. 494, no. 1, pp. 312–320, 2015.

[52] J. M. de Oliveira, N. Andréo Filho, M. Vinícius Chaud, T. Angiolucci, N. Aranha, and A. C. Germano Martins, "Porosity measurement of solid pharmaceutical dosage forms

by gamma-ray transmission," *Appl. Radiat. Isot.*, vol. 68, no. 12, pp. 2223–2228, 2010.

[53] H. Y. Saw, C. E. Davies, A. H. J. Paterson, and J. R. Jones, "Correlation between powder flow properties measured by shear testing and Hausner ratio," *Procedia Eng.*, vol. 102, no. December, pp. 218–225, 2015.

[54] H. Hamilton *et al.*, "HIPing of Pd-doped titanium components : A study of mechanical and corrosion properties properties," *J. Food Sci.*, no. January, 2014.

[55] G. Mehos, "Powder flowability - FFC, FF, ff, and WTF!"

[56] A. J. Megarry, S. M. E. Swainson, R. J. Roberts, and G. K. Reynolds, "A big data approach to pharmaceutical flow properties," *Int. J. Pharm.*, vol. 555, no. November 2018, pp. 337–345, 2019.

[57] J. W. Carson, B. H. Pittenger, and Jenike & Johanson Inc., "Bulk Properties of Powders," *ASM Handb.*, vol. 7, pp. 632–637, 1998.

3 Performance Evaluation of a High-precision Low-dose Powder Feeder

(This chapter is based on the publication Sara Fathollahi, Stephan Sacher, M. Sebastian Escotet-Espinoza, James DiNunzio, Johannes G. Khinast, Performance Evaluation of a High-precision Low-dose Powder Feeder, AAPS PharmSciTech. 2020 Nov 3;21(8):301.)

3.1 Abstract

Highly potent active pharmaceutical ingredients (APIs) and low-dose excipients, or excipients with very low density, are notoriously hard to feed with currently available commercial technology. The micro-feeder system presented in this work is capable of feeding low-dose rates of powders with different particle sizes and flow properties. Two different grades of lactose, di-calcium phosphate, croscarmellose sodium, silicon dioxide, a spray dried intermediate and an active ingredient were studied to vary material properties to test performance of the system. The current micro-feeder system is a volumetric feeder combined with a weighing balance at the outlet that measures feeder output rates. Feeding results are shown as a so-called "displacement-feed factor" curve for each material. Since the powder mass and volume are known in the micro-feeder system, in this work we characterized an observed density variation during processing via a "displacement-feed factor" profile for each of the fed powders. This curve can be later used for calibrating the system to ensure an accurate, constant feed rate and in addition predicting feeding performance for that material at any feed rate. There is a relation between powder properties and feeding performance. Powders with finer particles and higher compressibility show densification during their feeding process. However, powders with larger particles and lower compressibility show both "densification" and "powder bed expansion," which is the manifestation of dilation and elastic recovery of particles during the micro-feeding process. Through the application of the displacement-feed factor it is possible to provide precise feeding accuracy of low-dose materials.

3.2 Introduction

Continuous feeding of small quantities of powder is a challenge in a wide range of processes and industries, including the pharmaceutical industry (1,2). Especially, in the context of continuous manufacturing, continuous feeding of materials is one of most critical unit operations in the entire line. While continuous feeding of fluids is a fairly easy challenge,

creating a constant powder stream is challenging, especially for sticky and cohesive materials. Advantages of continuous manufacturing in terms of reduced footprint, advanced quality and scalability are well known (3,4). In the last years several modular continuous manufacturing implementations have been commercialized by different equipment companies, including GEA, Glatt or Bosch to name a few. In addition, personalized, individualized and small-scale manufacturing is increasingly important, also in the context of translational pharmaceutics.

Common to all continuous manufacturing operations is the need to create continuous powder flows (5–8). While feed rates of kilograms per hour can be attained using standard equipment, low feed rates in the range of grams per hour are difficult to achieve due to the intermittent nature of granular flows from small-scale screw conveyors. Even more problematic is the continuous feeding of cohesive or electrostatic materials, which flow in chunks or agglomerates. However, continuous low-dose feeding is increasingly important for two reasons: First, the pharmaceutical industry is in the process of adopting continuous manufacturing. Second, high-potency active pharmaceutical ingredients (HPAPIs), with doses in the range of milligrams or even micrograms per tablet, are becoming more frequent (9–11). Currently, no reliable equipment exists that can be used for continuous low-dose feeding of powders (12–16). Continuous feeding of fine powder at the low ratios needed for a given formulation is one of the key issues in continuous manufacturing processes (10,17).

Depending on the specific material density, fine powders with a particle size below 50-100 µm experience significant cohesive forces between individual particles (17). Van der Waals forces, electrostatic forces, and capillary forces are predominant in the dispersion of fine powders (17). These forces can lead to agglomeration and adhesion of particles to the walls of feeders (17). However, many APIs are powders with particles in the cohesive range. Thus, especially the continuous feeding of APIs in a continuous manufacturing framework is challenging, if not impossible with current systems. An overview of available micro-feeders and their feeding principle is provided in a previous study (18).

Powders with larger particles and better flow properties are relatively easy to feed by conventional loss-in-weight (LIW) feeders with feed rates in the range of 0.5-100 kg/h (10). However, the precision of such processes must be carefully monitored and feed rate deviations from the set point must be minimized by optimizing the process parameters (10,19). In addition to feed rate fluctuations that occur due to the fact that powder flows are always to a certain degree discrete, feed rate deviations happen in the LIW feeders due to refilling of the feeders (19,20). During refilling, LIW feeders operate in “blind-flight” volumetric mode, although

efforts are made by feeder companies to allow for a “smart refill”, which essentially is a prediction of the feed rate during refilling based on past experience. Of course, the accuracy of a volumetric feeding mode is strongly influenced by the variability of powder packing density (1). Density of powders is a strong function of powder properties, such as particle size distribution, shape, packing properties, of processing history, as well as environmental conditions such as vibration and humidity (1,21). Even batch-to-batch variations in the powder properties may introduce errors in the feeding system.

In this study, we introduce a micro-feeding system based on the volumetric principle combined with external feed rate monitoring by a high-precision balance. This system enables feeding powders with different particle sizes and powder properties for feed rates from below 1 g/h to about 100 g/h. The micro-feeder system contains a cartridge with a moveable piston inside. The feed rate is controlled via the displacement of the piston inside the cartridge. Since the cartridge dimensions and powder mass are known in this system, the feed rate can be adjusted by changing the displacement rate. Moreover, the total amount of powder fed over time is constant and known. The presented work is a follow up from the data presented by Besenhard et al. (22). A more advanced design of the micro-feeder system with a number of improvements compared to the previous one was developed (22). This includes the miniaturization of the system, control of the displacement rate via a controlled precision syringe pump and automated data recording. This work presents a detailed analysis of feeding performance of the novel micro-feeder in relation to the fed material properties.

Specifically, the feeding performance for two different grades of lactose, di-calcium phosphate, croscarmellose sodium, silicon dioxide, a model API and a spray dried intermediate (SDI) were tested. The first three powders are common excipients and silicon dioxide (a flow aid) is reported to be difficult to feed due to its low density and strong electrostatic behaviour (10). The API is low density crystalline material with poor flow characteristics. The SDI was selected for its cohesive and low bulk density characteristics which is representative of other SDI materials. Using these materials, this study aimed to characterize and assess the performance of the micro-feeder system.

3.3 Materials and methods

3.3.1 Materials

Two α-lactose-monohydrate excipients (CapsuLac60 and GranuLac200 from Meggle, Germany), di-calcium phosphate (dibasic calcium phosphate, Sigma-Aldrich, UK), croscarmellose sodium (sodium carboxymethylcellulose, Sigma-Aldrich, UK), Silicon dioxide

(CAB-O-SIL M-5P fumed silica, Cabot Switzerland GmbH, Switzerland), one active pharmaceutical ingredient, API A and one spray dried intermediate, SDI B (both provided by Merck & Co., Inc., Kenilworth, NJ, USA, known as MSD outside of the United States of America and Canada) were used in this study.

3.3.2 Micro-feeder system

The micro-feeder system presented in this study is based on advanced "volumetric" feeding principle, as shown in Figure 1. The micro-feeder contains a highly polished metal cartridge (using polishing "paper 420"), into which the powder is filled, with a moveable Teflon piston, a linear actuator and a scraper. Speed of the piston in the cartridge can be exactly controlled by the linear actuator via a syringe pump. Displacement of the piston in the cartridge replaces the powder from the cartridge in an exact way (volumetric filling principle).

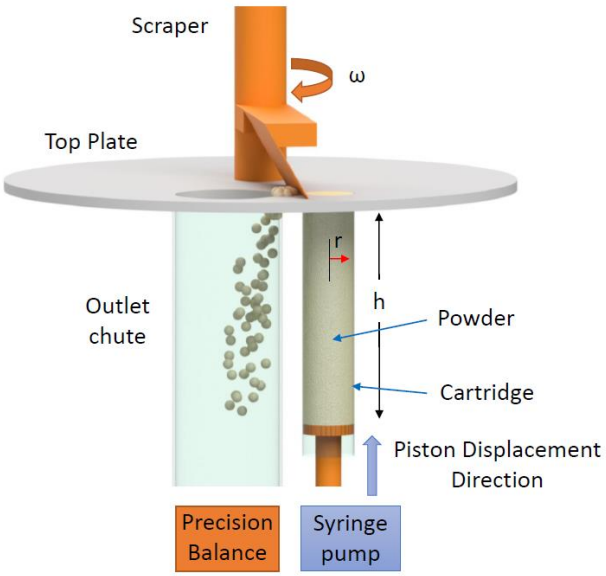

Figure 1. Principle of the micro-feeder system.

Since the total amount of powder in the cartridge, the cross-sectional area of the tube, and the piston displacement speed are known, the volumetric displacement rate over the process is constantly monitored and, in conjunction with a density value, can be used to calculate the mass flow rate. However, because density variations of the packed material occur, the instantaneous mass flow rate varies accordingly. Density variations can occur due to two effects: first, uneven distribution of the powder during filling and preparation of the cartridge. And second, due to a local densification during feeding caused by wall friction. Thus, the critical success factor for using such a device in routine manufacturing is to design the filling procedure in a way that density variations along the cartridge axis are minimized. Moreover, wall friction should be

kept low in order to reduce "in-process densification". Alternatively, weight loss over time can be monitored (i.e., "loss-in-weight principle") to control the piston speed. This, however, can be avoided with appropriate design of the micro-feeder.

As shown in Figure 1, in addition to the motor-controlled piston and the cartridge the system consists of a top plate with two openings. The first opening is for the cartridge powder to exit the cartridge. The second one is a hole for the powder to fall into a chute from which it is fed to the process. A scraper pushes powder from the first opening into the hole. Thus, periodically, exiting powder is transferred to the feeding chute. An anti-static kit integrated in the system can be used to prevent scattering or sticking of the powder material during the transfer process onto the balance.

In the present study a cartridge with the following dimensions was used: r = 11.5 mm, h = 100 mm. Clearly, longer/shorter and wider cartridges may be used, depending on the intended filling task.

In summary, this novel feeding system relies on four main principles:

- Volume at the bottom is continuously and constantly displaced
- Initial density in the cartridges is as constant as possible
- In-process densification is kept to a minimum by reducing wall friction
- The average feed rate is always known each second and the actual feed rate will not surpass a certain percentage threshold, which is guaranteed by the first three arguments

3.3.3 Experimental setup and detailed analysis of feeding process

In our experimental setup powder exits the cartridge on the top (due to piston displacement) and is removed by a scraper by pushing the powder into an opening in the top plate. By gravity it falls through a hole into the chute and then further on a precise balance (Mettler Toledo, XPE204, 0-220 g). For all experiments shown in this work, the accumulated powder mass was recorded every second automatically using "BalanceLink" software (Mettler Toledo, version 4.1.3). Feed rates were determined once per second and converted to g/h from the generated data ($\dot{m}_f = \Delta m/\Delta t$). Due to the periodic scraper action, powder falling through the chute onto the balance fluctuates, the average feed rate per one (1) minute was used for further analysis.

Displacement of the piston at the bottom of the cartridge within one minute (ΔV) and the accumulation of mass at the scale (relating to powder exiting at the top) within one minute (Δm) are known. Volumetric displacement at the top of the cartridge is not known precisely, although it will be similar (yet not necessarily identical) to ΔV. We thus define a property calls "effective

displacement density" as $\frac{\Delta m}{\Delta V}$, which is a good approximation of the actual bulk density of the powder at the exit. We normalized it by the tapped density ρ_T and call it "relative effective displacement density", ρ_{ED}^*. Thus,

$$\rho_{ED}^* = \frac{\Delta m}{\Delta V\, \rho_T} \qquad \text{Eq. 1}$$

3.3.4 Micro-feeding process

In order to try and maintain a constant mass flow rate, the volumetric displacement feeding unit requires a pre-conditioning of material to reduce the powder density variation along the cartridge's axis. The poured bulk density of materials (ρ_B) is a function of the filling procedure, powder particle packing property and wall friction effect. It also changes during manipulation and thus will change during feeding since particles will rearrange, leading to a densification during feeding. Without pre-conditioning, four process phases exist in the presented micro-feeder:

1. Starting phase: A lag time is observed due to compaction of the powder by piston displacement and wall friction. The duration depends on the bulk density after the filling process and the powder state.
2. Increasing feed rate: The feed rate increases until the powder is compacted to a "saturated volume" in the cartridge due to the frictional effects.
3. Stable feed rate: The feed rate stays constant. This period can be used for steady process feeding.
4. Process end: The feed rate drops, when the powder in the cartridge is depleted.

In order to avoid densification during the feeding process (i.e., steps 1 and 2), a pre-conditioning procedure was developed. During pre-conditioning the powder is densified to the tapped density to achieve saturated density faster.

3.3.5 **Pre-conditioning**

The pre-conditioning procedure consists of the following steps: After pouring powder in the cartridge, finger tapping (strokes by the side), and refilling of powder is performed as long as densification can be observed. This step helps powder particles to pack more effectively. Subsequently, by closing the upper/open part of the cartridge by a plate (lid) and raising the piston for a defined distance (h_0, see Eq. 2) the powder is compacted until the tapped density is achieved. Since powder mass in the cartridge (m) and cartridge volume (V_c) are known, the

tapped density of the material (value is known from powder characterization, see below) is achieved by compression. The piston displacement for reducing the volume of the powder mass in the cartridge (the defined distance of h_0) is calculated as:

$$h_0 = \frac{(M-m)\,h}{M} \qquad \text{Eq. 2}$$

Where, h is the cartridge height (in this study h = 100 mm) and M is the mass of powder that could be filled in the cartridge at tapped density ($M = V_c\ \rho_T$). After removing the lid on top and before starting the micro-feeding process, the powder that spills out on the top is removed and recorded. This is a small amount only that can be neglected for further analysis.

During the feeding process the piston displacement in the cartridge pushes the powder upwards. The feed rate is controlled by the piston speed. The piston speed set point is calculated based on the amount of powder in the cartridge after pre-conditioning and the desired feed rate. The piston's displacement rate (mm/min) is controlled by the syringe pump, leading to a constant volumetric displacement.

The micro-feeder device was tested using powders with different particle sizes and properties to assess the range of industrial applicability. Feeding performance, reproducibility and impact of various critical process parameters (e.g., syringe pump speed and scraper angular speed) were studied. After pre-conditioning, feeding consistency was tested for three fixed feed-rate set points of 5, 10 and 15 g/h. Each feed-rate set point was adjusted by a fixed piston displacement speed, which was calculated from the initial density in the cartridge and the desired feed rate. For all materials, the lowest possible displacement speed of 0.1 mm/min was tested. Due to the low density of silicon dioxide, feed rates of 1.5 and 2.5 g/h – calculated from the density and volumetric displacement – were studied. All experiments were performed in triplicate.

The scraper pushes the powder periodically to the vertical chute. The scraper speed defines the time interval of powder falling on the balance. For all experiments done in this study, the scraper speed was set to 10 rpm (which equals one rotation every 6 seconds) and the material amount discharged to the "process" is recorded in a 1 second interval. Constant set-up and parameters (except displacement) were used for all feeding experiments. Pre-conditioning (finger tapping and pre-compaction to achieve the material tapped density) was done for all test runs.

3.3.6 Material characterization

3.3.6.1 Particle Size distributions

HELOS/KR (OASIS/L dry dispersing system Sympatec, Clausthal-Zellerfeld, Germany) was used to measure the particle size distributions of materials. HELOS is a laser light diffraction technique that is capable of measuring particle size range of 0.45 µm to 875 µm. All measurements were done in triplicate.

3.3.6.2 Powder density measurement

Pharmatest PT-TD200, a standardized method described in the United States Pharmacopeia (USP 2011, h616i), was used to measure the bulk (poured) and tapped density of materials. The bulk density (ρ_B, g/cm^3) was measured by pouring powder in a standard 250 mL cylinder. After mechanically tapping the powder, the tapped density was determined (ρ_T, g/cm^3). Hausner ratio ($\boldsymbol{H_R = \rho_T/\rho_B}$), the ratio of the tapped to the bulk density, is a common parameter, to indicate the flowability of powders (23). All measurements were done in triplicate to determine powder density.

3.3.6.3 FT4 powder rheometer

A FT4 powder rheometer system (Freeman Technology, Tewkesbury, UK) was used to measure the wall friction angle at 15 kPa stress. The standard wall friction test procedure was applied using the 25 mm diameter FT4 glass vessel. A stainless-steel disc with a roughness of 0.28 µm was used for this measurement, in order to represent the highly polished stainless-steel cartridge of the micro-feeder.

Furthermore, the FT4 powder rheometer system was used in this study to measure the elastic behaviour of materials. The elastic behaviour is measured by recording the powder bed height while undergoing direct uniaxial, vertical compression of 15 kPa, followed by unloading. This compression method is mentioned in the literature as "quasi-static testing" method (24). In this test, the bed height was recorded at the beginning (powder bed height at zero-pressure, L_0), starting from both the poured and tapped state. Then a direct pressure of 15kPa was applied to the powder bed and the height was recorded (powder bed height at-pressure, L_1). The difference between the powder bed height at zero-pressure and at the applied pressure (in percentage) is the compressibility of powder at 15 kPa. After removing the load, the powder bed height was recorded once again (L_2). These data provide useful information on the elastic behaviour of the powder bed.

Powder bed height data of the materials were measured starting from poured powder state and tapped state. ΔL % at 15 kPa pressure is also termed compressibility at 15 kPa. This is a common measurement for compressibility and is reported in many studies (25–28). However, it is not reported how the powder bed expands after removing the pressure (i.e., compressibility after removing the 15 kPa pressure). The "difference between compressibility at-pressure and after removing it" is defined as the elastic recovery of powders. This value defines the powder bed height expansion (in percentage) after removing the direct pressure, i.e., the elastic recovery.

3.4 Results and discussion

Materials with different particle sizes and properties were used to represent a wide range of powder properties. For example, CapsuLac60 (d_{50} = 244 µm) and GranuLac200 (d_{50} = 31 µm), both being α-lactose-monohydrate excipients, were used to represent opposite material behaviour in terms of flowability (free flowing vs. cohesive). GranuLac200 with a $\boldsymbol{H_R}$ greater than 1.22 (23) exhibits poor flowability. In contrast, CapsuLac60 has good flowability ($\boldsymbol{H_R}$ = 1.10). Lactose is a common filler for tableting and capsule filling in pharmaceutical industry. Di-calcium phosphate (d_{50} = 184 µm) and croscarmellose sodium (d_{50} = 43 µm) are common excipients in pharmaceutical formulations for tableting. Silicon dioxide (d_{50} = 20 µm) is a multifunctional excipient for pharmaceutical solid dose manufacturing. It is commonly used as an anti-caking and anti-blocking agent, spray aid, carrier, thickening and stabilization agent.

In Figure 2, all four process phases (described above) can be seen during feeding of di-calcium phosphate without pre-conditioning (i.e., filled close to the poured density ρ_B). For all materials in this section, pre-conditioning was done prior to feeding process. The detailed information on pre-conditioning is summarized in Table I.

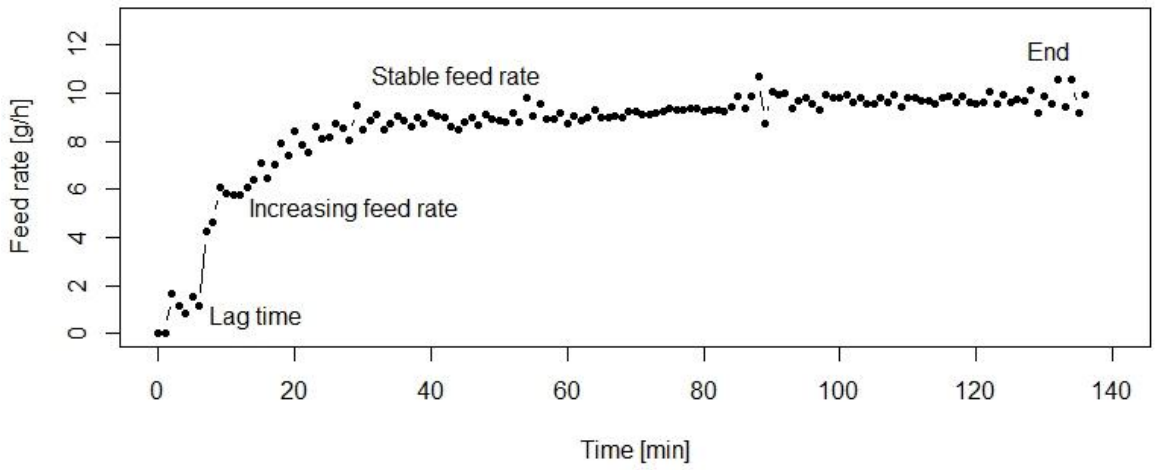

Figure 2. Feeding process without pre-conditioning step. Material: Di-calcium phosphate; feed rate of 10 g/h (displacement speed: 0.46 mm/min).

Table I. Detailed pre-conditioning information for all used materials. ± Represents one standard deviation (n = 3).

Materials	**CapsuLac60**	**Di-calcium phosphate**	**Croscarmellose sodium**	**GranuLac200**	**Silicon dioxide**
Bulk (poured) density ρ_B [g/cm³]	0.68 ± 0.00	0.70 ± 0.00	0.51 ± 0.00	0.52 ± 0.00	0.04 ± 0.00
Tapped density ρ_T [g/cm³]	0.75 ± 0.00	0.87 ± 0.00	0.77 ± 0.00	0.93 ± 0.00	0.05 ± 0.00
Powder density after finger tapping and refilling [g/cm³]	0.67 ± 0.01	0.82 ± 0.01	0.69 ± 0.01	0.55 ± 0.01	0.04 ± 0.00
Powder in the cartridge [g] *	27.85 ± 0.63	33.90 ± 0.42	28.56 ± 0.35	26.69 ± 0.40	1.55 ± 0.04
**h_0 [mm]	10.61 ± 2.01	6.47 ± 1.17	10.23 ± 1.09	41.27 ± 1.04	23.94 ± 2.08
Powder spill after pre-conditioning [g]	0.18 ± 0.06 (0.6%)	0.22 ± 0.07 (0.6%)	0.45 ± 0.23 (1.6%)	0.26 ± 0.04 (1%)	0.03 ± 0.03 (1.9%)
Powder density in the cartridge before starting the feeding process [g/cm³]	0.75 ± 0.00	0.87 ± 0.00	0.73 ± 0.00 ***	0.93 ± 0.00	0.05 ± 0.00

*after finger tapping and refilling; **calculated from Equation 2; *** For croscarmellose only a density of 0.73 g/cm³ could be achieved in the cartridge.

Figure 3 shows an overview of the feeding performance for the five different materials. For better visibility, reproducibility (defined as the repeatability of the feeding curves for a particular displacement condition) is only shown for the lowest and highest feed rates in Figure 3. Note that the duration of feeding of silicon dioxide is shorter than other materials due to the very low density of silicon dioxide (0.04 g/cm^3). Powder properties of materials (before feeding process) are summarized in Table II.

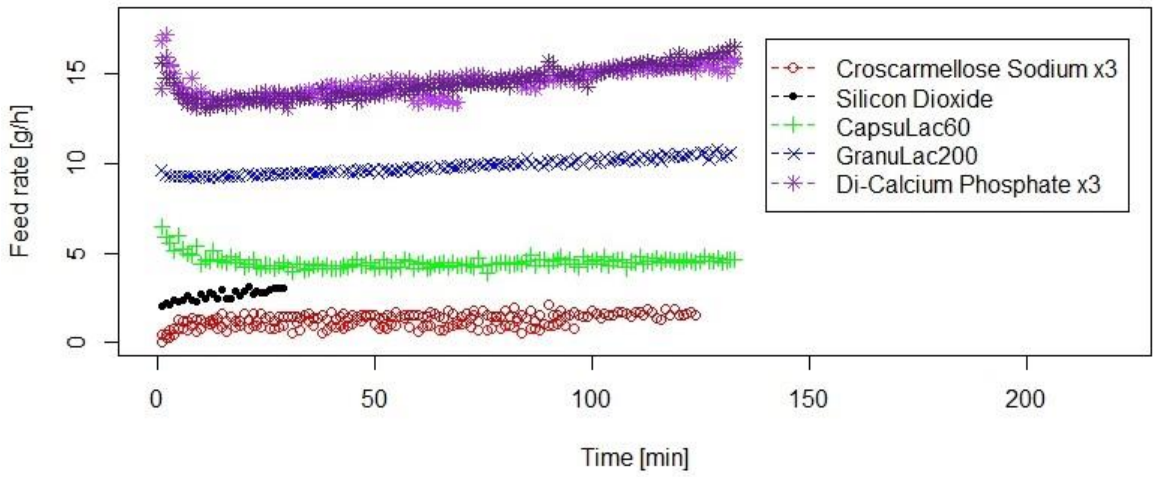

Figure 3. Overview of feeding experiments in the micro-feeder. Feed rate of 2.5 g/h for Silicon dioxide, 5 g/h for CapsuLac60 and 10 g/h for GranuLac200 are shown. All triplicate test runs (TR) are shown for croscarmellose sodium (feed rate of 1.5 g/h) and di-calcium phosphate (feed rate of 15 g/h). Short feeding duration for silicon dioxide is due to very low bulk density of this powder.

Table II. Powder properties of investigated materials (before feeding process). ± Represents 1 standard deviation (n = 3).

Materials	**CapsuLac60**	**Di-calcium phosphate**	**Croscarmellose sodium**	**GranuLac200**	**Silicon dioxide**
X10 [µm]	121.5 ± 5	14.6 ± 1	19.5 ± 0	4.7 ± 0	7.6 ± 0
X50 [µm]	243.7 ± 6	184.4 ± 5	43.4 ± 0	30.5 ± 0	20.2 ± 0
X90 [µm]	426.6 ± 30	314.5 ± 3	119.5 ± 2	102.2 ± 0	75.2 ± 1
Hausner ratio ($\boldsymbol{H_R}$)	1.10	1.24	1.51	1.79	1.25
Wall friction angle [°]	25.28 ± 0.83	25.58 ± 0.17	28.79 ± 0.94	28.90 ± 0.44	*

*SiO_2 showed difficulties during FT4 rheometer system (Freeman Technology, Malvern, UK) measurements

From Figure 3, different conclusions can be drawn: First, feeding performance is highly reproducible for a given powder. Second, feed rates between 1.5 g/h and 15 g/h can be obtained. Third, for a constant piston speed the feed rate deviations do not exceed 10-20% for the total course of feeding. Lastly, the characteristics (shape) of the feed rate versus time curve is sensitive to powder properties. Di-calcium phosphate and CapsuLac60 (similar properties, see Table II and Table III) have higher feed rates at the beginning, followed by a decrease, and later, an increase, suggesting an initial expansion of the powder bed, followed by densification. However, for GranuLac200 and croscarmellose sodium, feed rate increases continuously, suggesting a continuous densification during feeding. Silicon dioxide behaves similarly.

Table III. A summary of the powder bed height data starting from powder poured state (parameters were used to define the elastic behaviour of materials). Experiments were done in triplicate.

Materials	**L_0 [mm]**	**L_1 [mm]**	**L_2 [mm]**	**Compressibility at 15 kPa Pressure $(L_0-L_1)/ L_0$ [%]**	**Compressibility after removing the pressure $(L_0-L_2)/ L_0$ [%]**	**Difference between at pressure and after removing the pressure* [%]**
CapsuLac60	19.03 ± 0.03	18.30 ± 0.10	18.53 ± 0.09	4	3	32
Di-calcium phosphate	19.03 ± 0.01	18.34 ± 0.06	18.56 ± 0.06	4	2	32
GranuLac200	19.08 ± 0.02	11.89 ± 0.20	12.03 ± 0.20	38	37	2
Croscarmellose sodium	19.06 ± 0.03	17.26 ± 0.08	17.56 ± 0.07	9	8	17

L_0 : powder bed height at zero-pressure , L_1 : powder bed height at pressure, L_2 : powder bed height after removing the load

*Elastic recovery of powder bed, $[(L_2-L_1)/(L_0-L_1)]$

Powder bed height data of the materials are summarized in Table III and Table IV, respectively, starting from the poured powder state and tapped state. As can be seen CapsuLac60 and di-calcium phosphate show some compressibility for the poured initial state. GranuLac200 had significant compressibility and croscarmellose sodium had a compressibility of 9%. Elastic recovery was moderate in all cases. This is interesting since the materials with high compressibility greatly densified upon pressure without significant elastic recovery, i.e.,

internal structure was modified and internal voids were irreversibly destroyed due to rearrangement and shear. For the tapped density states, small compressibility was observed, with some elastic recovery which in relative terms was between 40 and 50%. For silicon dioxide FT4 measurements could not be performed (no data are available for this powder in both Table III and Table IV).

Table IV. A summary of the powder bed height data starting from powder tapped state (parameters were used to define the elastic behaviour of materials). Experiments were done in triplicate.

Materials	**L_0 [mm]**	**L_1 [mm]**	**L_2 [mm]**	**Compressibility at 15kPa Pressure $(L_0-L_1)/ L_0$ [%]**	**Compressibility after removing the pressure $(L_0-L_2)/ L_0$ [%]**	**Difference between at pressure and after removing the pressure* [%]**
CapsuLac60	19.50 ± 0.06	19.08 ± 0.06	19.28 ± 0.05	2	1	49
Di-calcium phosphate	19.78 ± 0.19	19.21 ± 0.10	19.47 ± 0.15	3	2	46
GranuLac200	19.68 ± 0.16	19.11 ± 0.07	19.33 ± 0.05	3	2	40
Croscarmellose sodium	19.95 ± 0.08	19.27 ± 0.09	19.56 ± 0.05	3	2	43

L_0 : powder bed height at zero-pressure , L_1 : powder bed height at pressure, L_2 : powder bed height after removing the load

*Elastic recovery of powder bed, $[(L_2-L_1)/(L_0-L_1)]$

3.4.1 Detailed analysis of feeding experiments

In this section the feeding performance of powders with different powder properties is discussed. Feed rates and "relative effective displacement density, ρ_{ED}^* ", for both GranuLac200 and croscarmellose sodium are shown in Figure 4A and Figure 4B, respectively, for various feed rates. Different displacement speeds (given in brackets) were used to obtain the feed rate. For a better comparison, the feed rate and effective displaced density are plotted versus displacement instead of time, since feed rates with slower displacement speed of 0.1 mm/min take a much longer time.

A

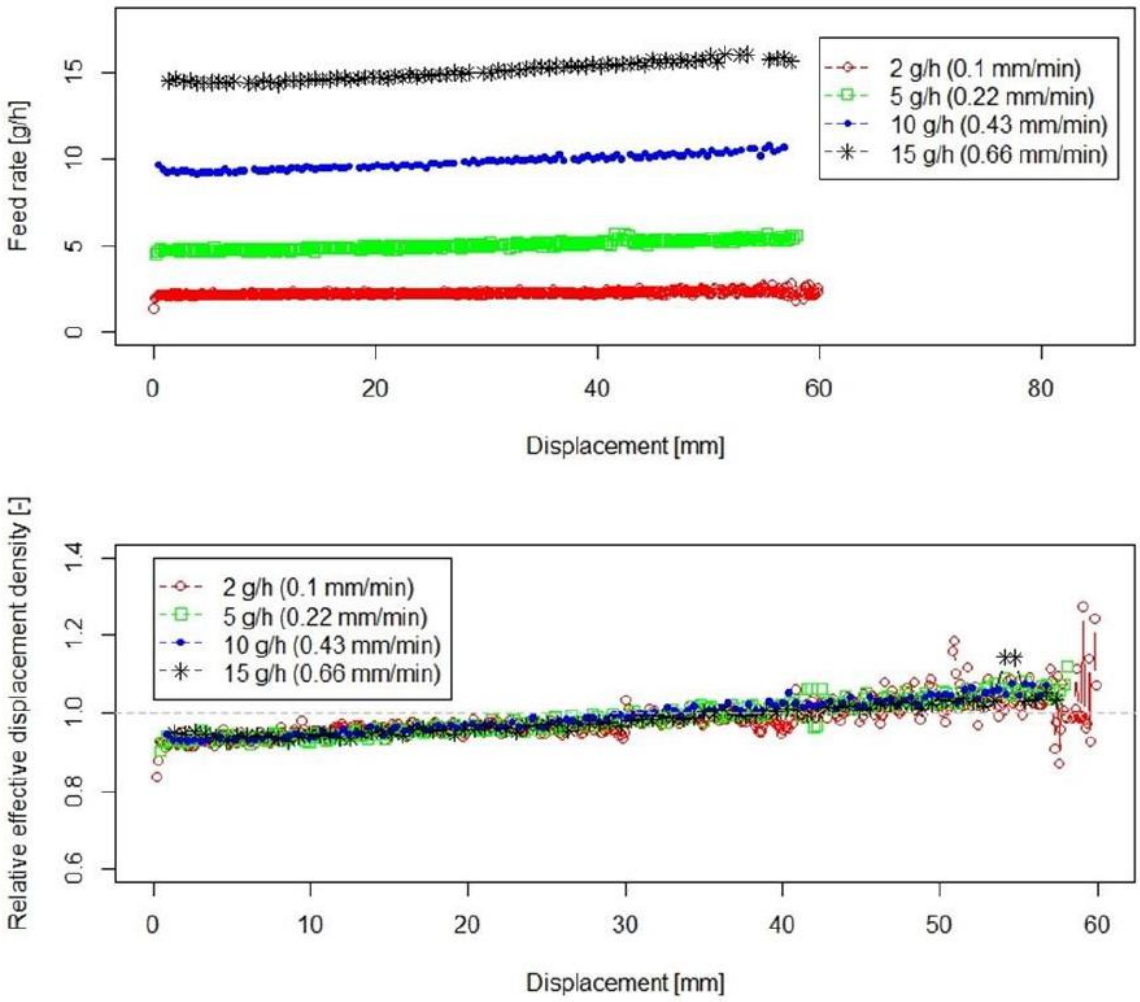
Feed rate [g/h]
0
5
10
15
0
20
40
60
80
Displacement [mm]
2 g/h (0.1 mm/min)
5 g/h (0.22 mm/min)
10 g/h (0.43 mm/min)
15 g/h (0.66 mm/min)
Relative effective displacement density [-]
0.6
0.8
1.0
1.2
1.4
0
10
20
30
40
50
60
Displacement [mm]
2 g/h (0.1 mm/min)
5 g/h (0.22 mm/min)
10 g/h (0.43 mm/min)
15 g/h (0.66 mm/min)

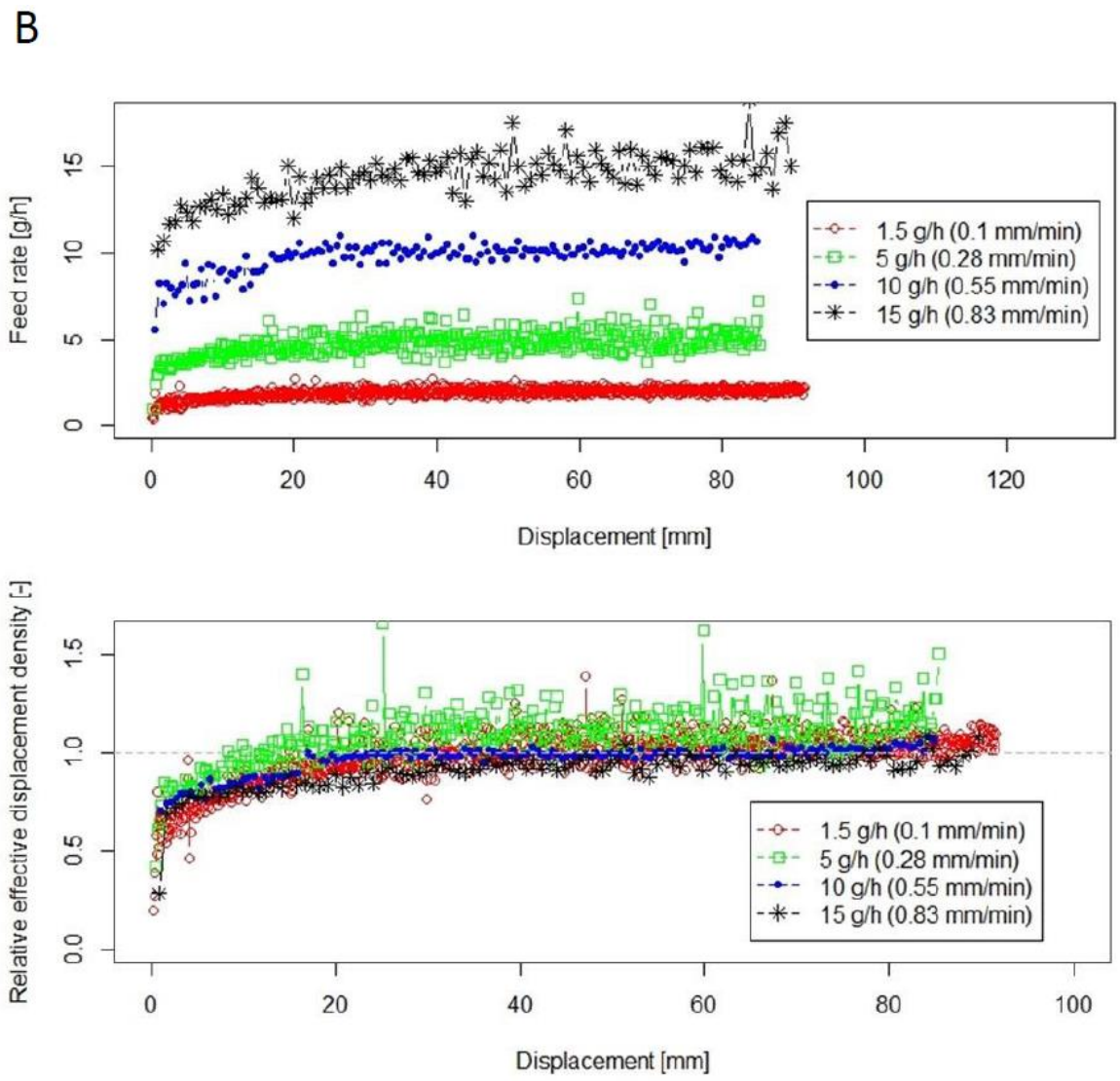

Figure 4. Feeding of GranuLac200 (A) and croscarmellose sodium (B) at different feed rates. Feed rate (upper plot) and relative effective displacement density (lower plot) during the feeding process versus displacement. The "relative effective displacement density" data are shifted to origins (h_0, pre-conditioning compaction range of 41.27 ± 1.04 mm for GranuLac200 and 10.23 ± 1.09 mm for croscarmellose sodium). Displacement speed is given in brackets for each feed rate.

A

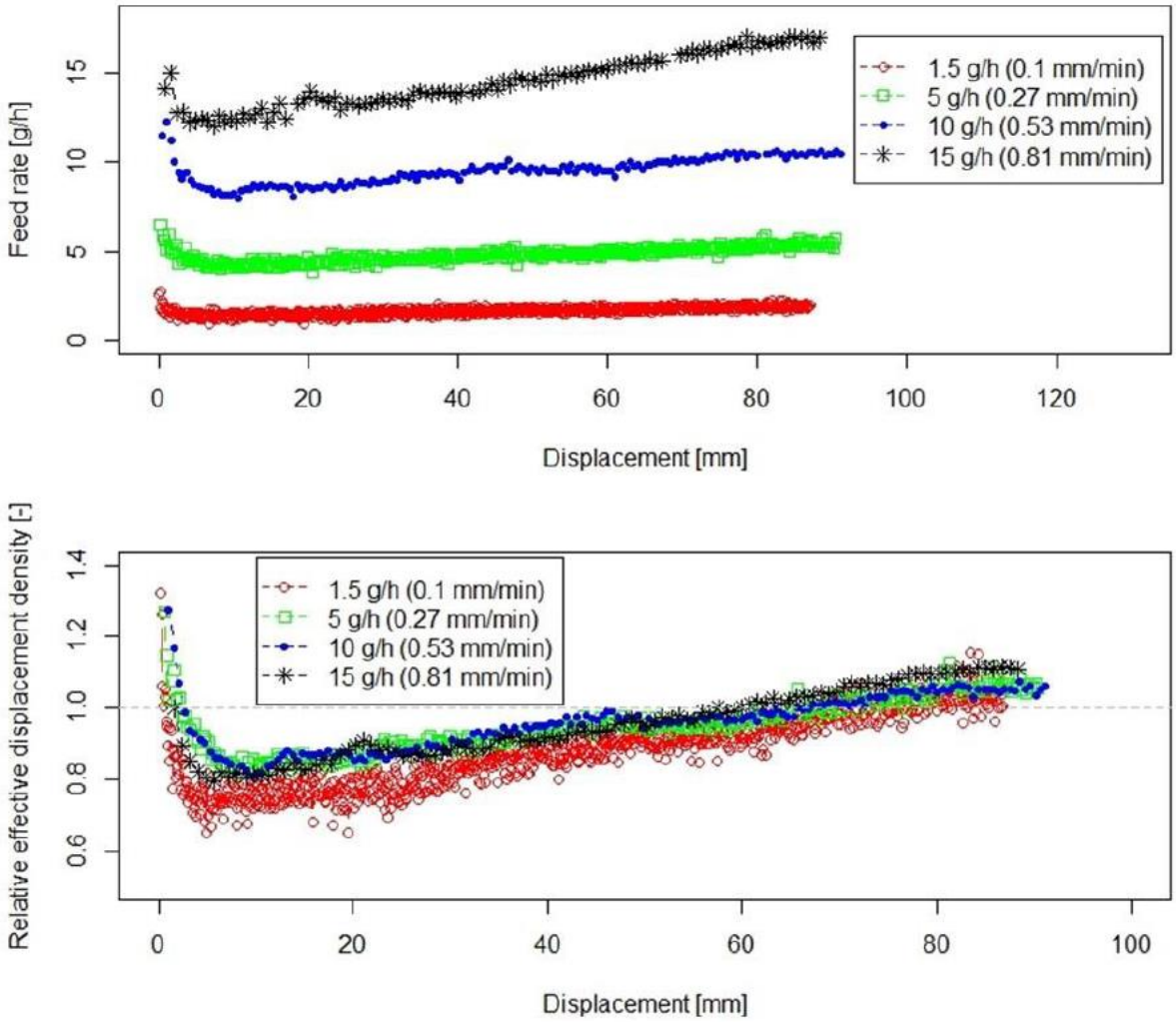
Feed rate [g/h]
0
5
10
15
0
20
40
60
80
100
120
Displacement [mm]
1.5 g/h (0.1 mm/min)
5 g/h (0.27 mm/min)
10 g/h (0.53 mm/min)
15 g/h (0.81 mm/min)

Relative effective displacement density [-]
0.6
0.8
1.0
1.2
1.4
0
20
40
60
80
100
Displacement [mm]
1.5 g/h (0.1 mm/min)
5 g/h (0.27 mm/min)
10 g/h (0.53 mm/min)
15 g/h (0.81 mm/min)

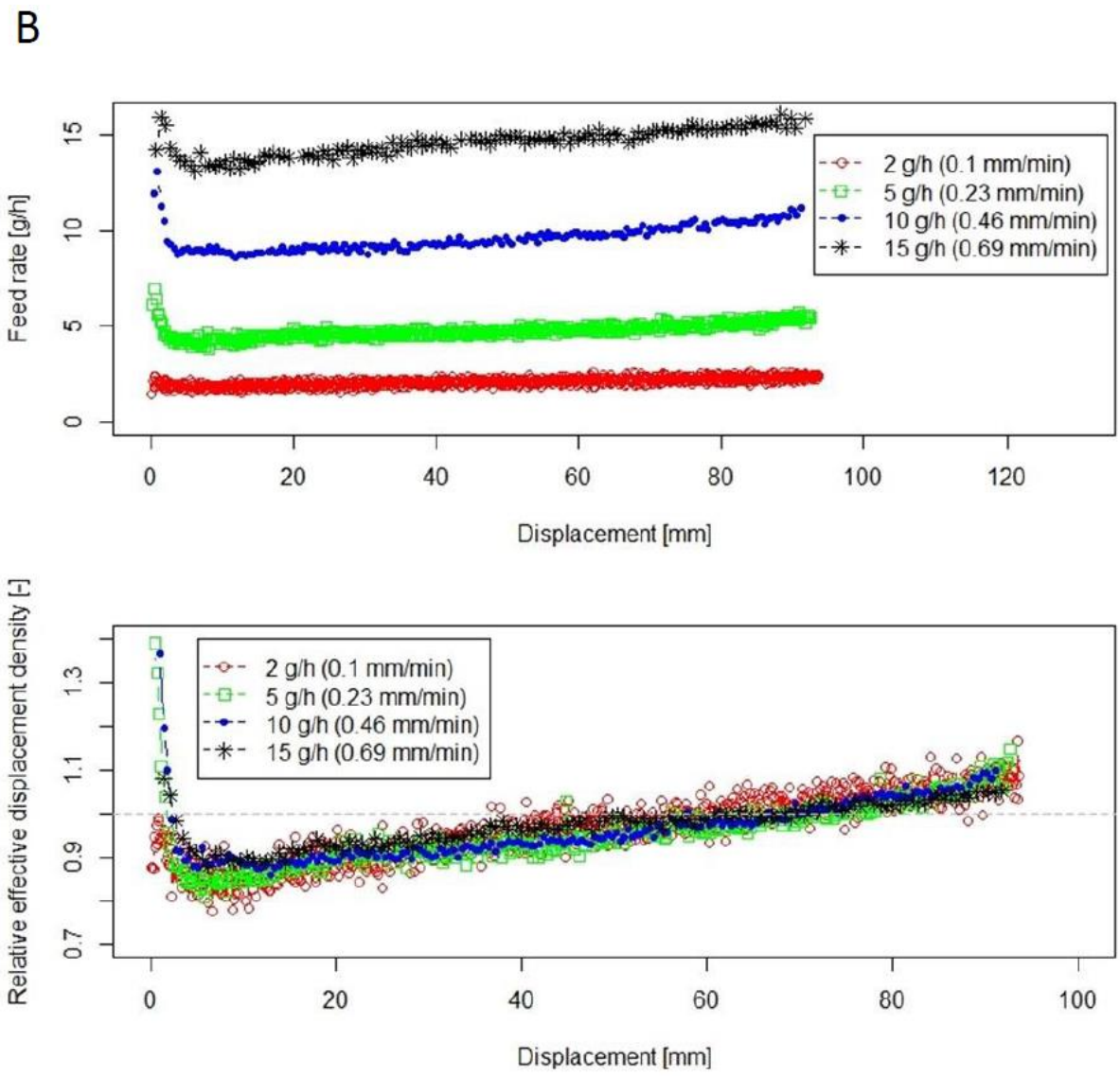

Figure 5. Feeding of CapsuLac60 (A) and di-calcium phosphate (B) at different feed rates. Feed rate (upper plot) and relative effective displacement density (lower plot) during feeding process versus displacement. The relative effective displacement density data are shifted to origins (h_0, pre-conditioning compaction range of 10.61 ± 2.01 mm for CapsuLac60 and 6.47 ± 1.17 mm for di-calcium phosphate). Displacement speed is given in brackets for each feed rate.

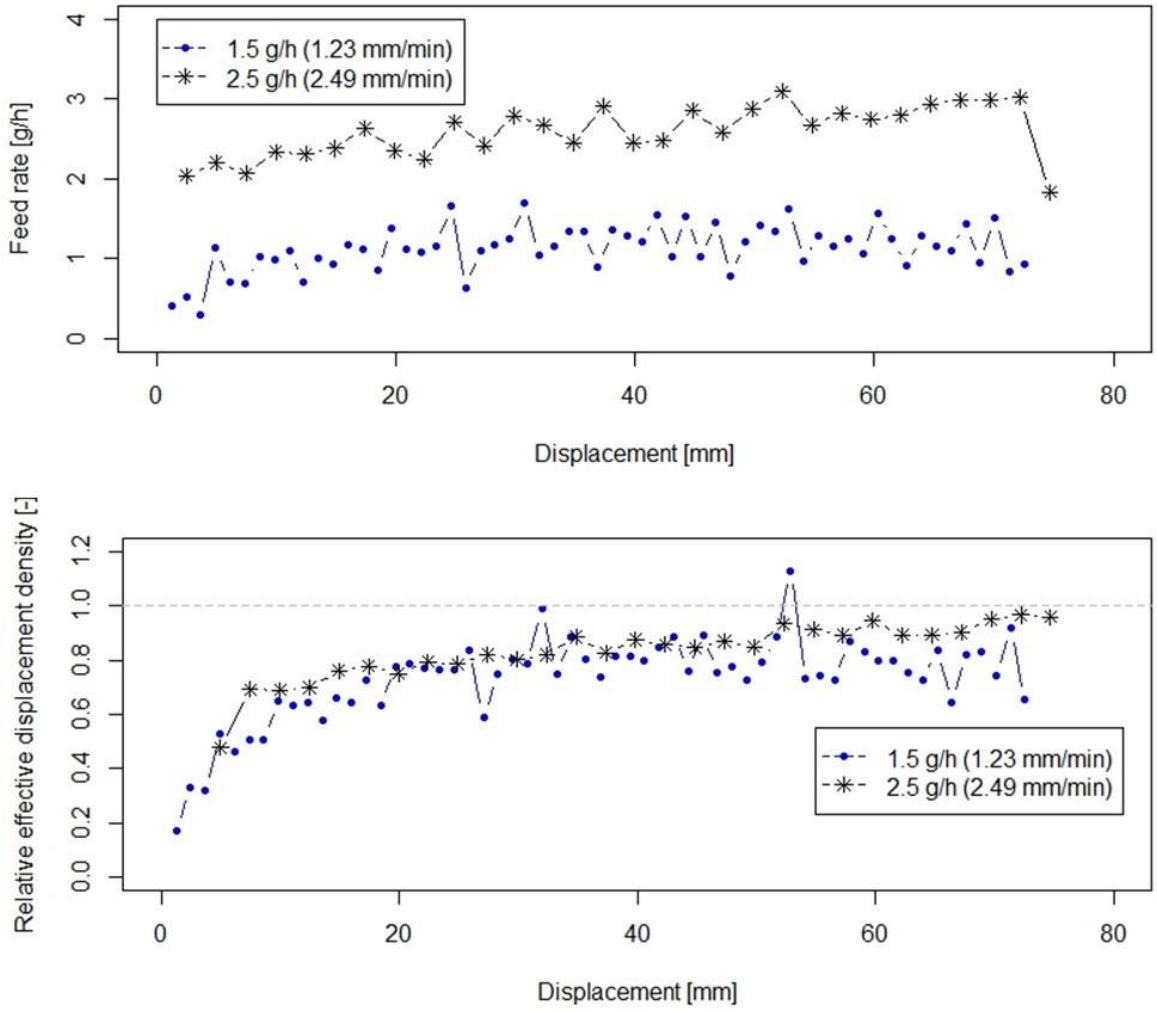

Figure 6. Feeding of silicon dioxide at different feed rates. Displacement speeds are given in brackets for each feed rate. Feed rate (upper plot) and relative effective displacement density (lower plot) during feeding process of silicon dioxide. The relative effective displacement density data are shifted to origins (h_0, pre-conditioning compaction range of 23.94 ± 2.08 mm).

For both fine powders, i.e., GranuLac200 and croscarmellose sodium, the feed rate increases slightly over the feeding process. There are two explanations: possibly a density gradient was created during pre-conditioning or powder densification occurs along the cartridge during feeding (due to the friction at the walls). Likely, both effects contribute to this observation.

As can be seen in Figure 4A and Figure 4B, the first material leaving the cartridge was below tapped density (ρ_{ED}^* <1) and during feeding the density increased to a value greater than tapped density (ρ_{ED}^* >1). Note that the average ρ_{ED}^* needs to be 1, since the cartridge was compressed to obtain powder of exactly tapped density. As can be seen in Figure 4A and Figure 4B the feed rates initially increase significantly.

For both GranuLac200 and croscarmellose sodium, the feed-rate slope (top plots) seems steeper for higher feed rates. However, the ρ_{ED}^{*} curves (bottom plots) show the same increase in slope for different feed rates. This plot thus enables a better understanding of the process. The feed rate is equal to ρ_{ED}^{*} times the displaced volume per time, which is a constant. The plots show that ρ_{ED}^{*} for both GranuLac200 and croscarmellose sodium (see Figure 4A and Figure 4B) evolve independently of the feed rate (displacement speed). According to Amonton's law of friction, the frictional forces are directly proportional to the normal forces, independently of the area of contact and the sliding velocity (29). Thus, the results agree with this law. Most importantly, every powder has the same densification profile, which once measured can be used to control the piston speed. In summary, feed rate changes are mild at constant piston speed.

Feeding process and relative effective displacement density, ρ_{ED}^{*}, for CapsuLac60 and di-calcium phosphate are shown in Figure 5A and Figure 5B, respectively. In contrast to the other finer powders, the feed rate for both powders decreases at the beginning to a minimum level and then it increases again. Feeding performance of CapsuLac60 and di-calcium phosphate are thus significantly different from GranuLac200 and croscarmellose sodium. CapsuLac60 and di-calcium phosphate have larger particles, lower compressibility, and larger elastic recovery compared to GranuLac200 and croscarmellose sodium (see powder properties in Table II and Table III).

As can be seen from Table II and Table III, the powder bed height of CapsuLac60 decreased 4% at 15 kPa direct pressure (see Table III). However, after removing the pressure, the particle bed expanded and the powder bed height increased by 32%. In contrast, GranuLac200's elastic recovery was low, at only 2% powder bed expansion. Croscarmellose sodium's elastic recovery was about 17%, and thus, also much lower than the recovery of CapsuLac60 and Di-calcium phosphate (32%). For the compression analysis from the tapped state the trends were similar, yet not as pronounced. Thus, we hypothesize that the observed initial high feed rate and high density is due to a non-uniform expansion of the powder bed in the cartridge after the pre-conditioning. This effect led to displacement of more mass per time interval at the beginning of the feeding process, manifesting as initially higher feed rates, followed by a lower density/feed rate phase.

Slight differences in the effective displacement density curves may be a result of small differences of powder mass in the cartridge (see Table I). This led to slightly different density levels in the cartridge. The similar shape of the curves supports this hypothesis.

The feeding experiments for silicon dioxide are shown in Figure 6. Silicon dioxide is reported to be difficult to handle due to its low density, high cohesion, and electrostatic properties (10). However, the novel micro-feeder was capable of feeding the glidant at feed rates of 1.5 and 2.5 g/h without significant fluctuations where similar behaviour was noted to the other fine powders tested in this study. As can be seen in Figure 6, the relative effective displacement density, ρ_{ED}^{*} of silicon dioxide is slightly less than unity (1). Due to very low bulk density (0.04 g/cm^3) and electrostatic properties, some material may have been lost during experimental execution. Alternatively, the resolution of the scale might have been insufficient for the low weights associated with silicon dioxide.

Generally, it was found that powders with larger particles and lower compressibility show first a higher feed rate, and therefore, initial densification during the micro-feeding process. In contrast, powders with finer particles and higher compressibility only slightly densify during the feeding process. Thus, feeding performance of powders is dependent on the particle size distributions, bulk density, compressibility and elastic behaviour of powders. However, the plots of the relative effective displacement density, ρ_{ED}^{*}, over displacement is similar for all different feed rates for all investigated materials. Thus, once this curve has been measured for one powder for one feeding rate, displacement speed can be controlled such that a uniform feed rate can be obtained. Using the ρ_{ED}^{*}, curve as a "displacement-feed factor calibration" for programming the syringe pump can ensure a constant feed rate. Average of the relative effective displacement density, ρ_{ED}^{*} and relative standard deviation (RSD) for all investigated materials are summarized in Table V.

Table V. Summary of ρ_{ED}^{*} [-] ± RSD [%] for all investigated material at discrete points of 25, 50 and 75 mm displacement.

Materials / Displacement	CapsuLac60	Di-calcium phosphate	Croscarmellose sodium	GranuLac200	Silicon dioxide
25 mm	0.82 ± 6%	0.90 ± 3%	1.03 ± 17%	0.97 ± 1%	0.81 ± 4%
50 mm	0.93 ± 3%	0.96 ± 2%	1.05 ± 9%	1.05 ± 5%	0.82 ± 4%
75 mm	1.02 ± 3%	1.02 ± 2%	1.05 ± 9%	*	*

*no data is available at this discrete point (see h_0 range in captions of Figure 4 and Figure 6)

Table VI. Particle size distribution of CapsuLac60 samples taken at the beginning, in the middle and at the end of the feeding process for two different feed rates of 20 and 75 g/h.

Material	Feed rate [g/h]	Sample taken	X10 [µm]	X50 [µm]	X90 [µm]
CapsuLac60	20	At the beginning	143	242	355
		In the middle	140	240	353
		At the End	141	240	351
CapsuLac60	75	At the beginning	137	235	347
		In the middle	137	239	350
		At the End	133	234	344

3.4.2 Segregation in the micro-feeder system

Due to the filling procedure, pre-conditioning and feeding, powder segregation may occur. CapsuLac60 has a wide particle size distribution and is relatively free-flowing which may increase the likelihood of size segregation. In order to study the segregation along the cartridge in the micro-feeder system, samples of 3 g were taken during the feeding process. First sample (3 g) was taken at the beginning, then the next sample (3 g) in the middle and the last one (3 g) at the end of the feeding process. The particle size distributions of these samples were measured subsequently by QICPIC (OASIS/L dry dispersing system Sympatec, Clausthal-Zellerfeld, Germany). Table VI shows the particle size distributions of the CapsuLac60 samples taken at different times during the feeding process for two different feed rates of 20 and 75 g/h. No significant difference in particle size distribution was noted between the collected data and the data summarized in Table II (before feeding process). Since no size segregation for CapsuLac60 (having the highest segregation potential) was observed, we assume that all other materials also do not exhibit segregation.

Table VII. Particle size distribution and detailed pre-conditioning information of the active ingredients (API and SDI) provided by Merck & Co., Inc (MSD).

Materials	**API A (API)**	**SDI B (SDI)**
X10 [µm]	8.13	21
X50 [µm]	19.11	42
X90 [µm]	38.65	79
Bulk (poured) density ρ_B [g/cm^3]	0.25 ± 0.00	0.32 ± 0.00
Tapped density ρ_T [g/cm^3]	0.41 ± 0.00	0.44 ± 0.00
Hausner ratio ($\boldsymbol{H_R}$)	1.64	1.38
Powder in the cartridge [g] *	13.94 ± 0.12	14.02 ± 0.15
Powder density after finger tapping and refilling [g/cm^3]	0.34 ± 0.00	0.34 ± 0.00
**h_0 [mm]	17.13 ± 0.70	22.77 ± 0.82
Powder spill after pre-conditioning [g]	0.03 ± 0.00 (0.2%)	0.12 ± 0.02 (0.9%)
Powder density in the cartridge before starting the feeding process [g/cm^3]	0.40 ± 0.00	0.43 ± 0.00

*after finger tapping and refilling **calculated from Equation 2

3.4.3 Micro-feeding of industrial API and SDI

API A and SDI B were used as received to expand the feasibility study for industrial relevant API and SDI, respectively. The particle size distribution and detailed pre-conditioning information of these materials is summarized in Table VII. Based on the PSD and $\boldsymbol{H_R}$ we assume that both materials are highly cohesive and sticky (30). Figure 7 shows the low-throughput feeding performance for both API and SDI (following the micro-feeding process section) for a maximum feeding duration of two hours. For feed rates of 10 and 15 g/h, the feeding duration is shorter due to the available powder mass in the cartridge.

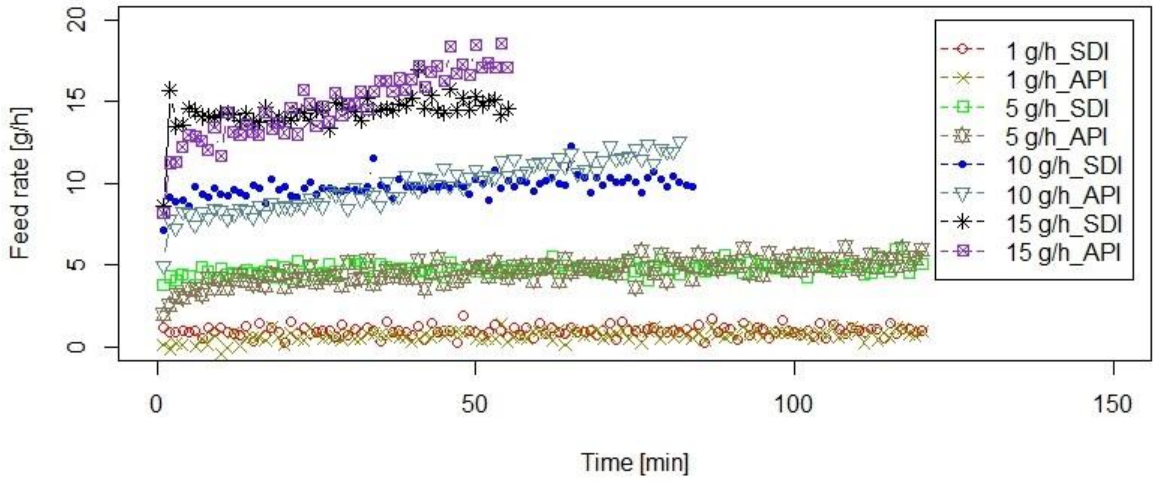

Figure 7. Micro-feeding of commercial APIs. The displacement speeds for API to adjust the feed rates of 1, 5, 10 and 15 g/h, are respectively 0.1, 0.5, 0.99 and 1.49 mm/min. The displacement speeds for SDI: are respectively 0.1, 0.46, 0.93 and 1.39 mm/min for adjusting 1, 5, 10 and 15 g/h feed rates.

Again, performance was reproducible for both API and SDI over the 3 runs performed at each displacement rate. SDI B had a stable constant feed rate at lower flow rates, but deviations were noted for the 10 and 15 g/h set points. Similarly, API A showed deviations for higher feed rates of 10 and 15 g/h. This feeding behaviour is similar to the GranuLac200 (see Figure 4A) and croscarmellose sodium (see Figure 4B) feeding. The possible reasons are explained above in "Detailed analysis of feeding experiments" section.

With these results we have shown the potential industrial applicability of the micro-feeder system was evaluated using fine and cohesive APIs at various low feed rates of 1, 5, 10 and 15 g/h. It is important to note that with the observed flow rate deviations of 10-20%, it would not be possible to implement the feeding system "as is". However, we see the potential of this unit to be part of a manufacturing process as it overcame the cohesivity and stickiness API attributes (see particle size distribution and $\boldsymbol{H_R}$ data in Table VII) and was able to dispense the material at very low rates. During the micro-feeding process, the powder is actively transported over all contact surfaces. It is pushed upward via the piston on the plate and is moved by the scraper from the plate onto the balance. Therefore, the potential for sticking on free surfaces is small. During all test runs no significant adhesion or agglomeration was observed and the full amount of powder in the cartridge was collected at the end on the balance (no powder was lost during the feeding process), except for silicon dioxide where small amounts may have lost.

The unit may be able to allow for single API dispensing and allow manufacturers to move away from having to process APIs with excipients to allow for feeding operations (e.g., APIs being mixed with excipients and flow aids to improve their flowability). Thus, the novelty of the micro-feeder system is to overcome a powder's poor flowability allowing the feeding of very fine and cohesive powders reproducibly, as described by the displacement-feed factor curve. Moreover, by using a combination between the micro-feeder and a loss-in-weight setup, precise and low powder flow rates – required for a commercial scale process – may be achieved.

3.5 Conclusions

In this study, the feeding performance and the impact of powder properties on feeding were analysed and discussed for four excipient materials. In addition, one API and one SDI (both highly cohesive) were evaluate to highlight the industrial applicability of the micro-feeder. A density-displacement curve was plotted for all materials investigated. The shape of the curve is highly reproducible, yet different for each material depending on powder properties. We found that large- and small-particle systems had qualitatively the same density-displacement curves; i.e., di-calcium phosphate and CapsuLac60 had similar curves, significantly different from the small-particle system (GrabuLac200 and croscarmellose sodium). For a specific material these curves are independent from the feed rate. Therefore, these data can be used to calibrate the syringe pump to ensure a constant accurate feed rate. In summary, the following conclusions can be made:

- Low feeding rates down to 1g/h can be achieved consistently for the tested materials.
- A wide variety of different powders, even low-density cohesive materials, can be fed.
- Repeatability and consistency of feeding, as described by the displacement-feed factor curve, were good. Most importantly, the density-displacement plot is unique for each material. We call this a "displacement-feed factor". The dependence can be used to control piston speed to achieve a constant and low feed rate for a range of feeding rates (1-20g/h tested in the study).
- Segregation is not a significant issue in this process (which is another major advantage of the proposed micro-feeding system).

A major benefit of the micro-feeder system is that it requires less material for testing when compared to other feeders (i.e., tens of mL of powder can be used to test micro-feeding system compared to 1-2 kg of powder needed for larger feeders). This is important for highly potent (and expensive) APIs and also during early stages of development.

Future work will address the closed-loop control of this feeder, making it ready for integration in GMP continuous manufacturing lines given the need to better control the flow rate over time. For automation of the system, finger tapping (strokes by the side in the cartridge) during the pre-conditioning process would be replaced by automatically hammering the cartridge periodically during the filling process.

3.6 Acknowledgements

RCPE is a K1 COMET Centre within the COMET – Competence Centres for Excellent Technologies programme. The COMET programme is operated by the Austrian Research Promotion Agency (FFG) on behalf of the Federal Ministry for Transport, Innovation and Technology (BMVIT) and the Federal Ministry for Digital and Economic Affairs (BMDW). Our projects are also funded by Land Steiermark and the Styrian Business Development Agency (SFG). Furthermore, we would like to thank Viktoria Magosi for the technical support of the experimental studies presented in this work.

3.7 References

1. Yang S, Evans JRG. Metering and dispensing of powder; the quest for new solid freeforming techniques. Powder Technol. 2007 Sep;178(1):56–72.

2. Wang Y, Koynov S, Glasser BJ, Muzzio FJ. A method to analyze shear cell data of powders measured under different initial consolidation stresses. Powder Technol. 2016;294:105–12.

3. Schaber SD, Gerogiorgis DI, Ramachandran R, Evans JMB, Barton PI, Trout BL. Economic analysis of integrated continuous and batch pharmaceutical manufacturing: A case study. Ind Eng Chem Res. 2011;50(17):10083–92.

4. Rantanen J, Khinast J. The Future of Pharmaceutical Manufacturing Sciences. J Pharm Sci. 2015;104(11):3612–38.

5. Rogers L, Briggs N, Achermann R, Adamo A, Azad M, Brancazio D, et al. Continuous Production of Five APIs in Flexible Plug-and-Play Modules - A Demonstration Campaign. Org Process Res Dev. 2020;

6. Azad MA, Osorio JG, Brancazio D, Hammersmith G, Klee DM, Rapp K, et al. A compact, portable, re-configurable, and automated system for on-demand pharmaceutical tablet manufacturing. Int J Pharm. 2018;539(1–2):157–64.

7. Adamo A, Beingessner RL, Behnam M, Chen J, Jamison TF, Jensen KF, et al. On-demand continuous-flow production of pharmaceuticals in a compact, reconfigurable system. Science (80-). 2016;352(6281):61–7.

8. Stelzer T, Wong SY, Chen J, Myerson AS. Evaluation of PAT Methods for Potential Application in Small-Scale, Multipurpose Pharmaceutical Manufacturing Platforms. Org Process Res Dev. 2016;20(8):1431–8.

9. Stauffer F, Vanhoorne V, Pilcer G, Chavez PF, Schubert MA, Vervaet C, et al. Managing active pharmaceutical ingredient raw material variability during twin-screw blend feeding. Eur J Pharm Biopharm. 2019;135(October 2018):49–60.

10. Engisch WE, Muzzio FJ. Loss-in-Weight Feeding Trials Case Study: Pharmaceutical Formulation. J Pharm Innov. 2014;10(1):56–75.

11. Bostijn N, Dhondt J, Ryckaert A, Szabó E, Dhondt W, Van Snick B, et al. A multivariate approach to predict the volumetric and gravimetric feeding behavior of a low feed rate feeder based on raw material properties. Int J Pharm. 2019;557(September 2018):342–53.

12. Lu X, Yang S, Evans JRG. Studies on ultrasonic microfeeding of fine powders. J Phys D Appl Phys. 2006;39(11):2444–53.

13. Lu X, Yang S, Evans JRG. Ultrasound-assisted microfeeding of fine powders. Particuology. 2008 Feb;6(1):2–8.

14. Matsusaka S, Yamamoto K, Masuda H. Micro-feeding of a fine powder using a vibrating capillary tube. Adv Powder Technol. 1996;7(2):141–51.

15. Qi L, Zeng X, Zhou J, Luo J, Chao Y. Stable micro-feeding of fine powders using a capillary with ultrasonic vibration. Powder Technol. 2011 Dec;214(2):237–42.

16. Chen X, Seyfang K, Steckel H. Development of a micro-dosing system for fine powder using a vibrating capillary. Part 2. The implementation of a process analytical technology tool in a closed-loop dosing system. Int J Pharm. 2012 Aug;433(1–2):42–50.

17. Leschonski K, Rüthele S, Menzel U. A Special Feeder for Diffraction Pattern Analysis of Dry Powders. Part Part Syst Charact. 1984;1(1–4):161–6.

18. Besenhard MO, Karkala SK, Faulhammer E, Fathollahi S, Ramachandran R, Khinast JG. Continuous feeding of low-dose APIs via periodic micro dosing. Int J Pharm. 2016;509(1–2):123–34.

19. Engisch WE, Muzzio FJ. Feedrate deviations caused by hopper refill of loss-in-weight feeders. Powder Technol. 2015;283:389–400.

20. Engisch WE, Muzzio FJ. Method for characterization of loss-in-weight feeder equipment. Powder Technol. 2012;228:395–403.

21. Yu AB, Standish N. Estimation of the Porosity of Particle Mixtures by a Linear-Mixture Packing Model. Ind Eng Chem Res. 1991;30(6):1372–85.

22. Besenhard MO, Fathollahi S, Siegmann E, Slama E, Faulhammer E, Khinast JG. Micro-feeding and dosing of powders via a small-scale powder pump. Int J Pharm. 2017;519(1–2):314–22.

23. Hao T. Understanding empirical powder flowability criteria scaled by Hausner ratio or Carr index with the analogous viscosity concept. RSC Adv. 2015;5(70):57212–5.

24. Hentschel ML, Page NW. Elastic properties of powders during compaction. Part 1: Pseudo-isotropic moduli. J Mater Sci. 2007;42(4):1261–8.

25. Søgaard S, Bryder M, Allesø M, Rantanen J. Characterization of powder properties using a powder rheometer. 2019;825.

26. Fu X, Huck D, Makein L, Armstrong B, Willen U, Freeman T. Effect of particle shape and size on flow properties of lactose powders. Particuology. 2012;10(2):203–8.

27. Dudhat SM, Kettler CN, Dave RH. To Study Capping or Lamination Tendency of Tablets Through Evaluation of Powder Rheological Properties and Tablet Mechanical Properties of Directly Compressible Blends. AAPS PharmSciTech. 2017;18(4):1177–89.

28. Gnagne EH, Petit J, Gaiani C, Scher J, Amani GN. Characterisation of flow properties of foutou and foufou flours, staple foods in West Africa, using the FT4 powder rheometer. J Food Meas Charact. 2017;11(3):1128–36.

29. Friction DOF, Laws THE, Friction OF. Friction 3.1. 2017. In: https://reader.elsevier.com/reader/sd/pii/B9780081009109000039?token=4780A3F361861693B871057678B4B752C13BD127EFA844463E5FFECB95E1DB833E66BF9B55A74A48DF8F483AA376E909. Accessed 15 March 2020.

30. Adhikari B, Howes T, Bhandari BR, Truong V. Stickiness in foods: A review of mechanisms and test methods. Int J Food Prop. 2001;4(1):1–33.

4 Development of a Controlled Continuous Low-dose Feeding Process

(This chapter is based on the publication Sara Fathollahi, Julia Kruisz, Stephan Sacher, Jakob Rehrl, M. Sebastian Escotet-Espinoza, James DiNunzio, Benjamin J. Glasser, Johannes G. Khinast, Under review, May 2021)

4.1 Abstract

This paper proposes a feed rate control strategy for a novel volumetric micro-feeder, which can accomplish low-dose feeding of pharmaceutical raw materials with significantly different powder properties. The developed feed-forward control strategy enables a constant feed rate with a minimum deviation from the set-point, even for materials that are typically difficult to accurately feed (e.g., due to high cohesion or low density) using conventional continuous feeders.

Density variations observed during the feeding process were characterized via a displacement feed factor profile for each powder. The characterized effective displacement density profile was applied in the micro-feeder system to proactively control the feed rate by manipulating the powder displacement rate (i.e., computing the feed rate from the powder displacement rate). Based on the displacement feed factor profile, the feed rate can be predicted during the feeding process and at any feed rate set-point. Three pharmaceutically relevant materials were used for the micro-feeder evaluation: di-calcium phosphate (large-particle system, high density), croscarmellose sodium (small-particle system, medium density) and barium sulphate (very small-particle < 10 µm, high density). A significant improvement in the feeding performance was achieved for all investigated materials. The feed rate deviation from the set-point and its relative standard deviation were minimal compared to operations without the control strategy.

4.2 Introduction

Tablets and capsules are the most common forms of drug products (1). Many factors, such as the raw material's variability (e.g., bulk properties) and manufacturing process disturbances (2), can affect the quality of final drug products. The drug product's quality and consistency are assured through well-designed development and manufacturing process within the Quality by Design (QbD) framework (3). Over the last ten years continuous manufacturing has been increasingly applied in the pharmaceutical industry due to its many potential benefits (4,5).

Continuous powder feeding is a common unit operation for all continuous manufacturing (CM) processes for both active pharmaceutical ingredients (APIs) and excipients (6). Powder feeders play an important role in the CM process: *they maintain the steady state of the process and deliver the pharmaceutical ingredients to the downstream process* (5,7), e.g., continuous granulation, tableting and coating. Individual feeders continuously deliver the APIs and excipients according to the formulation and at a pre-defined feed rates (5). Consistent feeding of materials requires good understanding of the material properties and the manufacturing process. Additionally, an automated process control system is essential to address both the measurable and the non-measurable process disturbances in real time (2). Control of the feeding operation is a primary component of a system's control strategy since the input of the continuous process directly affects the output, and thus, the critical quality attributes of a drug product, such as assay and content uniformity (5).

Loss-in-weight (LIW) feeders are frequently used in pharmaceutical CM process to maintain consistent feeding into subsequent unit operations. The principle of LIW feeding involves the constant monitoring of the mass (i.e., weight) of material in the feeder while discharging and constantly adjusting the rate of discharging to maintain a mass flow rate (8). The mass of the feeder is monitored via a balance under the feeding unit. LIW feeding stands in contrast to gain-in-weight (GIW) because in the latter the balance is placed outside of the feeding unit to collect the material discharged out of the feeder. From a processing perspective, the use of LIW feeders can be used in conjunction to other unit operations while the GIW feeders need to terminate into the balance in which the material mass is being measured.

The feeding range of feeders depends on the feeder's size and tooling (e.g., screws and screens) and the material properties (8). Although the use of feeders is well established in many industries and has been successfully applied in various processes, there are limitations as to the specific types of materials and the minimum feasible feed rate. Especially at low feed rates (< 1 kg/h), LIW feeding is challenging due to feed-rate fluctuations associated with the screw conveying principle, problems during the hopper refilling and associated feed-rate variations due to changes in the powder bed height. Moreover, bridging and adhesion of cohesive materials are associated with the screw conveying method, leading potentially to blockage of the feed channel (9–12). In continuous processes, blending elements are typically designed to reduce the variability caused by the feeding operation (5). However, some studies (13,14) indicate that the variability and disturbance during the feeding operation can affect the performance of downstream unit operations and the final product quality. To control the feeding performance of LIW feeders, the feeder tooling selection was matched to the material properties

(8,11,12,15,16). In addition, individual feeder control strategies have been developed to reduce the variability of the fed material's concentration (5,17).

To control the feed rate, feeders an integrated balance to inform a closed-loop controller that then adjusts the discharging rate by speeding or slowing the discharging element (e.g., screws or paddles). The close-loop controlled can be either proportional integral (PI) or proportional integral derivative (PID) (10). Such a feed-back control strategy allows one to monitor the plant's output (i.e., the feed rate computed based on the balance raw signal) and take actions (e.g., adjusting the screw speed) in order to attenuate the effects of any disturbance in the feed rate. A feed-forward control strategy makes it possible to take actions based on the process knowledge and the measured disturbances (a feed-forward signal) before these disturbances affect the plant's output (2). However, it is impossible to monitor the feed rate in real-time and actively take actions if deviations from the feed-forward signal (unmeasured disturbances) occur. Especially with regard to pharmaceutical products, it is important to monitor the process in-line, detect possible disturbances (deviations from the feed-forward signal) and take actions before the process disturbances (indicated by the feed-forward signal) affect the final product quality. For example, in the tableting environment this can affect the content uniformity, weight and functionality of the final tablets (18).

A strategy combining feed-back and feed-forward control is required to supress predictable (measured) disturbances proactively and to monitor the process for possible unmeasured disturbances in real time (2). Some studies investigated control at a system level, using feed-back control strategies (19–22) and feed-forward control models (23,24) to control the manufacturing processes. Other authors (2,25,26) proposed a combined feed-forward feed-back control system for continuous manufacturing process. Furthermore, there are studies on the application of iterative learning control for weighing the powder materials (27,28).

Low-dose feeding of cohesive materials, such as highly-active APIs and lubricants (7), is a challenge due to the inherent feeder variability (10). In our previous study (29), a novel micro-feeder system was introduced, which enables feeding of powders with diverse powder properties (e.g., size, density, flow properties, cohesivity, etc.) at feed rates as low as 1 g/h. Based on the volumetric feeding principle, this micro-feeder system yields a constant volume of powder per unit time. In the absence of a control strategy, a consistent feed rate is determined by the constant powder mass distribution in the feeder cartridge. Depending on the formulation, even slight deviations in density and feed rate may lead to an out-of-specification event during continuous manufacturing of low-dose drug products. To address this issue, in this follow-up

study a strategy for controlling the feed rate during the feeding process was developed and evaluated by feeding di-calcium phosphate, croscarmellose sodium and barium sulphate.

4.3 Materials and methods

4.3.1 Materials

Di-calcium phosphate (dibasic calcium phosphate, Sigma-Aldrich, UK), croscarmellose sodium (sodium carboxymethylcellulose, Sigma-Aldrich, UK) and barium sulfate (Sigma-Aldrich, UK) were used in this work. They were selected to demonstrate the feeding variability relative to the various powder properties.

4.3.2 Powder characterization techniques

4.3.2.1 Particle size distribution measurement

Particle size distributions (PSDs) of the materials were measured via laser light diffraction techniques (Helos/KR, OASIS/L dry dispersing system Sympatec, Clausthal-Zellerfeld, Germany). A vibrating chute was used to transport the powder in a controlled way to the dispersing unit. A dispersion pressure of 2.5 bar was applied.

4.3.2.2 Bulk and tapped density measurements

The bulk (poured) and tapped densities (BD and TD) of materials and mixtures were analyzed via a Pharmatest PT-TD200, a standardized method described in the United States Pharmacopeia (30).

4.3.3 Methods

4.3.3.1 Experimental set up

The micro-feeder system, described by Fathollahi et al. (29), was augmented to include an LIW option. The micro-feeder consists of a cartridge, which contains the powder, a moveable piston actuated via a syringe pump to displace the powder and a scraper to transport the material to the process. It is combined with a weighing balance (Mettler Toledo, XPE204, 0-220g with a readability of 0.0001 g) at the outlet that measures the feeder's output rates by recording the accumulated mass at the outlet of feeder (gain in weight (GIW)). Additionally, the micro-feeder is placed on another balance (Mettler Toledo, XSR32001L, 0.1-32100g with a readability of 0.1 g) to monitor the weight loss over time (LIW). A schematic of the micro-feeder system is shown in Figure 1.

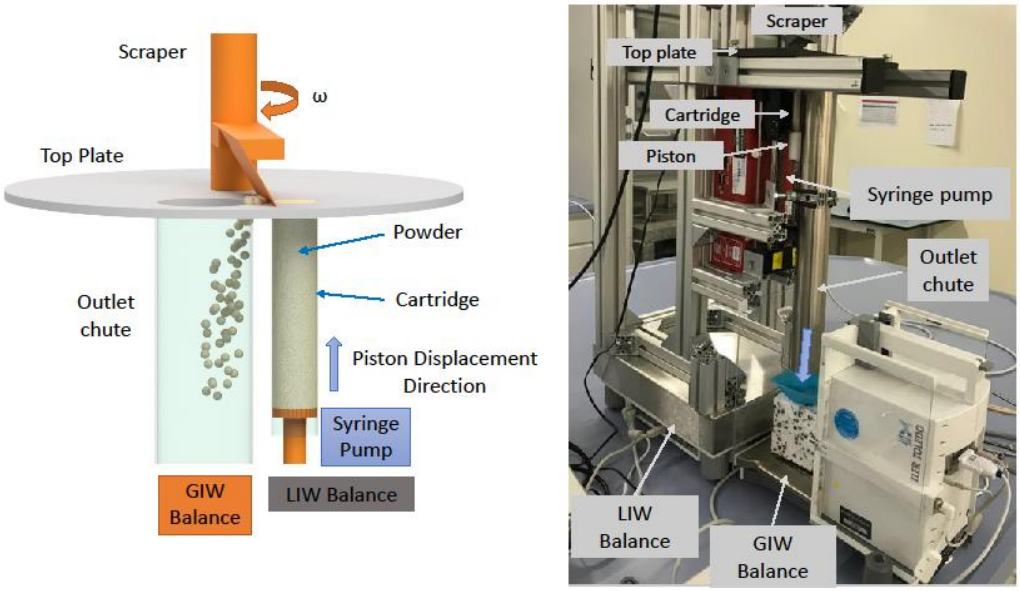

Figure 1. Micro-feeder system: schematic of the system (left), experimental setup (right). (LIW=loss in weight, GIW=gain in weight)

4.3.3.2 Data acquisition and equipment integration

The piston is driven by a syringe pump (NE-1000 programmable single syringe pump, New Era instruments via New Era pump systems, USA), which can be connected to a PC via a serial port (RS232). The dosed volume can be read from the serial connection. Furthermore, it is possible to write a new displacement speed set-point and start/stop the pump via the serial port. Both balances are also connected via the serial interface. They provide the actual weight value that is differentiated and filtered in a post-processing step (see

Figure 2). All available parameters are acquired at a sampling frequency of 1Hz using Matlab® (Mathworks, Natick USA). At each time point, the data acquired from the syringe pump and the balances is recorded and the piston position is computed (see Eq. (1)).

$$p = V_{in}/A_{cart}, \tag{1}$$

where p is the calculated position of piston, V_{in} is the dosed volume (which is read from the pump via the RS232 interface) and A_{cart} is the cross-sectional area of the cartridge. The set-point for displacement speed v is written to a text file, including a timestamp to allow time-aligned data processing.

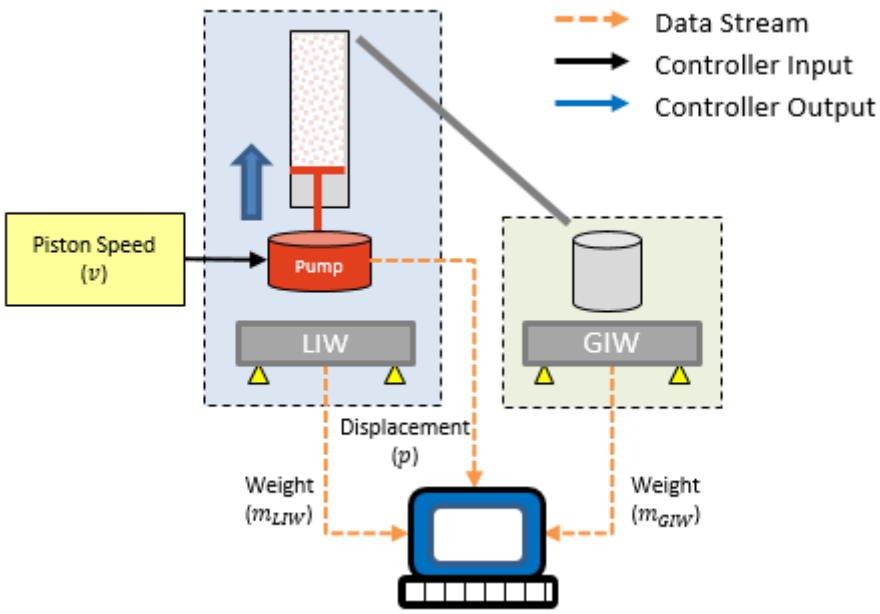

Figure 2: Schematic of the set up for the calibration runs

4.3.3.3 Data processing

All data processing discussed in this work was performed using Matlab® (Mathworks, Natick USA). The feed rate was obtained via a Savitzky-Golay derivative filter (31,32) with window lengths of 2 minutes for the GIW data and of 10 minutes for the LIW data, both using a second order polynomial.

4.3.3.4 Micro-feeder characterization methodology

The feed rate in the micro-feeder system can be adjusted through the piston's displacement speed. The micro-feeder system assumes the piston displaces the cartridge volume continuously and at the specified rate (i.e., instantaneous adjustment). This ensures a constant mass feed rate, provided that the density in the cartridge is constant initially and during feeding due to pre-conditioning. The pre-conditioning procedure is designed as an essential step prior to the feeding process to eliminate cavities and inter-particle voids. During this step, the powder in the cartridge is tapped and compacted to the powder tapped-density state. Details of the pre-conditioning procedure are provided in our previous work (29).

In this study, the scraper rotating speed was set to 10 rpm. The high-precision balance was used as a catch (gain-in-weight) balance (i.e., GIW data) at the outlet of the micro-feeder to measure the accumulated mass of the material fed. At the same time, the other balance, on which the micro-feeder is located, recorded the mass loss (i.e., LIW data) of the micro-feeder.

Volumetric displacement ΔV of the powder on top of the cartridge during time interval Δt is not known precisely. However, it can be approximated via the volumetric piston displacement at the bottom of the cartridge ($\Delta V \approx v \cdot A_{cart} \cdot \Delta t$), where v is the constant piston displacement speed in the cartridge and A_{cart} is the cross-sectional area of the cartridge. Accumulation of mass at the catch balance (relating to the powder exiting at the top, Δm) was measured. We defined a property termed "the effective displacement density," ρ_{ED} as $\frac{\Delta m}{\Delta V}$, which is an approximation of the actual bulk density of the powder at the exit. The feed rates are determined based on the generated data each second ($\dot{m}_f = \Delta m/\Delta t$). Since the micro-feeder system is based on the volumetric principle, a variation in the effective displacement density along the cartridge causes the feed rate variation over the process time. The effective displacement density is plotted as a function of displacement for each material and is termed a "displacement feed factor." The displacement feed factor profile represents the uncontrolled feed rate profile for each material.

A benefit of the micro-feeder system is that the system is robust, stable, and feeding is reproducible. Specifically, the displacement feed factor is reproducible yet unique (29) for each material and depends on the powder properties, such as the particle size, elastic behaviour, and bulk and tapped densities. Most importantly, the displacement feed factor is not affected by the feed rate (29) for the tested materials in the investigated ranges. This property makes it possible to apply the displacement feed factor in a feed-forward control strategy. The piston displacement speed is calculated from the actual piston position to compensate for the displacement feed factor profile and achieve a feed rate closer to the set-point over the entire length of the cartridge.

4.3.3.5 Calibration runs

Calibration runs were performed prior to controlled feeding to determine the displacement feed factor for each material. A schematic of the setup of the calibration runs is shown in Figure 2. The piston displacement speed (Eq. (2)) is calculated based on the powder mass (M) in the cartridge length (L) considering the desired feed rate ($\dot{m}_{set}$),

$$Piston\ speed, v\ [\frac{mm}{min}] = \frac{\dot{m}_{set}\ [\frac{g}{min}]}{\frac{M}{L}\ [\frac{g}{mm}]}. \quad (2)$$

The initial powder mass is assumed to be constantly distributed along the cartridge and to remain constant during the feeding process. Therefore, the piston displacement speed is set to a fixed value for the entire run.

The calibration runs were performed at feed rates of 5 g/h, 10 g/h and at the lowest possible piston displacement speed of 0.1 mm/min, which is the limit for the syringe pump. The data from the GIW balance were used to calculate the displacement feed factor profile of each material.

4.3.3.6 Control strategy

The feed rate in the micro-feeder system was determined based on the displacement speed of the piston in the cartridge and the displacement feed factor, i.e., the piston displacement speed acted as a manipulated variable. The control concept consisted of two stages: (1) feed-forward control and (2) iterative learning control.

4.3.3.7 Feed-forward control

Actual piston displacement information and the material-specific feeding behaviour was used to control the feed rate in the feed-forward mode. The piston position data were obtained from the syringe pump. The material-specific feeding behaviour was represented by the displacement feed factor, which was determined in the calibration runs. A polynomial function describing the displacement feed factor over the displacement based on the calibration results was defined for each material and used to calculate the piston displacement speed required for achieving the desired feed rate. The polynomial function is given in Eq. (3) with the displacement p and the polynomial coefficients α:

$$\rho_{poly}(p) = \sum_{i=0}^{8} \alpha_i p^i \tag{3}$$

The high-order polynomial was chosen in order to capture the more complex shape of the displacement feed factor curve of di-calcium phosphate (29).

For the feed-forward control, the syringe pump was run at the calculated piston displacement speed, which was adapted according to the piston displacement. Nominal feed rate $\dot{m}_{nom}$ for feed-forward control in Eq.(4) can be expressed as a function of the effective displacement density (modelled by the polynomial in Eq. (3)) in the calibration run in combination with piston displacement speed v and cartridge cross-sectional area A_{cart},

$$\dot{m}_{nom} = \rho_{poly}(p) \cdot v \cdot A_{cart}. \tag{4}$$

By rearranging Eq. (4), the required piston displacement speed can be calculated The feed-forward control is based on the idea that the nominal feed rate is identical to the feed rate set point $\dot{m}_{ref}$, i.e $\dot{m}_{nom} = \dot{m}_{ref}$. Consequently, the piston speed is computed by

$$v = \frac{\dot{m}_{ref}}{\rho_{poly}(p) \cdot A_{cart}}. \quad (5)$$

A schematic of the control strategy is shown in Figure 3.

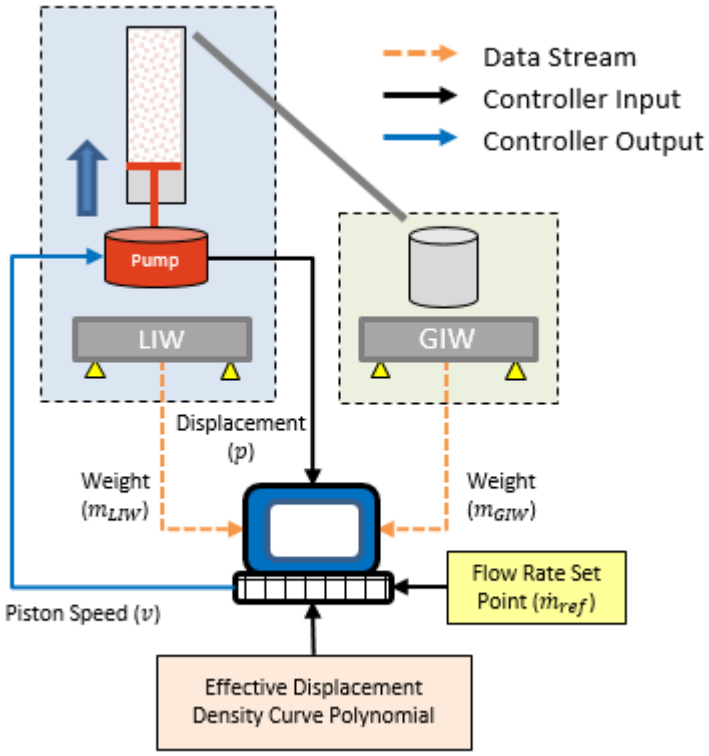

Figure 3. Schematic of the feed-forward control strategy.

4.3.3.8 Iterative learning control

An iterative learning control (27,28) algorithm was developed and implemented in the process controller for correcting an offset in the displacement feed factor profile. Factors that change the effective displacement feed factor (e.g., batch-to-batch variability, inconsistent preconditioning, operator dependency) can result in an offset of the displacement feed factor.

During these runs, the pump was run in the feed-forward control mode based on the displacement feed factor data from the calibration. The LIW data were then used to compensate for disturbances at regular time intervals. Specifically, a deviation from the dosed mass obtained from the LIW data was compared to the desired dosed mass according to the set-point. This error was used to correct the offset coefficient, α_0, in Eq. (3). However, the offset only affected the last polynomial coefficient and did not alter the shape of the displacement feed factor curve. This offset correction was applied after a certain predefined time. We call this method the ”corridor control” principle. Alternatively, it can be applied at a certain piston displacement.

After the time interval or displacement that corresponded to one iteration, the actual measured feed rate was once again compared to the set-point and the polynomial function was updated accordingly. In our case, coefficient α_0 of the polynomial was updated. The update law is given by Eq. (6):

$$\alpha_{0,k+1} = \alpha_{0,k} + K \cdot e_k. \tag{6}$$

Error e_k is the difference between the desired dosed mass per time (feed rate $\dot{m}_{nom}$) and the actual dosed mass per time (feed rate $\dot{m}_{LIW}$) during the previous time interval (or displacement interval), k. The appropriate choice of constant K will be outlined below. The nominal feed rate was assumed to be:

$$\dot{m}_{nom} = \left(\sum_{i=1}^{8} \alpha_i p^i + \alpha_{0,k} \right) \cdot v \cdot A_{cart} \tag{7}$$

The actual feed rate is composed of the nominal feed rate and additive disturbance $\dot{m}_d$. Under the assumption that only α_0 is uncertain (unknown offset d), the actual feed rate can be written as:

$$\dot{m}_{LIW} = \dot{m}_{nom} + \dot{m}_d = \left(\sum_{i=1}^{8} \alpha_i p^i + \alpha_{0,k} + d \right) \cdot v \cdot A_{cart} \tag{8}$$

This actual feed rate should now correspond to the updated polynomial:

$$\alpha_{0,k+1} = \alpha_{0,k} + d \tag{9}$$

The integral deviation of the measured feed rate from the set-point during one integration period, which is equal to one iteration, can be calculated using Eq. (10):

$$e_k = \int_{t-t_{int}}^{t} e(\tau)\, d\tau = \int_{t-t_{int}}^{t} (\dot{m}_{nom} - \dot{m}_{LIW}) d\tau = \int_{t-t_{int}}^{t} (-d \cdot v \cdot A_{cart}) d\tau \tag{10}$$

Since d and A_{cart} are constant, after performing the integration of velocity and considering Eq. (6) and (9), K can be computed as follows:

$$e_k = -d \cdot A_{cart} \int_{t-t_{int}}^{t} v\, d\tau = -d \cdot A_{cart}\, [p(t) - p(t - t_{int})] \tag{11}$$

$$K = \frac{d}{e_k} = -\frac{1}{A_{cart}\,[p(t) - p(t - t_{int})]} \tag{12}$$

Furthermore, for a time-invariant set-point $\dot{m}_{set}$, Eq. (10) can be simplified to Eq. (13) for the benefit of using the measured mass values from the balance, which provides inherently integrated values of the feed rate:

$$e_k = \int_{t-t_{int}}^{t} (\dot{m}_{nom} - \dot{m}_{LIW})d\tau = \dot{m}_{nom} \cdot t_{int} + (m_{LIW_t} - m_{LIW_{t-t_{int}}}). \tag{13}$$

A schematic of the control strategy is shown in Figure 4.

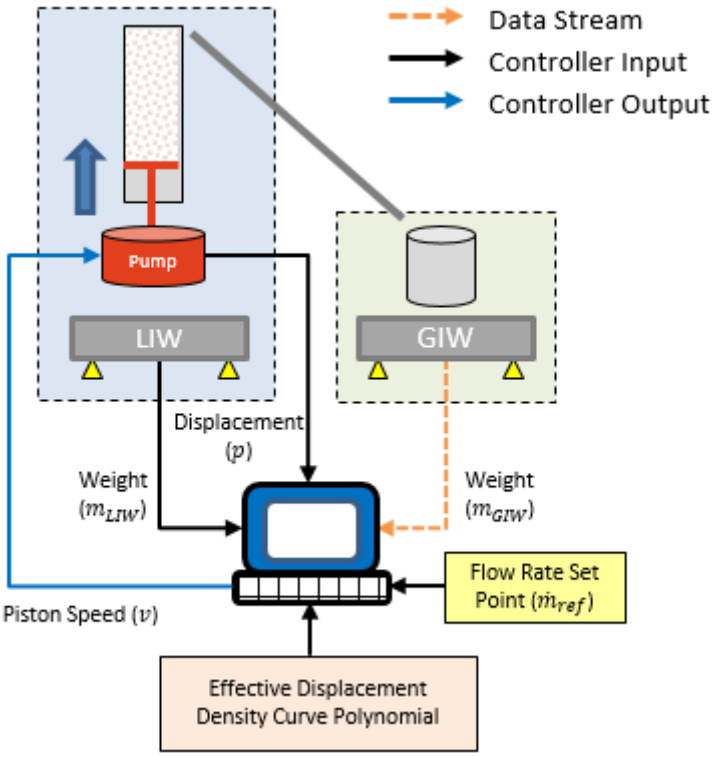

Figure 4. Schematic of the iterative learning control strategy.

To show the effect of iterative learning control, the initially well-fitted polynomial displacement feed factor profile used in feed-forward control was offset by -10%, resulting in 10% higher displacement speed compared to the set-point at the beginning of the experiment. Start-up and integration time were chosen in accordance with a filtering window time.

The algorithm was then used to control the actual micro-feeding system, and two experiments were performed. First, the iterative learning control based on the LIW balance data was tested. Second, a feed-forward controlled run using the wrong polynomial displacement feed factor was run for the purpose of quantifying the capabilities of iterative learning control. During this

run, the displacement speed was the one obtained in the calibration run but increased by 10% according to the disturbance introduced. No control action based on LIW balance data was taken.

4.3.3.9 Feeding Performance Metrics

The feeding performance evaluation of the feed rate $\dot{m}$ is based on the following standardized methods: the average relative standard deviation ($RSD_{\%}$) given by Eq. (16), with s denoting the standard deviation and the average relative deviation from the set-point ($RDtS_{\%}$) as a quotient of the average deviation from the set-point over the feed rate set-point $\dot{m}_{set}$ (see Eq. (18)). The relative deviation of mean to set-point ($RDMtS_{\%}$) is calculated by Eq. (18), where $\dot{m}_{mean}$ is mean feed rate.

$$\dot{m}_{mean} = \frac{1}{N}\sum_{1}^{N}\dot{m} \tag{14}$$

$$s = \sqrt{\frac{\sum_1^N(\dot{m} - \dot{m}_{mean})^2}{N}} \tag{15}$$

$$RSD_{\%} = \frac{s}{\dot{m}_{mean}} \cdot 100 \tag{16}$$

$$RDtS_{\%} = \frac{\frac{1}{N}\sum_1^N|\dot{m} - \dot{m}_{set}|}{\dot{m}_{set}} \cdot 100 \tag{17}$$

$$RDMtS_{\%} = \frac{|\dot{m}_{mean} - \dot{m}_{set}|}{\dot{m}_{set}} \cdot 100 \tag{18}$$

4.4 Results and discussion

Di-calcium phosphate, croscarmellose sodium and barium sulphate were used for evaluating the performance of the feed-forward control strategy. The main reason for choosing these materials was to represent a spanning range of material properties (e.g., the particle size distribution and flow properties). The powder properties of the investigated materials are summarized in Table I. Di-calcium phosphate is an example of a large-particle system (x50 = 184 µm) with a fair flowability (1.19 < $\boldsymbol{H_R}$ < 1.25), and croscarmellose sodium represents a small-particle system (x50 = 43 µm) with a very poor flowability (1.46 < $\boldsymbol{H_R}$ < 1.59). As our previous study (29) indicated, systems with similar PSDs have qualitatively the same displacement feed factor in the micro-feeder system. Barium sulphate was chosen to represent

an extremely small particle system (x50 < 10 µm) with an extremely poor flowability ($\boldsymbol{H_R}$ > 1.6).

Table I. Powder properties of the investigated materials. ± Represents 1 standard deviation (n = 3).

Materials	**Di-calcium phosphate**	**Croscarmellose sodium**	**Barium sulphate**
X10 [µm]	14.6 ± 1	19.5 ± 0	0.74 ± 0
X50 [µm]	184.4 ± 5	43.4 ± 0	3.06 ± 0
X90 [µm]	314.5 ± 3	119.5 ± 2	7.94 ± 0
Hausner ratio ($\boldsymbol{H_R}$)*	1.24	1.51	1.81
Bulk density [g/cm^3]	0.70 ± 0.00	0.51 ± 0.00	0.73 ± 0.00
Tapped density [g/cm^3]	0.87 ± 0.00	0.77 ± 0.00	1.32 ± 0.00

*$\boldsymbol{H_R}$ = tapped density / bulk density

4.4.1 Calibration Runs: defining the displacement feed factor

In the calibration runs, the piston displacement speed was set to a fixed value for the entire run. The piston displacement speeds in all calibration runs are summarized in Table II. The results of calibration runs are shown in Figure 5. These are the displacement feed factor profiles of all three materials investigated. The effective displacement density of each material was calculated using the 10 g/h feed rate calibration run (without control) based on the GIW balance data. Results of the calibration runs demonstrate that the displacement feed factor is unique for each material. For di-calcium phosphate, the effective displacement density is higher in the beginning and later decreases to a minimum value. Afterwards, the effective displacement density increases again during the feeding process. Croscarmellose sodium shows a constant increase in the effective displacement density data along the cartridge. Barium sulphate shows strong fluctuations due to its very cohesive nature (see H_R in Table I). The effective displacement density of barium sulphate is lower in the beginning and becomes denser during the feeding process. Based on these displacement feed factor profiles, the polynomial function (Eq. (3)) can be defined for each material and used for adjusting the piston displacement speed to achieve a constant feed rate.

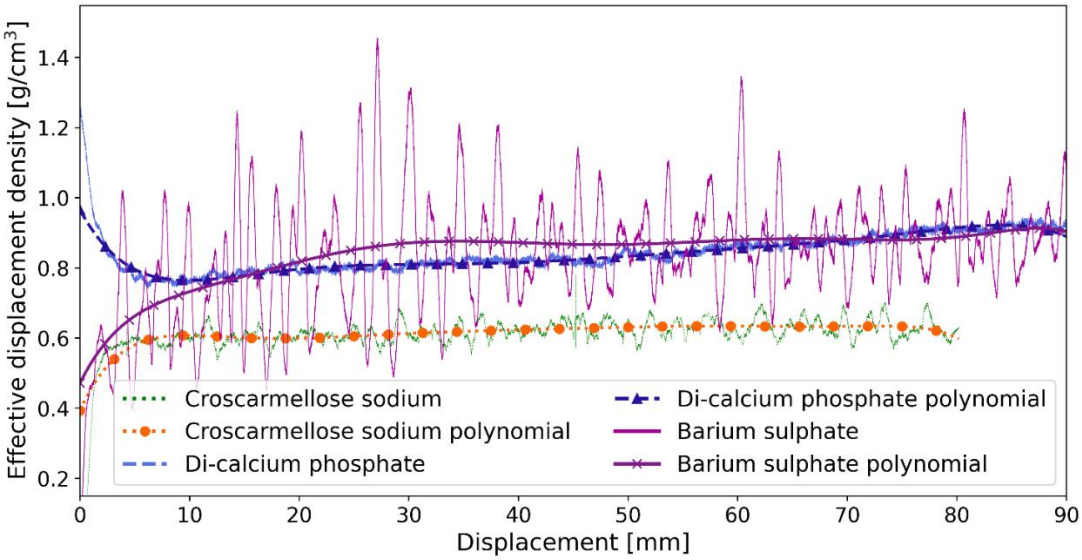

Figure 5. Displacement feed factor profile and the fitted polynomial function for all three materials; calculated using the 10 g/h feed rate calibration run (without control) based on the GIW balance data.

As pointed out above the effective displacement density profile is unique for every material but does not depend on the displacement speed. Figure 6 shows the effective displacement density at three piston displacement speeds for croscarmellose sodium. The shapes and slopes of the curves for different feed rates (piston displacement speeds) are almost identical. Most importantly, the polynomial function fitted to the 10 g/h feed rate curve matches those of the other two feed rates well. Therefore, the polynomial function of 10 g/h feed rate can be used to model the effective displacement density at all selected feed rates, which can be extended to the two other materials as well.

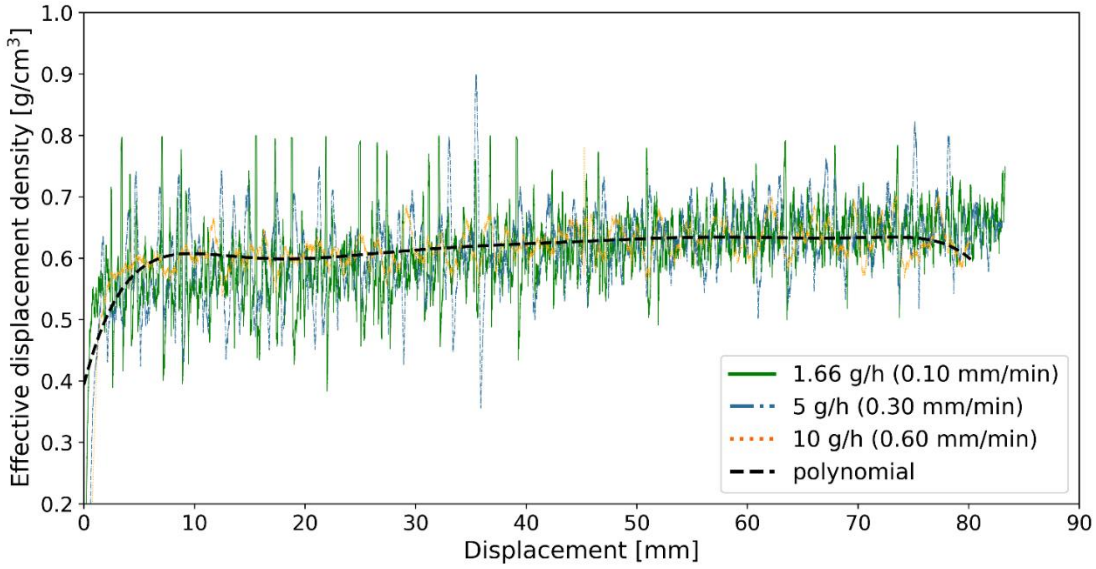

Figure 6. Displacement feed factor profile at all three feed rates selected for croscarmellose sodium; data is obtained from the calibration runs (without control) based on the GIW balance data. The shown polynomial function fitted to the 10 g/h feed rate curve fits to all other feed rates as well. The piston displacement speeds are provided in brackets.

4.4.2 Feed-forward control

In this section, the ability of the feed-forward control strategy to minimize deviations from the set-point was evaluated. For this purpose, the fitted polynomial function at the 10 g/h feed rate, shown in Figure 5, was used to predict the effective displacement density. Subsequently, this polynomial function was used to adjust the piston displacement speed in each position to ensure a constant feed rate. Since the displacement feed factors for the investigated materials are not affected by the feed rate (e.g., see Figure 6 for croscarmellose sodium), the polynomial function fitted to the 10 g/h set-point was used to control the runs at various feed rates for each material. The feed-forward control strategy was evaluated by comparing the control runs to the calibration runs in terms of deviation from the set-points (see Eq. (17) and Eq. (18)) and the RSD (see Eq. (16)).

The feeding curves of di-calcium phosphate, croscarmellose sodium and barium sulphate in the calibration and feed-forward control runs are shown in Figure 7, Figure 8 and Figure 9, respectively. The figures provide comparisons of the feed rate and the piston displacement speed in the calibration and control runs for all three feed-rate set-points. As Figure 7, Figure 8 and Figure 9 indicate, the control runs were executed until the cartridge was empty, while the calibration runs were shorter for the lower feed rate set-points of di-calcium phosphate and barium sulphate. This is because the micro-feeder system is very stable over the studied range. As shown in Figure 6 for croscarmellose sodium, the polynomial function fitted to the 10 g/h

set-point fits the other set-points as well. Due to this fact, for other materials the calibration runs for lower set-points (< 10 g/h) were done only for reduced amounts of time. The reason for fitting the polynomial function of 10 g/h feed rate to the other feed rates is that this run is the shortest one in terms of time and the longest one in terms of displacement. Therefore, in a short time all required information, which is required to control the feed rate of a material, can be obtained. Hence, the duration of calibration runs at various feed rates differ in terms of displacement in Figure 7 and Figure 9 while the lower set-points were executed with a maximum duration of 6 hours. The execution time of the lowest possible feed rate with a piston displacement speed of 0.1 mm/min was 6 hours, which is equivalent to 36 mm displacement. The execution time at the 5 g/h feed rate was 3 hours (displacement of 60 mm), while the 10 g/h run lasted less than 2 hours (displacement of 90 mm).

Figure 7 shows that the feed rate of the calibration runs for di-calcium phosphate is very high in the beginning and subsequently decreases to a minimum value. Afterwards, the feed rate increases continuously with a constant slope. The feed rate of the calibration run for 10 g/h set-point is at the desired set-point only for a short period (displacement of 55-70 mm). However, during the feed-forward controlled run the feed rate is at the set-point for the entire run. A comparison of the piston displacement speed in the calibration runs (set to a fixed value for the entire run) and the control runs (changed based on the model) is provided in Figure 7.

The same improvement in the feed rate deviation from the set-point can be observed for croscarmellose sodium in Figure 8. The feed rate of the calibration runs for croscarmellose sodium is out of the desired set-point for the first 40 mm of displacement. However, the control runs show a much closer feed rate to the set-point along the entire run.

The feed rate deviation for barium sulphate improved remarkably in the control run as well. As shown in Figure 9, the feed rate is much lower than the set-point in the beginning of the calibration run (less than half of the set-point for almost 10 mm for 10 g/h set point). The reason is that pre-conditioning was performed differently for this material due to setup issues. Barium sulphate was only tapped and not compacted to the tapped density state, which may be the main explanation for the observed low feed rate in the beginning of the calibration run. Nevertheless, the feed-forward control run led to much smaller feed rate deviation from the set-point. The last point was particularly notable at the beginning of the run.

All in all, the results show that, despite pre-conditioning prior, the powder density is not constant or does not remain constant along the cartridge. This leads to feed rate deviation from the set-point when no control is applied (calibration runs). However, what was noted was the

changes in density along the cartridge were reproducible and measurable using an effective displacement density profile. Using this profile, the feed-forward controlled runs were able to reach the specified set-point and maintain a stable feed rate at this level. It is important to note that even with the implementation of a feed-forward control, there was a short start-up phase were deviations from the set point were notable. These deviations were most pronounced for di-calcium phosphate, possibly due to an initially larger deviation between the model and the measurement data of the displacement feed factor.

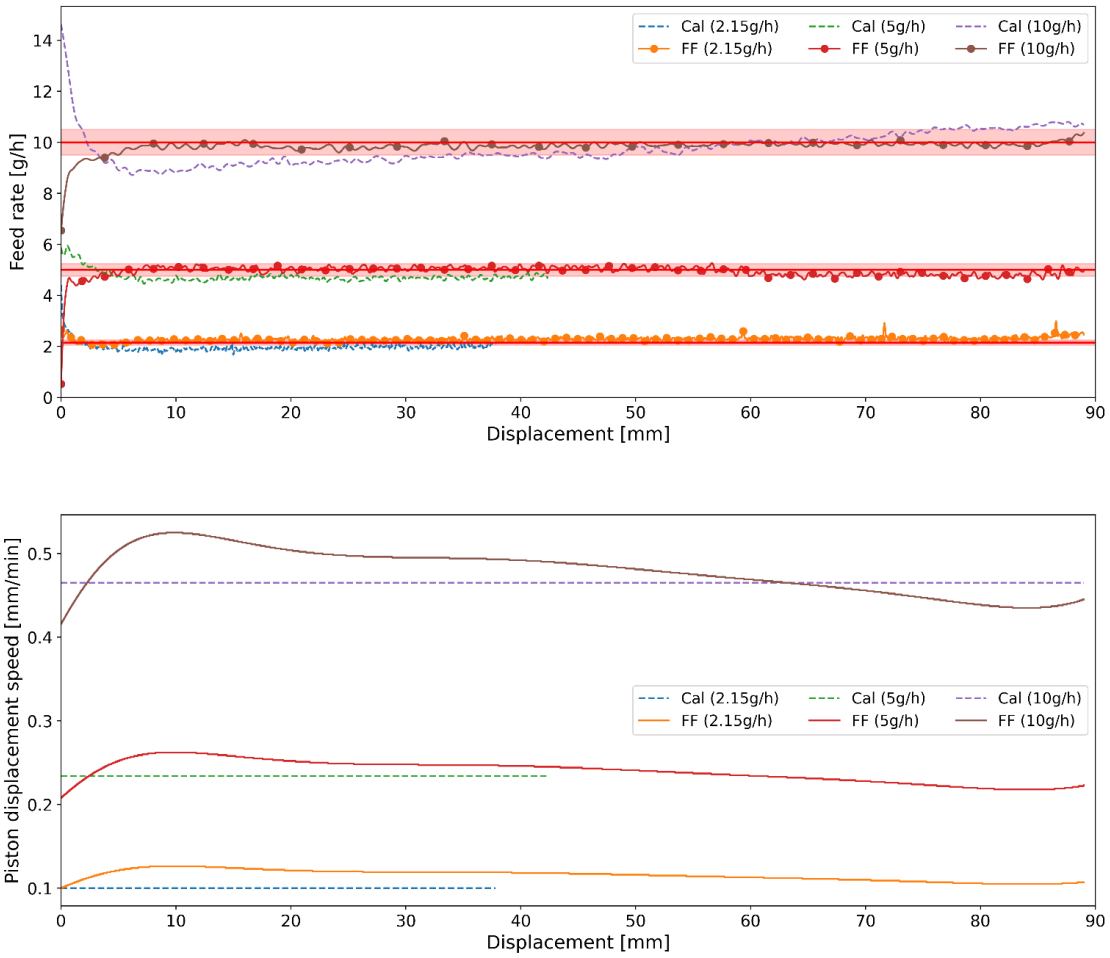

Figure 7. Feeding of di-calcium phosphate at various feed rate set-points: comparison of feeding without (Cal) and with control (FF). The piston displacement speed for the calibration run was set to 0.47 mm/min, 0.23 mm/min and 0.1 mm/min respectively for feed rate set-points of 10 g/h, 5 g/h and 2.15 g/h. For better visibility the set-point ± 5% is shown with a highlighted red line.

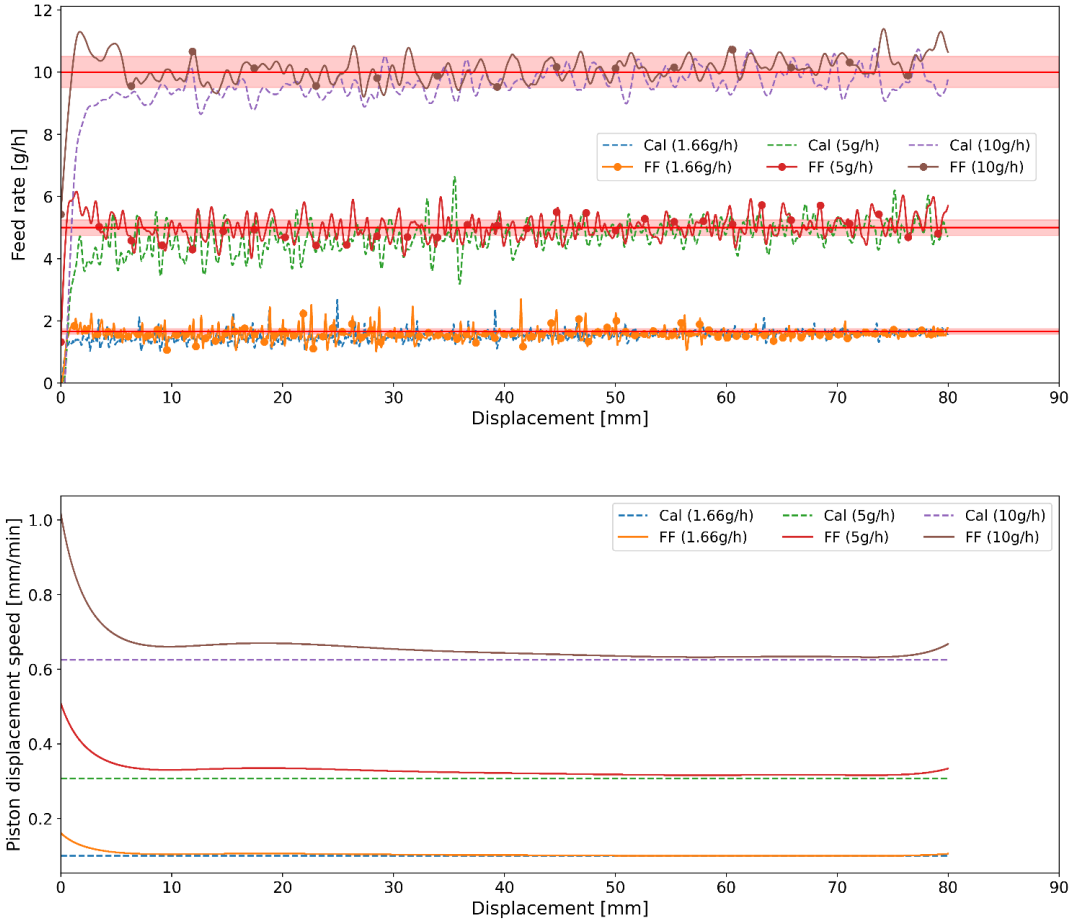

Figure 8. Feeding of croscarmellose sodium at various feed rate set-points: comparison of feeding without (Cal) and with control (FF). The piston displacement speed for the calibration run was set to 0.61 mm/min, 0.31 mm/min and 0.1 mm/min respectively for feed rate set-points of 10 g/h, 5 g/h and 1.64 g/h. For better visibility the set-point ± 5% is shown with a highlighted red line.

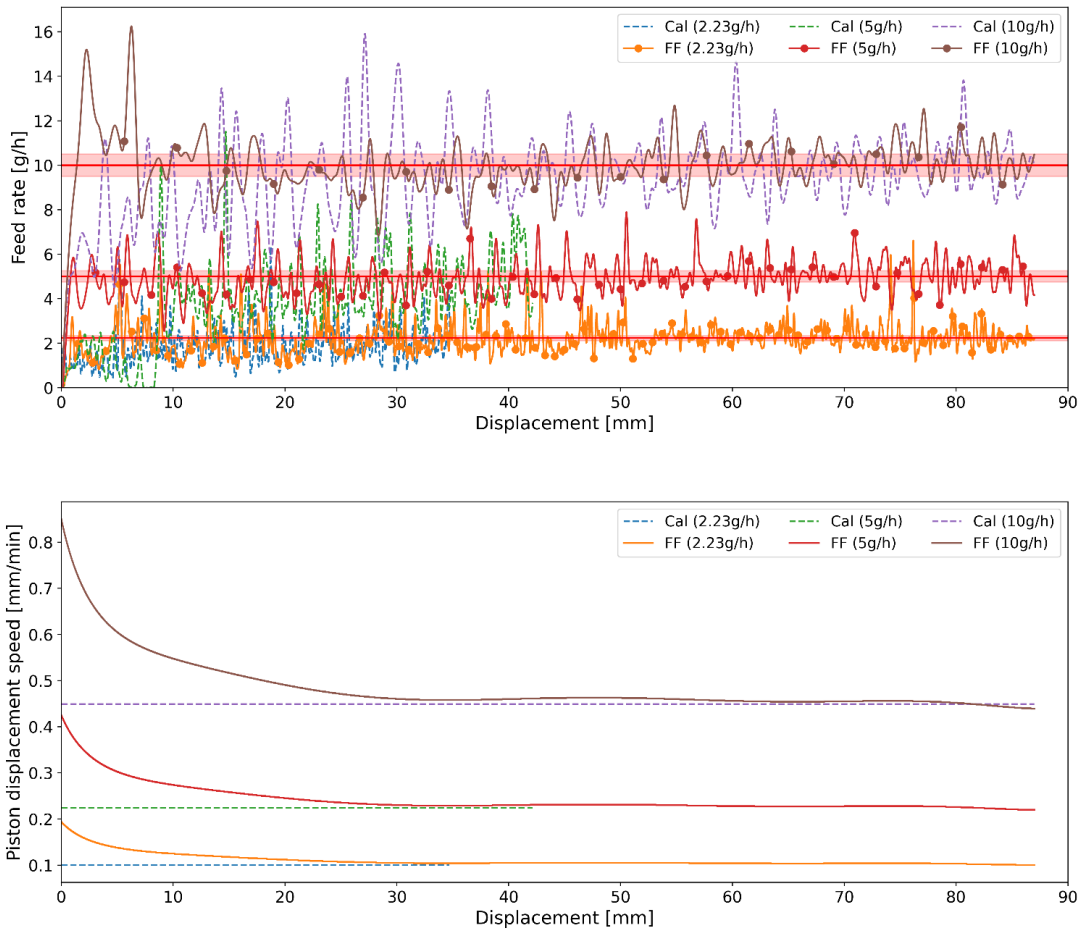

Figure 9. Feeding of barium sulphate at various feed rate set-points: comparison of feeding without (Cal) and with control (FF). The piston displacement speed for the calibration run was set to 0.45 mm/min, 0.22 mm/min and 0.1 mm/min respectively for feed rate set-points of 10 g/h, 5 g/h and 2.23 g/h. For better visibility the set-point ± 5% is shown with a highlighted red line.

Results for the feed rate set-points of all materials, deviation from set-points as well as average relative standard deviation in the controlled and calibration runs, are summarized in Table II. The results were compared for the control and calibration runs by determining the RSD (see Eq. (16)) and the feed rate deviation from the set-point (see Eq. (17) and Eq. (18)). RSD represents the distribution of feed rate measurements around the average feed rate normalized by the average feed rate. The deviation from the set-point are a measure on how close the set-point is met.

Table II indicates that the feed rate set-point in the calibration runs and the feed-forward controlled runs is not the same at the lowest feed rate. Since the minimum possible piston displacement speed was 0.1 mm/min (syringe pump limitation), the piston displacement speed was fixed at this value in the calibration runs at the minimum throughput. However, the minimum throughput in the feed-forward control runs is determined by the maximum

displacement feed factor in combination with the minimum piston displacement speed. This minimum set-point can be calculated by rearranging Eq. (5) and using the maximum displacement feed factor. Using a lower feed rate set-point would result in a truncation of the piston displacement speed at 0.1 mm/min. This equipment limitation hinders achieving the desired set-point. Therefore, the feed rates at the lowest piston displacement speed cannot be compared to the lowest possible set-point for the feed-forward control, which takes the displacement feed factor into account.

Table II. Summary of feed rates, average relative deviation from the set-point and average relative standard deviation in the calibration and feed-forward runs. Cal= calibration run, FF= feed-forward control run.

Material		Barium sulphate			Croscarmellose sodium			Di-calcium phosphate		
Piston displacement speed [mm/min]	Cal	0.45	0.22	0.1	0.61	0.31	0.1	0.47	0.23	0.1
Evaluation range [mm]	-	5-85	5-40*	5-35*	5-75**	5-75	5-75	5-85	5-40*	5-35*
Set-point [g/h]	Cal	10	5	2.23	10	5	1.64	10	5	2.15
	FF	10	5	2.28	10	5	1.66	10	5	2.41
Mean feed rate [g/h]	Cal	9.53	3.94	1.92	9.65	4.72	1.52	9.67	4.67	1.94
	FF	9.98	4.71	2.15	10.06	4.97	1.57	9.88	5.05	2.25
Relative deviation of mean to set-point, RDMtS [%]	Cal	4.7	21.2	13.9	3.5	5.6	7.3	3.3	6.6	9.8
	FF	0.2	5.8	5.7	0.6	0.6	5.4	1.2	1.0	6.6
Average relative deviation to set-point, RDtS [%]	Cal	13.7	33.0	30.7	4.6	8.1	9.9	5.3	6.6	10.0
	FF	7.2	14.3	26.5	2.8	5.5	7.4	1.3	1.6	6.6
Average relative standard deviation, RSD [%]	Cal	18.0	45.9	40.8	4.2	9.4	10.0	5.3	1.6	3.7
	FF	9.9	17.8	35.5	3.5	6.8	11.1	0.9	1.7	2.3

*the evaluation range were chosen to compare the control results to the calibration ones (which were kept shorter)

**steady state range is shorter due to the longer pre-conditioning (22-23mm compression)

The mean feed rate and RSD data in Table II show a significant improvement in the feeding consistency for all materials using the feed-forward control strategy. The deviation from the set-point (AStS and RDtS) are significantly lower in all control runs. Notably, the RDtS is considering the average absolute difference between set-point and measured feed rate and thus, positive and negative deviations do not compensate each other. Therefore, the RSMtS (Eq. (18)) provides a better estimation and it is of course lower. The RSMtS decreased to lower than 7% in various set-points of feed-forward control runs.

RSD decreased for all control runs except for 5 g/h set-point of di-calcium phosphate and minimum set-point of croscarmellose sodium. Generally, the RSD is caused by deviation from the set-point, inconsistencies in feed rate and measurement noise (from the scale). As the feed rate is stable (following a horizontal profile in the considered range) for the feed-forward controlled experiments, the effect of this deviation to the set-point is removed and the remaining RSD can be attributed to material-inherent inconsistencies in feed rate as well as measurement noise. In particular, for croscarmellose sodium the RSD reduction is lower compared to other materials, since the effective displacement density is less dependent on the displacement (see Figure 8). Furthermore, a higher RSD at lower throughputs indicates that the RSD's absolute value is determined by the measurement noise, which is not affected by the throughput.

The RDtS is an important measure to quantify the feeding performance. It is clearly smaller for all feed-forward controlled runs compared to the calibration. A clear trend can be observed: a relative deviation from the set-point is lower at higher feed rates, which - in combination with the RSD - suggests that the feeding performance is better at higher throughputs. The largest deviation from the set-point of 2.28 g/h (cal) versus 2.15 g/h (FF) at the minimum throughput is observed for barium sulphate. This can be translated to feeding 0.13 g less of material in one hour. The deviation is most likely caused by a non-reproducible displacement feed factor curve due to inconsistencies during filling and pre-conditioning.

In summary a good feeding consistency was achieved using the feed forward control strategy. Nevertheless, to compensate for any deviation, an iterative learning control approach was adopted.

4.4.3 Iterative learning control

The concept of iterative learning control is demonstrated by introducing an error (artificial offset) in the polynomial density model. This error, mimicking a 10 % lower density than the one obtained in the calibration runs, results in a higher displacement speed and thus a too high

feed rate. The iterative learning approach was tested as a proof of concept using the micro-feeding system for di-calcium phosphate at a feed rate set-point of 10 g/h. The iterative learning control (iterative learning/feed-forward combined) was then compared to having only feed-forward control in place, with the same 10% higher feed rate. The basic idea of this concept is that LIW control, as it is used by standard LIW feeders, does not work well for the micro feeder, since the mass loss over time is low, and scale resolution is usually not good enough to provide data for the feed-back control in sufficiently small time intervals. Thus, we propose a concept where control is mostly feed-forward, and weight-loss data are used for an iterative learning approach. The iterative learning approach assures that the feed forward controlled feed rate remains within the permissible range of feed rates in order to achieve product with CQAs meeting approved targets. We call this concept a "corridor-control" approach. In this case, we demonstrate the corridor approach with a feed rate of 10 g/h with a corridor of ± 7.5%. This corridor is chosen considering the accuracy and readability of GIW (0.0001 g) and LIW (0.1 g) balances.

In general, the iterative learning control consists of the initialization phase and the iteration phase. The initialization phase is used to reach a stable feed rate. During this phase, the controller is not active. During the iteration phase, the controller is active and tracks the reference (set-point) in an iterative manner, either on iteration displacement or iteration time interval (applied in this work).

In the micro-feeder system, the LIW balance data are used for iterative learning control. An initialization step of 600 seconds was chosen. This 600 seconds (10 minutes) are chosen based on the displacement speed of approximately 0.5mm/min at the beginning of the experiment, corresponding to a piston displacement of 5mm. It can be seen in Figure 7, that after 5mm at a feed rate of 10 g/h, steady state is reached. Subsequently, the iteration step with an integration period of 1200 seconds was applied. This means that every 1200s the polynomial density model is updated to keep the feed rate close to the desired feed rate set-point.

The weight loss recorded by the LIW balance is used to calculate the correction term and update the polynomial for the next iteration step. The LIW balance values are smoothed by using a linear polynomial fit over 60s before the iteration step starts. This is done to obtain more robust results from the LIW balance, where disturbances, especially introduced by the scraper, influence the LIW balance data. The error for the polynomial density model is calculated from Eq.(13). This approach is done in a repetitive mode for each iterative step.

Figure 10 shows a comparison of iterative learning control active (corridor-control, Figure 10b) and only feed-forward control (Figure 10a). The results are summarized in Table III. As mentioned, Figure 10a depicts feeding of di-calcium phosphate with a 10% offset error in the initial feed rate. At the beginning, the feed rate is increasing and reaching a (too high) steady state after an initialization period. Towards the end of the experiment, the feed rate is decreasing. This can be explained by a deviation from the effective displacement density compared to the calibration experiment for which the polynomial density model was obtained to adjust the piston displacement speed. Possibly, preconditioning was not as effective in this illustrative example. As can be seen in the figure, the feed rate is out of spec for almost the entire run, since the control variable adjustment is not error based in the feed-forward control concept. In fact, two contributions to the off-specification feeding performance can be identified: first a 10% offset and second, a decrease of density during the run in contrast to the calibration experiments.

Figure 10b shows the corridor-control (feed-forward/iterative learning control combined) feeding of di-calcium phosphate with a 10% error. Compared to Figure 10a, there are stepwise changes in the feed rate apparent. At the initialization step (600s) and the first iteration step (integration period of 1200s), the feed-forward control was active. Therefore, the feed rates for the first 1800 seconds in Figure 10a and b are similar. However, after 1800s the computation of the difference between reference (set-point) and measured dosed mass (LIW balance signal recorded during first iterative step) leads to a set-point offset and the controller reduces the displacement speed. In the next iteration, at 3000s, the feed rate is too low and therefore the controller increases the displacement speed again. However, the controller is still following the initial shape of the polynomial density model for adjusting the displacement speed and is only adding or cutting the error. This approach keeps the feed rate close to the set-point in the defined corridor.

There are slight differences in the LIW and GIW data, which is due to the difference in accuracy and readability of these balances. Since the correction in the corridor control approach is based on the LIW balance data, only considering the LIW data, the feed rate is after the first iterative step for the entire run in the range of the set-point ± 5%. From a processing and GMP perspective, the LIW balance information can be used to provide material accountability at the end of the run and enable tracking of material in real time over a longer corridor. It is understood that the precision of the LIW balance will not be sufficient to control the process over short process windows were only milligrams (mg) of material are dispensed, however, over longer periods of time the data can be beneficial.

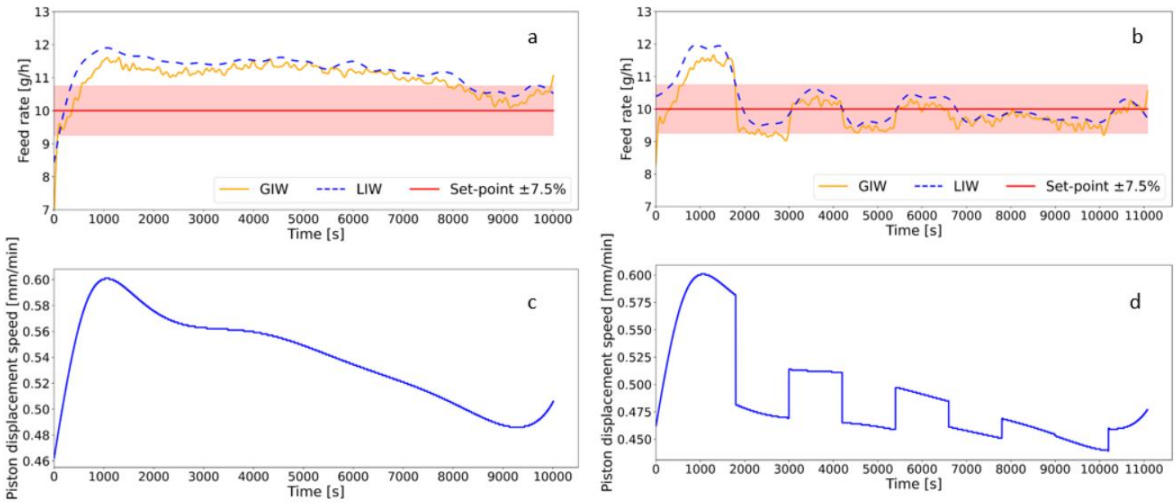

Figure 10: Comparison of iterative learning (IL) control active (b, and d) to IL inactive (a, and c) runs: di-calcium phosphate with a 10% feed rate off set. Figures a, and b show the feed rate as a function of time for IL control inactive and IL control active runs, respectively. Feed rate generated from both LIW scale (blue dotted line) and GIW scale (yellow line) data are presented. For better visibility the set-point of 10 g/h ± 7.5% is shown with a highlighted red line. Figures c, and d show the displacement speed profile of the syringe pump as a function of time for respectively IL control inactive and IL control active runs. The LIW scale signal is used for adapting the piston displacement speed.

Introducing stepwise changes in the displacement speed profile and hence in the feed rate increases the RSD of the signal. However, as can be seen from Table III, the RSMtS and RDtS are drastically reduced by means of iterative learning control. The RSMtS is reduced to less than 1.5% in iterative learning active runs. The RDtS is considering the average absolute difference between set-point and measured feed rate so the positive and negative deviations do not compensate each other. Therefore, this example shows that the RSD is not a suitable single measure for evaluation the feeding performance.

For the corridor control approach (iterative learning control active), the displacement speed decreases to a much lower speed after the first iteration step (see Figure 10d at 1800 s). This leads to a sharp decrease in feed rate and therefore resulting in a high RSD. Refinements on the timing of initialization step and iteration step are currently under investigation. Moreover, a reduction of the iteration step duration will allow a faster reaction to certain process disturbances however on the cost of robustness. Therefore, variable timing based on noise level is under consideration.

Table III. Summary of iterative learning control (IL) active and inactive feeding results based on GIW and LIW scale data. Material fed: Di-calcium phosphate

Scale for Data	Set-point [g/h]		Mean feed rate [g/h]		Relative deviation of mean to set-point, RDMtS [%]		Average relative deviation to set-point, RDtS [%]		Average relative standard deviation, RSD [%]	
	IL off	IL on	IL off	IL on	IL off	IL on	IL off	IL on	IL off	IL on
GIW	10	10	11.08	9.90	10.8	1.0	10.76	5.10	3.12	6.45
LIW	10	10	11.31	10.14	13.1	1.4	13.11	4.98	3.19	6.83

4.5 Summary and conclusions

A two-stage control strategy was developed for a novel micro-feeder system. The performance of the feed-forward control strategy was evaluated using di-calcium phosphate, croscarmellose sodium and barium sulphate representing powders with different material properties and feeding characteristics. A material-specific displacement feed factor, which is not affected by the feed rate, was obtained in the calibration runs for each material. This factor was used to predict the feed rate and proactively control the piston displacement speed as a manipulated variable. The influence of effective displacement density variation on the feed rate during processing was successfully minimized. Stable feed rates were achieved at the set-point levels via pre-defined modification of the piston displacement speed based on the prediction model (obtained in the calibration runs). The relative deviation from the set-point and the RSD decreased significantly, particularly for the materials with high feed rate fluctuations without control.

Furthermore, an iterative learning control strategy combined with the feed-forward control was developed and successfully transferred to the physical micro-feeding system. As a proof of concept, di-calcium phosphate was fed at 10 g/h using this control strategy to demonstrate its applicability to the micro-feeder. The results are highly promising and further optimization and refinements will be carried out in a follow-up study.

The results of this study attest to the potential of the proposed micro-feeder system for industrial implementation. By applying the proposed control strategy, the feeding performance of materials that are difficult to handle at low doses using conventional systems can be improved to fulfil the requirements of commercial manufacturing.

4.6 Acknowledgements

RCPE is a K1 COMET Centre within the COMET – Competence Centres for Excellent Technologies programme. The COMET programme is operated by the Austrian Research Promotion Agency (FFG) on behalf of the Federal Ministry for Transport, Innovation and Technology (BMVIT) and the Federal Ministry for Digital and Economic Affairs (BMDW). Our projects are also funded by Land Steiermark and the Styrian Business Development Agency (SFG). We would like to thank Elliot Koh for graphical support, Mohammed Feroz Bhuiyan and Michael Piller for technical support.

4.7 References

1. Markl D, Warman M, Dumarey M, Bergman EL, Folestad S, Shi Z, et al. Review of real-time release testing of pharmaceutical tablets: State-of-the art, challenges and future perspective. Int J Pharm [Internet]. 2020;582(April):119353. Available from: https://doi.org/10.1016/j.ijpharm.2020.119353
2. Singh R, Muzzio FJ, Ierapetritou M, Ramachandran R. A combined feed-forward/feed-back control system for a QbD-based continuous tablet manufacturing process. Processes. 2015;3(2):339–56.
3. Madarász L, Köte Á, Gyürkés M, Farkas A, Hambalkó B, Pataki H, et al. Videometric Mass Flow Control: A New Method for Real-Time Measurement and Feedback Control of Powder Micro-Feeding based on Image Analysis. 2020;
4. Vanarase A, Ricart B, Almaya A, Debelder L, Wyatt J. Results and Discussion Corporate Strategy for CM Implementation. 2020;(August):1–18.
5. Hanson J. Control of a system of loss-in-weight feeders for drug product continuous manufacturing. Powder Technol [Internet]. 2018;331:236–43. Available from: https://doi.org/10.1016/j.powtec.2018.03.027
6. Wang Y, Koynov S, Glasser BJ, Muzzio FJ. A method to analyze shear cell data of powders measured under different initial consolidation stresses. Powder Technol [Internet]. 2016;294:105–12. Available from: http://dx.doi.org/10.1016/j.powtec.2016.02.027
7. Moghtadernejad S, Escotet-Espinoza MS, Oka S, Singh R, Liu Z, Román-Ospino AD, et al. A Training on: Continuous Manufacturing (Direct Compaction) of Solid Dose Pharmaceutical Products. J Pharm Innov. 2018;13(2):155–87.
8. Li T, Scicolone J V., Sanchez E, Muzzio FJ. Identifying a Loss-in-Weight Feeder Design Space Based on Performance and Material Properties. J Pharm Innov. 2020;15(3):482–95.
9. Engisch WE, Muzzio FJ. Feedrate deviations caused by hopper refill of loss-in-weight feeders. Powder Technol. 2015;283:389–400.
10. Engisch WE, Muzzio FJ. Loss-in-Weight Feeding Trials Case Study: Pharmaceutical Formulation. J Pharm Innov. 2014;10(1):56–75.
11. Engisch WE, Muzzio FJ. Method for characterization of loss-in-weight feeder

equipment. Powder Technol. 2012;228:395–403.

12. C.A. Blackshields AMC. Continuous powder feeding for pharmaceutical solid dosage form manufacture: a short review. Pharm Dev Technol [Internet]. 2017; Available from: https://doi.org/10.1080/10837450.2017.1339197

13. Berthiaux H, Marikh K, Gatumel C. Continuous mixing of powder mixtures with pharmaceutical process constraints. Chem Eng Process Process Intensif. 2008;47(12):2315–22.

14. Vanarase AU, Muzzio FJ. Effect of operating conditions and design parameters in a continuous powder mixer. Powder Technol [Internet]. 2011;208(1):26–36. Available from: http://dx.doi.org/10.1016/j.powtec.2010.11.038

15. Cartwright JJ, Robertson J, D'Haene D, Burke MD, Hennenkamp JR. Twin screw wet granulation: Loss in weight feeding of a poorly flowing active pharmaceutical ingredient. Powder Technol [Internet]. 2013;238:116–21. Available from: http://dx.doi.org/10.1016/j.powtec.2012.04.034

16. Wang Y, Li T, Muzzio FJ, Glasser BJ. Predicting feeder performance based on material flow properties. Powder Technol [Internet]. 2017;308:135–48. Available from: http://dx.doi.org/10.1016/j.powtec.2016.12.010

17. Thayalan V, Landers RG. Regulation of powder mass flow rate in gravity-fed powder feeder systems. J Manuf Process. 2006;8(2):121–32.

18. Fathollahi S, Faulhammer E, Glasser BJ, Khinast JG. Impact of powder composition on processing-relevant properties of pharmaceutical materials: An experimental study. Adv Powder Technol [Internet]. 2020;31(7):2991–3003. Available from: https://doi.org/10.1016/j.apt.2020.05.027

19. Singh R, Sahay A, Karry KM, Muzzio F, Ierapetritou M, Ramachandran R. Implementation of an advanced hybrid MPC-PID control system using PAT tools into a direct compaction continuous pharmaceutical tablet manufacturing pilot plant. Int J Pharm [Internet]. 2014;473(1–2):38–54. Available from: http://dx.doi.org/10.1016/j.ijpharm.2014.06.045

20. Hsu SH, Reklaitis G V., Venkatasubramanian V. Modeling and control of roller compaction for pharmaceutical manufacturing. Part I: Process dynamics and control framework. J Pharm Innov. 2010;5(1–2):14–23.

21. Hsu SH, Reklaitis G V., Venkatasubramania V. Modeling and control of roller compaction for pharmaceutical manufacturing: Part II: Control system design. J Pharm Innov. 2010;5(1–2):24–36.

22. Kirchengast M, Celikovic S, Rehrl J, Sacher S, Kruisz J, Khinast J, et al. Ensuring tablet quality via model-based control of a continuous direct compaction process ☆. Int J Pharm. 2019;567(858704):118457.

23. Hattori Y, Otsuka M. Modeling of feed-forward control using the partial least squares regression method in the tablet compression process. Int J Pharm [Internet]. 2017;524(1–2):407–13. Available from: http://dx.doi.org/10.1016/j.ijpharm.2017.04.004

24. Celikovic S, Kirchengast M, Rehrl J, Kruisz J, Sacher S, Khinast J, et al. Model predictive control for continuous pharmaceutical feeding blending units. Chem Eng Res Des. 2019;154:101–14.

25. Singh R, Román-Ospino AD, Romañach RJ, Ierapetritou M, Ramachandran R. Real time monitoring of powder blend bulk density for coupled feed-forward/feed-back control of a continuous direct compaction tablet manufacturing process. Int J Pharm [Internet]. 2015;495(1):612–25. Available from: http://dx.doi.org/10.1016/j.ijpharm.2015.09.029

26. Rehrl J, Kruisz J, Sacher S, Khinast J, Horn M. Optimized continuous pharmaceutical manufacturing via model-predictive control. Int J Pharm [Internet]. 2016;510(1):100–15. Available from: http://dx.doi.org/10.1016/j.ijpharm.2016.06.024

27. An J, You F, Wu M, She J. Iterative Learning Control for Nonlinear Weighing and Feeding Process. 2018;2018.

28. You F, An J. Iterative Learning Control for Batch Weighing and Feeding Process. 2018;2904–8.

29. Fathollahi S, Sacher S, Escotet-espinoza MS, Dinunzio J, Khinast JG. Performance Evaluation of a High-Precision Low-Dose Powder Feeder. 2020;1–13.

30. USP. ⟨ 616 ⟩ Bulk Density and. United States Pharmacop Natl Formul. 2012;48(2012):2011–3.

31. Savitzky A, Golay MJE. Smoothing and Differentiation of Data by Simplified Least Squares Procedures. Anal Chem. 1964 Jul;36(8):1627–39.

32. Candan Ç, Inan H. A unified framework for derivation and implementation of Savitzky-Golay filters. Vol. 104, Signal Processing. 2014. p. 203–11.

5 Conclusion

The advantages of shifting from batch manufacturing to continuous manufacturing in the pharmaceutical industry are highlighted in chapter 1. Continuous manufacturing makes a great opportunity to adopt innovations in the pharmaceutical industry. APIs and excipients are continuously fed and blended in continuous pharmaceutical manufacturing. Optimization of these processes requires a good understanding of both the material properties and the manufacturing process.

In chapter 2, the dependence of macroscopic powder properties on the mixture composition of binary powder mixtures from 0-100% was investigated. Macroscopic powder properties (such as bulk and tapped density, Hausner ratio, compressibility, permeability, cohesivity, and flow function ffc) of binary mixtures are strongly dependent on the size ratio of the binary mixtures and the fraction of larger particles. Our results show that there is a smooth linear correlation between macroscopic powder properties for a binary mixture of symmetric particle size. However, this simple linear mixture rule does not apply to other binary mixture classes with significantly different size ratios, but there is a non-linear/non-monotonic dependence of powder properties on composition. This result is especially relevant in the context of continuous pharmaceutical manufacturing and suggests using particle mixtures with symmetric particle size if a stable operation of varying mixtures is needed.

The novel micro-feeder system is introduced in chapter 3. It is capable of continuously feeding small quantities of powder (down to 1 g/h) with significantly different flow properties (from powder with high cohesion to free-flowing). The feeding principle is based on volumetric feeding, that cartridge volume at the bottom is continuously and constantly displaced and transferred to the further process. The feeding performance and the impact of powder properties on feeding were analyzed and discussed. The feeding process was stable and reproducible for all investigated materials. A density displacement curve was plotted for all materials, which is unique and independent of the feed rate set point for each material. Results suggest that by calibrating the syringe pump based on the density displacement curve, a constant feed rate with high accuracy can be achieved.

In chapter 4, a two-stage control strategy was developed for the micro-feeder system. In the first stage, a material-specific displacement feed factor was used to predict the feed rate and proactively control it. The performance of the control strategy was evaluated. Results show stable feed rates at various set-points. This is achieved by modification of the piston displacement speed based on the prediction model. Furthermore, an iterative learning control

strategy combined with the feed-forward control was developed and successfully transferred to the micro-feeding system. The performance evaluation results are highly promising.

6 Outlook

The robustness of mixtures is a highly relevant property for direct compaction since a robust mixture is easier to blend. Robustness is defined as a material mixture that does not change macroscopic properties in a nonlinear way and does not show segregation upon changes in composition. Particularly segregation is a big problem for direct compaction. Therefore, it is suggested for future work to test segregation (e.g., Jenike & Johanson) to elaborate the robustness of mixtures. For an API of a given size, it is important to specify the excipient size to have a robust mixture, since the API size is usually defined by other factors e.g., bioavailability. Therefore, it is recommended to study the impact of powder composition and robustness of mixtures with an API of a given size and different-sized excipients. In addition, non-linear (non-ideal) mixture rules need to be developed to allow a rational design, optimization, scale-up, and control of pharmaceutical manufacturing operations. This is relevant for any process where materials are mixed and filled, e.g., mixing APIs with a carrier and filling it into a capsule body. Capsule filling is a volumetric process, and therefore, small changes in the composition can lead to large changes in fill weight due to the large changes in density. Thus, it is a prerequisite to limiting the size ratios of the components in the mixture for process stability, agility, and robustness.

For the micro-feeder system, first of all, full automation of the micro-feeder system needs to be developed. For example, finger tapping (strokes by the side in the cartridge) during the pre-conditioning process should be replaced by automatically hammering the cartridge periodically during the filling process. For making the system ready for longer feeding times (non-stop feeding) process, an additional (material-filled) cartridge with an automated refilling system needs to be developed and tested. Hence, while the first cartridge is in use, the other one is in the refilling station.

The corridor control (feed-forward/iterative control combined) of the micro-feeder should be finalized for integration in GMP continuous manufacturing lines, given the need to better control the flow rate over time. However, further optimization and refinements of the proposed corridor control need to be carried out in the future. In this thesis, as a proof of concept, the iteration step of 1200 s was used and tested for evaluating the corridor control strategy. However, the iteration steps need to be much shorter (in terms of time) to enable the control system to take appropriately quick action on process disturbances.

By applying the proposed control strategy, the feeding performance of materials that are difficult to handle at low doses (e.g., MgSt or colloidal silica) using conventional systems can

be improved to fulfill the requirements of commercial manufacturing. Further investigation and testing of corridor control strategy with more complex materials, such as lubricants, are required.

The idea for future work is to install the micro-feeder system in a continuous tableting line. Two micro-feeders will be installed in the continuous tableting line, one for the API feeding and one for the lubricant. The performance evaluation of both feeder and control strategy can be evaluated by the content uniformity of the final tablet. This study attests to the potential of the proposed micro-feeder system for industrial implementation.

7 Appendix

7.1 Publications

Research Papers

Sara Fathollahi, Eva Faulhammer, Benjamin J. Glasser, Johannes G. Khinast, Impact of Powder Composition on Processing-relevant Properties of Pharmaceutical Materials: An Experimental Study, Advanced Powder Technology, Volume 31, Issue 7, July 2020, Pages 2991-3003.

Sara Fathollahi, Stephan Sacher, M. Sebastian Escotet-Espinoza, James DiNunzio, Johannes G. Khinast, Performance Evaluation of a High-precision Low-dose Powder Feeder, AAPS PharmSciTech. 2020 Nov 3;21(8):301.

Besenhard MO, Karkala SK, Faulhammer E, Fathollahi S, Ramachandran R, Khinast JG. Continuous feeding of low-dose APIs via periodic micro dosing. Int J Pharm. 2016;509(1–2):123–34.

Besenhard MO, Fathollahi S, Siegmann E, Slama E, Faulhammer E, Khinast JG. Micro-feeding and dosing of powders via a small-scale powder pump. Int J Pharm. 2017;519(1–2):314–22.

M.O. Besenhard, E. Faulhammer, S. Fathollahi, G. Reif, V. Calzolari, S. Biserni, A. Ferrari, S.M. Lawrence, M. Llusa, J.G. Khinast, Accuracy of micro powder dosing via a vibratory sieve-chute system Eur. J. Pharm. Biopharm., 94 (2015), pp. 264-272.

Under review

Sara Fathollahi, Julia Kruisz, Stephan Sacher, Jakob Rehrl, M. Sebastian Escotet-Espinoza, James DiNunzio, Benjamin J. Glasser, Johannes G. Khinast, Development of a Controlled Continuous Low-dose Feeding Process, under review

Stephan Sacher, Sara Fathollahi, Johannes G. Khinast, Comparative study between a novel micro-feeder and loss-in-weight feeders, under review

Patent

Sara Fathollahi, Johannes Khinast, Thomas Klein, Eyke Slama, Maximilian Besenhard. System and a method for constant micro-dosing and feeding of powder material. Publication number:20200158549, publication date: May 21, 2020.

Talks and Poster

Poster: Sara Fathollahi, E.Faulhammer, Johannes G. Khinast, Influence of powder composition on macroscopic powder properties

Location: 14th Minisymposium Chemical and Process Engineering and 5th Austrian Particle Forum, Linz, April 2018

Talk: Sara Fathollahi, E.Faulhammer, Johannes G. Khinast, Influence of powder composition on macroscopic powder properties

Location: 12th Pharmaceutical Solid-State Research Cluster (PSSRC) Meeting in Leuven, Belgium, September 2018

Talk: Sara Fathollahi, E.Faulhammer, B.J.Glasser, Johannes G. Khinast, Influence of powder composition on macroscopic powder properties

Location: AIChE Annual Meeting, Orlando, USA, November 2019

Poster and a short talk: Sara Fathollahi, E.Faulhammer, B.J.Glasser, Johannes G. Khinast, Influence of powder composition on macroscopic powder properties

Location: Blending and Segregation Forum, Enschede, The Netherlands, December 2019

Talk: Sara Fathollahi, Stephan Sacher, Johannes G. Khinast, Performance evaluation of a high-precision low-dose powder feeder

Location: 14th Pharmaceutical Solid-State Research Cluster (PSSRC) 2020 Annual Meeting, Online.

7.2 Academic development

2017 – 2021	Graz University of Technology, Doctoral School of Chemical and Process Engineering, Institute of Process and Particle Engineering, Austria
2014 – 2016	Graz University of Technology, Master of Science, Institute of Biomedical Engineering, Austria
2008 – 2012	Islamic Azad university of Tehran, Institute of Biomedical Engineering, Bachelor of Engineering, Iran